C.P. No. 968

C.P. No. 968

MINISTRY OF TECHNOLOGY

AERONAUTICAL RESEARCH COUNCIL

CURRENT PAPERS

The Drag of Some Wedge Centre-body Intakes at Mach Numbers of 1.56, 1.86 and 2.14

by

R. A. Dutton and E. L. Goldsmith

LONDON: HER MAJESTY'S STATIONERY OFFICE

1967

PRICE 12*s* 6*d* NET

U.D.C. No. 533.697.25 : 533.6.013.12 : 531.652 : 533.6.011.72 : 533.6.011.5

C.P. No.968*
July 1966

THE DRAG OF SOME WEDGE CENTRE-BODY INTAKES AT MACH NUMBERS OF 1.56, 1.86 AND 2.14

by

R. A. Dutton
E. L. Goldsmith

SUMMARY

Experiments are described in which measurements have been made of the drag and pressure recovery of a wedge centre-body intake of rectangular cross-section. Intakes with four different wedges (12°, 16°, 20° and 24° semi apex angle) were tested at Mach numbers of 1.56, 1.86 and 2.14. The measurements were obtained for the following three different flow states; with both the wedge and cowl lip shocks attached, with only the wedge shock attached, and finally with the wedge shock detached. The results obtained from the drag measurements are compared with those from an approximate method of calculation. With the wedge shock attached, the spillage drag can be estimated reasonably well but when the wedge shock is detached the measure of agreement between experimental and calculated results is poor.

Curves showing the variation of capture ratio and pre-entry drag at full mass flow with M_∞ for particular wedge angles, and curves giving the cowl drag at full mass flow for families of both straight line and elliptical cowl profiles are presented.

---

* Replaces R.A.E. Tech. Report 66208 - A.R.C. 28449

CONTENTS

1 INTRODUCTION

A considerable amount of experimental work has been done on conical centre-body intakes but as yet, the equivalent wedge centre-body intake has received much less attention. For single- or twin-engine installations (engines in the fuselage or in separate nacelles on the wings) the conical centre-body intake is an obvious choice, since its geometry blends well with the remainder of the aircraft. For multi-engine applications however engines may be placed so as to occupy a fair portion of the wing span, either buried in the wing with intakes at the wing leading edge or positioned under the wing in a rectangular shaped nacelle. In these cases the wedge centre-body intake obviously applies. Where it is deemed advantageous to vary the geometry of the intake in flight the wedge centre-body intake may also offer improvements over the equivalent conical centre-body intake. Variable geometry in this instance is limited (by practical difficulties) to varying the fore and aft position of the centre-body with respect to the cowl whereas with the wedge centre-body intake the angle of the wedge, the position of the cowl lip and the fore and aft position of the centre-body can all be varied, either separately or together.

The shock pressure recovery of wedge centre-body intakes is readily calculable and for a given wedge surface Mach number and internal geometry it should be possible to estimate the losses other than shock losses from tests of equivalent conical centre-body intakes.

If the wedge centre-body and the cowl lip shock are attached it should be possible to calculate the pre-entry and cowl drag of infinite span intakes reasonably accurately using shock-expansion theory. However, at Mach numbers below design this flow configuration does not continue indefinitely, as first the cowl shock detaches and then the centre-body shock wave becomes detached.

As the following table shows these shock detachment Mach numbers can be considerably higher for wedge centre-body intakes than for equivalent conical centre-body designs.

/Table

Intake type	Design Mach No.	Centre-body semi-angle	Shock pressure recovery	Centre-body surface Mach No.	Cowl lip shock detachment Mach No.	Centre-body shock detachment Mach No.
Conical	2.5	25	0.76	1.75	1.80	1.33
Wedge	2.5	20	0.75	1.64	2.21	1.84

* For an internal cowl angle of 10°, $M_{\omega\ell} = 2.5$.

Thus the main aim of the present investigation has been to measure drag of centre-body intakes having centre-body angles which enable all these three flow states to be achieved at the test Mach numbers of 1.56, 1.86 and 2.14. The tests have been made on intakes with height-to-width ratios which are fairly typical of fighter aircraft installations so that the departure from the infinite span conditions of the theoretical estimates can be assessed. A check on a proposed method of drag calculation at full mass flow[1] (treating the intake as a spilling pitot type intake) where the centre-body shock wave is detached has been made. The drag under spillage conditions has been measured and compared with calculated values using methods of estimation originally developed for conical centre-body intakes[2,3].

2 CALCULATION OF MAXIMUM MASS FLOW, PRE-ENTRY AND COWL DRAGS

2.1 General

We require to know the drag and maximum mass flow in the flow states shown in Fig.1. When the shock waves are attached to the nose of the wedge and the cowl lip and the external flow is everywhere supersonic as in Fig.1(a) the mass flow and pre-entry drag can be calculated exactly by consideration of the supersonic flow around wedges (see Section 2.2). The cowl drag can be calculated by the method of characteristics or by shock-expansion theory (as in Section 2.3). The latter method although not exact is probably sufficiently accurate for most practical purposes at least up to a Mach number of 3.0, and is of course much easier to apply.

At some Mach numbers below the design figure the required deflection of the flow at the cowl lip will preclude the attachment of the shock at the lip. It is not easy to formulate even approximate methods for calculating the drag in this condition particularly if (as is most likely) the lip shock is detached

due to excessive deflection of the internal flow. In this case by ignoring the effect of this shock detachment on the external flow the cowl and pre-entry drags can still be calculated. If the shock detachment is caused by excessive deflection of the external flow however the drag is not readily calculable by any method.

At low Mach numbers the nose wedge shock is detached and it was suggested in Ref.7 that the drag at full mass flow in this condition could be calculated by the approximate methods, already available, to estimate the drag of pitot intakes under conditions of spillage. Thus the maximum mass flow is calculated for choking at the entry plane (assuming that the detached shock is normal over the entry streamtube area) and the drag is calculated as for a pitot intake operating at this mass flow. This method might be expected to give reasonable results at Mach numbers well below the nose shock detachment Mach number. It has also been suggested[4] that it might easily be modified to take account of the shock curvature over the entry streamtube by assuming a hyperbolic form for the detached wave.

So far only the drag at full mass flow has been considered. The calculation of the increased drag arising when the intake is spilling can again be considered in two parts (a) when the wedge shock is attached and (b) when it is detached.

For the first set of conditions the method developed for conical centre-body intakes in Ref.2 has been adapted and used.

When the wedge shock is detached the spillage drag is calculated by the method already outlined when the full mass flow drag was discussed earlier in the section. The intake is treated as a spilling pitot and the method proposed by Fraenkel in Ref.5 is used.

The actual details of these methods are not given in the present report because they have already been summarised in Refs.3 and 5 respectively.

In the remaining part of this section details are given for the calculation of mass flow, the pre-entry drag and the cowl drag at full mass flow for both straight line and elliptical cowl profiles. Finally the method of obtaining the total drag is summarised.

2.2 Calculation of the maximum mass flow $\left(\frac{A_\infty}{A_{en}}\right)_{max}$ and the pre-entry drag $C_{D_{pre_o}}$ at maximum mass flow

The maximum mass flow is given by (Appendix A):-

$$\left(\frac{A_\infty}{A_{en}}\right)_{max} = \left(\frac{h_\infty}{h_{en}}\right)_{max} = \frac{\cot \theta_\ell - \cot \delta}{\cot \theta_\omega - \cot \delta}$$

and pre-entry drag at maximum mass flow is given by (Appendix A):-

$$C_{D_{pre_o}} = \frac{\left(\frac{p_1}{p_\infty} - 1\right)\left(\frac{\cot \theta_\omega - \cot \theta_\ell}{\cot \theta_\omega - \cot \delta}\right)}{\frac{q_\infty}{p_\infty}}$$

using the notation given in Fig.2.

These two quantities have been calculated for wedge angles of 4°, 8°, 12°, 16°, 20° and 24° in the Mach number range 1.2 - 3.0 and for a suitable range of lip position angles θ_ℓ and are presented in Figs.3 and 4.

2.3 Calculation of cowl drag ($C_{D_{cowl_o}}$) at full mass flow for straight line and elliptical cowl profiles

2.3.1 Straight line profiles

For an intake having parallel sides the cowl drag at full mass flow is given simply by

$$C_{D_{cowl_o}} = \frac{\left(\frac{p_1}{p_\infty} - 1\right)\left(1 - \frac{h_{en}}{h_{max}}\right)}{\frac{q_\infty}{p_\infty}}$$

or

$$C_{D_{cowl_o}} = \frac{\left(\frac{p_1}{p_\infty} - 1\right)\frac{L \tan \eta_o}{h_{max}}}{\frac{q_\infty}{p_\infty}}$$

since in this case

$$\tan \eta_o = \frac{h_{max} - h_{en}}{L} \quad .$$

In Fig.5, $C_{D_{cowl_o}} \Big/ \frac{L}{h_{max}}$ is plotted versus M_∞ for various values of η_o.

Strictly in calculating the cowl drag the effect of the pre-entry flow on the flow over the cowl should be considered, i.e. the loss in total pressure across the wedge shock, the Mach number and stream direction immediately ahead of the cowl lip, should be taken into account. However the cowl drag obtained in this way is found to be only slightly greater than that calculated neglecting the pre-entry flow and assuming that free-stream conditions apply at the cowl lip. This can be seen from Figs.6 and 7. In Fig.6 $C_{D_{cowl_o}} \Big/ \frac{L}{h_{max}}$ is plotted versus δ for various values of η_o and a particular free-stream Mach number. Here it can be seen that the difference between the drag calculated considering the pre-entry flow and that obtained neglecting it (the value of $C_{D_{cowl_o}} \Big/ \frac{L}{h_{max}}$ when $\eta_o = \delta_1$) is always small (2½%) independent of whether a shock or an expansion occurs at the cowl lip. Fig.7 shows the variation of $C_{D_{cowl_o}} \Big/ \frac{L}{h_{max}}$ with M_∞ for a particular wedge and cowl slope and again it is seen that the two methods of drag calculations differ only slightly over the range of Mach number considered.

Hence the curves presented in Fig.5 can be used to obtain sufficiently accurate values of the cowl drag when the centre-body intake is operating under full mass flow conditions, if it is assumed that free-stream conditions apply immediately ahead of the cowl lip.

2.3.2 Elliptical cowl profiles

A series of elliptical profiles covering a range of initial slopes, fineness ratios and area ratios will include most cowl profiles (having zero slope at the maximum cross section) that are likely to be encountered in practice. The drag of a representative series has therefore been determined.

The ordinates of several elliptical profiles have been calculated from the expression

$$h = \frac{-\frac{(h_{max}-h_{en})^2}{L} \pm \sqrt{\left[-\frac{(h_{max}-h_{en})^4}{L^2} - \left\{\tan\eta_o - 2\left(\frac{h_{max}-h_{en}}{L}\right)\right\}\left\{\frac{x}{L}(h_{max}-h_{en})^2 \tan\eta_o\left(\frac{x}{L}-2\right)\right\}\right]}}{\left\{\tan\eta_o - 2\frac{(h_{max}-h_{en})}{L}\right\}}$$

which is derived in Appendix B together with the expression below for the gradient at each of the chosen ordinates.

$$\frac{dh}{dx/L} = \frac{\left(1-\frac{x}{L}\right)}{\left\{\frac{L\tan\eta_o - 2(h_{max}-h_{en})}{(h_{max}-h_{en})^2 \tan\eta_o}\right\} h + \frac{1}{\tan\eta_o}}$$

The cowl drag has been obtained by graphically integrating the pressure coefficients which were found at each chosen point on the cowl by Prandtl/Meyer expansion theory.

The results are presented in Fig.8 where $C_{D_{cowl_o}}$ is plotted versus M_∞ for various values of h_{en}/h_{max}, L/h_{max} and η_o. As with the straight line cowl profiles $C_{D_{cowl_o}}$ can be determined from these curves assuming free-stream conditions to apply at the cowl lip.

2.4 General calculation of total drag

In the preceding part of this section details are given of suggested methods for the calculation of the fundamental drag components of two dimensional wedge centre-body intakes. The total external drag is obtained as follows: under full mass flow conditions

$$C_{D_{ext}} = C_{D_{pre_o}} + C_{D_{cowl_o}} + C_{D_{side\ walls}}$$

and Fig.4 enables $C_{D_{pre_o}}$ to be obtained for a range of M_∞ and various values of θ_ℓ. Also, Figs.5 and 8 show the variation of $C_{D_{cowl_o}}$ for both straight line and

elliptical cowl profiles over the same Mach number range and for various values of initial cowl angle and cowl fineness ratio.

The calculation of side plate drag depends of course on their shape. If swept back side plates are used their drag can be calculated by a method developed for swept back wing sections and given in Ref.6.

When the intake is spilling the external drag coefficient is given by the expression:-

$$C_{D_{ext}} = C_{D_{cowl_o}} + C_{D_{side\ plates}} + C_{D_{spill}}$$

where $C_{D_{spill}} = C_{D_{pre}} + \Delta C_{D_{cowl}}$

and is calculated by either of the methods described in Section 2.1 depending on whether the wedge shock is attached or detached.

3 EXPERIMENTAL APPARATUS AND PROCEDURE

The experiments were carried out in the No.4 5½ in. sq supersonic tunnel at the R.A.E. Details of the model intake are shown in Fig.9. Four wedges (12°, 16°, 20° and 24° semi apex angle) could be inserted in the intake and each one was positioned so that the wedge shock would impinge on the cowl lip at $M_\infty = 2.10$. The wedge centre-body dimensions are given in Fig.10. Side walls were attached to the wedges, each pair being swept back at the wedge shock angle for $M_\infty = 1.86$. Tests were made at Mach numbers of 1.56, 1.86 and 2.14 and at Reynolds numbers of 0.294×10^6, 0.266×10^6 and 0.235×10^6 respectively based on cowl height. Both pressure recovery and drag were measured over a range of mass flows through the intake. Similar measurements were also made at each Mach number with the intake operating as a pitot intake, i.e. with the centre-body removed.

The pressure recovery was obtained by taking an arithmetic mean of the readings of 42 pitot tubes situated in the exit plane. This method was adopted after checking that it gave approximately the same results as an area mean method. The positions of the pitot tubes are shown diagramatically in Fig.11 the irregular shaped exit area being necessary to obtain the required mass flows with the existing sting attachment.

The total drag of the intake was measured on a strain gauge balance and the external drag obtained using the relation below:-

$$C_{D_{ext}} = \frac{p_\infty}{q_\infty A_{max}} \left[\frac{W}{P_\infty} - \left(1 - \frac{P_{en}}{P_\infty} B_\infty\right) A_{exit} - \left(1 - \frac{p_{base}}{p_\infty}\right) A_{base} + \left(\frac{p_{bal}}{p_\infty} - 1\right) A_{bal} \right] - C_{D_{SF}}$$

i.e. internal, base and skin friction drags and the pressure force on the end of the balance sting are subtracted from the measured total load. The base drag was found from the arithmetic mean of 4 pitot tubes positioned immediately downstream of both the fixed and interchangeable exit plugs as shown in Fig.11. The skin friction drag was estimated from Ref.7.

Schlieren photographs were taken to show the shock configurations existing with the intake operating at full mass flow.

4 RESULTS AND COMPARISON WITH THEORY

4.1 General

In this section the experimental results are split up for convenience into two main groups. In the first, full mass flow conditions are considered. The results obtained with the intake operating as a pitot intake, are presented to indicate the general accuracy of the measurements. The remaining results are discussed under the three main headings outlined in the Introduction, i.e. when the flow round the intake is completely supersonic (both the wedge shock and the cowl shock are attached), when the wedge shock is attached but the cowl shock is detached and finally when the wedge shock is detached.

In the second group the drag results obtained with the intake spilling are compared with theoretical calculations. The variation of pressure recovery with mass flow is also given although these results are included mainly for completeness as the wedges were designed specifically for the drag tests and not to give high pressure recovery.

The theoretical intake drag for both maximum mass flow and spillage conditions has been calculated by the methods referred to in Section 2.

4.2 Drag at full mass flow

4.2.1 Pitot intakes

Fig.12 gives a comparison between the theoretical and experimental results obtained at each Mach number with the intake operating as a pitot intake. Fairly good agreement is obtained between the two results at each Mach number, the measured drag being slightly less than the theoretical at two Mach numbers. This

is to be expected because the theoretical drag is based on two dimensional theory even though the model is nearly square in cross-section.

It will also be noted that the value of $\left(\frac{A_\infty}{A_{en}}\right)_{max}$ determined from the experimental results is slightly greater than 1.0 at $M_\infty = 1.56$ and $M_\infty = 1.86$. This overestimation of mass flow through a pitot intake, although it often occurs, is difficult to explain. It is calculated (assuming choking to occur in the exit plane) from the relation,

$$\frac{A_\infty}{A_{en}} = \frac{P_{ex}}{P_\infty} \times \frac{A_{ex}}{A_{en}} \times \frac{A_\infty}{A_\infty}$$

and hence if the pressure recovery is obtained accurately $\left(\frac{A_\infty}{A_{en}}\right)_{max}$ is overestimated only if $\frac{A_{ex}}{A_{en}}$ is too great. A_{en} can of course be measured accurately but because of small boundary layer effects and the blockage produced by the pitot tubes (situated in the exit plane) the estimation of the effective A_{ex} is slightly doubtful. In the present investigation the effective A_{ex} was taken as:-

$$\text{Actual Exit Area} - \pi r^2 N$$

where r is the external radius of the pitot tubes and N is the number of tubes in the flow. This applies a quite significant correction to $\left(\frac{A_\infty}{A_{en}}\right)$ but the fact that $\left(\frac{A_\infty}{A_{en}}\right)_{max}$ is still slightly in excess of 1.0 indicates that such a correction is necessary.

At $M_\infty = 2.14$ $\left(\frac{A_\infty}{A_{en}}\right)_{max}$ is slightly less than 1.0 although the schlieren photograph Fig.12 shows clearly that under full mass flow condition the shock is attached across the intake plane.

4.2.2 Wedge centre-body intakes

Comparisons between the theoretical and experimental drag results obtained with each wedge, are made in Figs.13 to 16. In general the agreement between the calculated and measured values of $C_{D_{ext}}$ is poor, a fact which must be attributed to the consistently low experimental values of $\left(\frac{A_\infty}{A_{en}}\right)_{max}$ compared with the theoretical values. This can be seen from Figs.13(b) to 16(b).

This tendency to measure low mass flow through the intake (the reverse of what generally happens with pitot type intakes) is probably an effect of wedge tip and side wall bluntness (the Mach number component perpendicular to the swept back edge of the side walls is too low to ensure shock attachment). At the low Reynolds numbers of the tests the boundary layer growth on the wedges and the side walls will also be an important factor.

The effect of the initial wedge thickness can be seen by comparing the theoretical shock wave angles with those measured on the schlieren photographs (greatly enlarged). For the 12° wedge at Mach numbers 1.56 and 1.86 the theoretical shock angles are 57.4° and 45° whereas the measured angles are 59° and 46°. These changes lead to approximately 1% reductions in the corresponding mass flows. For the 16° wedge at $M_\infty = 1.86$ the reduction in mass flow is approximately 4%.

The detached shock on the swept back side walls will undoubtedly force the wedge shock forward (locally on each side of the intake) and will therefore cause a reduction in mass flow and an increase in drag.

(a) Wedge and cowl lip shocks attached

The above conditions apply to:

(i) the 12° wedge at $M_\infty = 1.86$ (Fig.13)

(ii) the 12° and 16° wedges at $M_\infty = 2.14$ (Figs.13 and 14).

Although the agreement between experiment and theory is better with the 12° wedge the experimental drag is quite appreciably greater than the theoretical results in all cases. It will be seen from the schlieren photographs shown in Figs.13 and 14 that the wedge shock angles are greater than their theoretical values (the shock should lie along the swept back edge of the side walls at $M_\infty = 1.86$), also although the cowl lip shock is theoretically attached it is seen to be detached on one side of the 16° wedge at $M_\infty = 2.14$. As has already been mentioned these differences between the theoretical and experimental shock positions will lead to increases in the measured drag over the theoretical values.

(b) Wedge shock attached but cowl lip shock detached

These conditions apply to:

(i) the 12° wedge at $M_\infty = 1.56$ (Fig.13)

(ii) the 16° and 20° wedges at $M_\infty = 1.86$ (Figs.14 and 15)

(iii) the 20° and 24° wedges at $M_\infty = 2.14$ (Figs.15 and 16).

The intake drag under these conditions is calculated in precisely the same way as for case (a), i.e. the presence of the detached shock at the cowl lip is ignored as it was expected that this would cause only a small increase in drag. Again the agreement between theory and experiment is generally poor. Good agreement is obtained only with the 12° wedge at $M_\infty = 1.56$. However, the agreement is no worse than occurred in (a) the experimental drag is greater than the estimated drag and it would appear that if the correct mass flow had been obtained the agreement would have been much more reasonable.

(c) Wedge shock detached

This condition applies to

(i) the 16°, 20° and 24° wedges at $M_\infty = 1.56$ (Figs.14, 15 and 16)
(ii) the 24° wedge at $M_\infty = 1.86$ (Fig.16).

Already it has been mentioned that under these conditions the drag is calculated assuming that the intake is operating as a spilling pitot intake and that the detached shock is normal to the free-stream direction. Quite good agreement between experiment and theory for the 24° wedge at $M_\infty = 1.86$ was obtained but for the remaining three cases large discrepancies occur.

The good agreement obtained with the 24° wedge is fortuitous because (as the schlieren photograph shows) the wedge shock is not detached. When the flow pattern does approximate to that about a spilling pitot intake we note;

(1) The mass flow is considerably less than the theoretical choking mass flow and in the absence of pitot measurements in the entry plane no adequate explanation can be given for this.

(2) The calculation of the drag of a spilling pitot for this choking mass flow ratio by the Fraenkel method[5] does in any case overestimate the drag (see Fig.17(a)). Thus it is probably better to apply a method similar to the one suggested by Seddon in Ref.8.

On the basis of work described in Ref.4 it has been suggested that the detached shock is of a hyperbolic form. If we assume that the location of the shock wave upstream of the wedge tip is the same for the intake as for an isolated wedge, the drag can be determined by finding the static pressure rise across a curved shock instead of a normal shock. The schlieren photographs indicate that this would appear to be a more correct procedure but it was found to make only a very small improvement to the agreement between calculations and measurements.

4.3 Drag and pressure recovery under spillage conditions

Figs.17 to 21 show both the variation of external drag and pressure recovery with mass flow for each particular intake. The pressure recovery results obtained with the wedges are included only for completeness. The wedges were designed primarily for the drag tests and their pressure recoveries cannot be regarded as typical.

4.3.1 Comparison between theoretical and experimental drag rise with spillage

(a) Pitot intakes

The variations of drag for the pitot intakes under spillage conditions at each Mach number is shown in Fig. 17(a), (b) and (c). The agreement with the theory is fairly good which again indicates that the influence of "end effects" is probably small.

(b) Wedge centre-body intakes

The method of predicting the external intake drag with spillage suggested for conical centre-body intakes in Ref.2 has been used here for the wedge centre-body intakes when the wedge shock is attached. For the detached wedge shock conditions the increase in drag is obtained by again assuming that the intake operates as a spilling pitot.

When the wedge shock is attached the agreement between the theory and the experimental results is fairly good as can be seen from Figs.18, 20(b) and (c), and 21(c). However Figs.19(a), 20(a) and 21(a) and (b) show that when the wedge shock is detached treating the intake as a spilling pitot results in approximately 25% overestimation of the drag. Again in the calculation of this spilling pitot drag it has been assumed that the detached shock is normal to the free-stream direction. This assumption was made partly for simplicity and partly because taking a hyperbolic shape again failed to give much improvement.

4.3.2. Pressure recovery

(a) Pitot intakes

Fig. 17(a), (b) and (c) show that the pressure recovery obtained at each Mach number is only slightly less than the normal shock pressure recovery.

(b) Wedge centre-body intakes

As mentioned in Section 4.1 the wedges were not designed to give good pressure recovery and as can be seen from Figs.18 to 21 the sudden expansion and "corner" effects lead in each case to pressure recoveries far below the theoretical shock values.

5 CONCLUSIONS

(1) With the centre-body removed the experimental drag and pressure recovery are in quite good agreement (under both full mass flow and spillage conditions) with the theoretical results for pitot intakes.

This result, obtained with a model of almost square cross section, indicates that the influence of "end" effects is fairly small.

(2) The spillage drag of a two-dimensional wedge centre-body intake can be estimated reasonably well by adapting the method proposed in Ref.2 for conical centre-body intakes.

(3) Treating a two dimensional wedge centre-body intake as a spilling pitot when the wedge shock is detached overestimates the drag by some 25%.

(4) Two possible reasons (apart from the low Reynolds number of the tests) can account for the low maximum mass flow values through the wedge centre body intakes: First the components of the free-stream Mach number perpendicular to the edge of the swept back side walls is always too low to ensure an attached shock and secondly the wedge tip bluntness can account for a small but significant forward displacement of the wedge shock.

Appendix A

THE CALCULATION OF $\left(\frac{A_\infty}{A_{en}}\right)_{max}$ AND $C_{D_{cowl_o}}$ FOR TWO DIMENSIONAL WEDGE CENTRE-BODY INTAKES WITH STRAIGHT LINE PROFILES

From Fig.2

$$L_N - \ell = \frac{h_\infty}{\tan \theta_\omega}$$

and

$$\ell = \frac{h_{en} - h_\infty}{\tan \delta}$$

Hence

$$L_N - \left(\frac{h_{en} - h_\infty}{\tan \delta}\right) = \frac{h_\infty}{\tan \theta_\omega}$$

or

$$h_\infty = \frac{(L_N \tan \delta - h_{en}) \dfrac{\tan \theta_\omega}{\tan \delta}}{1 - \dfrac{\tan \theta_\omega}{\tan \delta}}$$

and

$$\frac{h_\infty}{h_{en}} = \frac{\left(\dfrac{L_N}{h_{en}} \tan \delta - 1\right) \tan \theta_\omega}{\tan \delta - \tan \theta_\omega}$$

when the wedge shock impinges on the cowl lip:-

$$\frac{L_N}{h_{en}} = \cot \theta_\ell$$

and under these conditions the entering mass flow reaches its maximum value, hence

$$\left(\frac{A_\infty}{A_{en}}\right)_{max} = \left(\frac{h_\infty}{h_{en}}\right)_{max} = \frac{\cot \theta_\ell - \cot \delta}{\cot \theta_\omega - \cot \delta}$$

The pre-entry drag (based on A_{en}) in this full mass flow condition is defined as

$$C_{D_{pre_o}} = \frac{\left(\frac{p_1}{p_\infty} - 1\right)(h_{en} - h_\infty)}{\frac{q_\infty}{p_\infty} h_{en}}$$

$$= \frac{\left(\frac{p_1}{p_\infty} - 1\right)\left(\frac{\cot \theta_\omega - \cot \theta_\ell}{\cot \theta_\omega - \cot \delta}\right)}{\frac{q_\infty}{p_\infty}}$$

Appendix B

THE CALCULATION OF $C_{D_{cowl_o}}$ FOR TWO DIMENSIONAL WEDGE CENTRE-BODY INTAKES WITH ELLIPTICAL COWL PROFILES

Assume that the profile shape is given by

$$x^2 + ah^2 + bx + ch + d = 0 \quad . \tag{B7}$$

Using the notation given in the diagram below and the following boundary conditions:

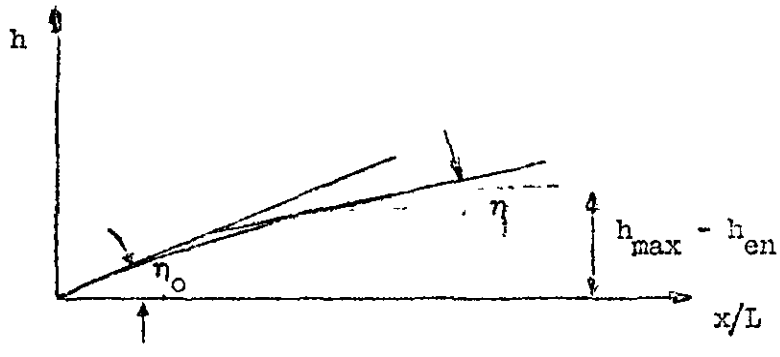

$x = 0, \qquad h = 0$

$x = L, \qquad h = h_{max} - h_{en}$

$\frac{dh}{dx} = \tan \eta_o$ when $x = 0$, and $h = 0$

$\frac{dh}{dx} = 0$ when $x = L$, and $h = h_{max} - h_{en}$

Equation (B7) can be rewritten as

$$x^2 + \frac{L^2 \tan \eta_o - 2L(h_{max} - h_{en})}{(h_{max} - h_{en})^2 \tan \eta_o} h^2 - 2Lx + \frac{2Lh}{\tan \eta_o} = 0 \quad .$$

Hence the ordinates and the tangents to the curve at each one may be obtained from

$$h = \frac{\pm\left(\frac{h_{max}-h_{en}}{L}\right)^2 \pm (h_{max}-h_{en}) \times \sqrt{\left[\frac{(h_{max}-h_{en})^2}{L^2} - \left\{\tan \eta_o - 2\frac{(h_{max}-h_{en})}{L}\right\}\left\{\frac{x}{L}\tan \eta_o \left(\frac{x}{L} - 2\right)\right\}\right]}}{\left\{\tan \eta_o - 2\frac{(h_{max} - h_{en})}{L}\right\}}$$

and

$$\frac{dh}{dx/L} = \frac{\left(1 - \frac{x}{L}\right)}{\left\{\frac{L \tan \eta_o - 2(h_{max} - h_{en})}{(h_{max} - h_{en})^2 \tan \eta_o}\right\} h + \frac{1}{\tan \eta_o}}$$

knowing the ordinates and tangents at arbitrarily chosen points the Prandtl-Meyer expansion theory can be used to obtain a series of pressure coefficients along the cowl profile. These can then be integrated graphically to give $C_{D_{cowl_o}}$.

NOTATION (See also Fig.2)

A	cross-sectional area
h	ordinate measured from and perpendicular to intake axis
x	distance measured from cowl lip parallel to intake axis
L	length of cowl, i.e. distance between entry and maximum cowl cross-sectional areas
L_n	distance between wedge tip and entry plane
δ	semi-apex angle of wedge centre-body
θ	inclination with respect to the intake axis of a line through the tip of the wedge
η_o	initial inclination of the outside surface of the cowl
η_i	initial inclination of the inside surface of the cowl
P	total pressure
p	static pressure
q	dynamic pressure $\frac{1}{2} \rho v^2$
M	Mach number
$M_{\omega \ell}$	free stream Mach number at which the wedge or cone shock falls on the cowl lip
$C_{D_{cowl_o}}$	cowl wave drag coefficient at full mass flow (based on A_{max})
$C_{D_{pre_o}}$	pre-entry drag coefficient at full mass flow (based on A_{en} for Fig.4
$C_{D_{ext_o}}$	total external drag coefficient at full mass flow (based on A_{max})
$C_{D_{ext}}$	total external drag coefficient at any mass flow (based on A_{max})
$(\ )_\infty$	free-stream
$(\ )_{en}$	in the entry plane
$(\ )_{ex}$	in the exit plane
$(\ )_\omega$	immediately behind the wedge shock
$(\ )_\ell$	immediately ahead of the cowl lip

REFERENCES

No.	Author	Title, etc.
1	E. L. Goldsmith	A review of supersonic air intakes. R.A.E. Tech. Note Aero 2429, (A.R.C. 18878) November 1955
2	E. L. Goldsmith C. F. Griggs	The estimation of pressure recovery and drag of conical centre-body intakes at supersonic speeds. (A.R.C. R.& M. 3035), May 1952
3	E. L. Goldsmith C. F. Griggs	A comparison of the estimated and measured performance of conical centre-body intakes at Mach numbers from 2.14 to 3.27. (A.R.C. R.& M. 3035), November 1953
4	W. E. Moeckel	Approximate method for predicting form and location of detached shock waves ahead of plane or axially symmetric bodies. NACA Tech. Note 1921, July 1949
5	L. E. Fraenkel	The external drag of some pitot type intakes at supersonic speeds. Part I R.A.E. Report Aero 2380, (A.R.C. 13537), June 1950
6	E. Lapin	Charts for the computation of lift and drag of finite wings at supersonic speeds. Douglas Report No. SM-13480, (P32182)
7	W. F. Cope	The turbulent boundary layer in compressible flow. (A.R.C. R.& M. 2840), November 1943
8	J. Seddon	Note on the spillage drag of pitot type air intakes at transonic speeds. R.A.E. Tech. Note Aero 2315, (A.R.C. 17380), August 1954

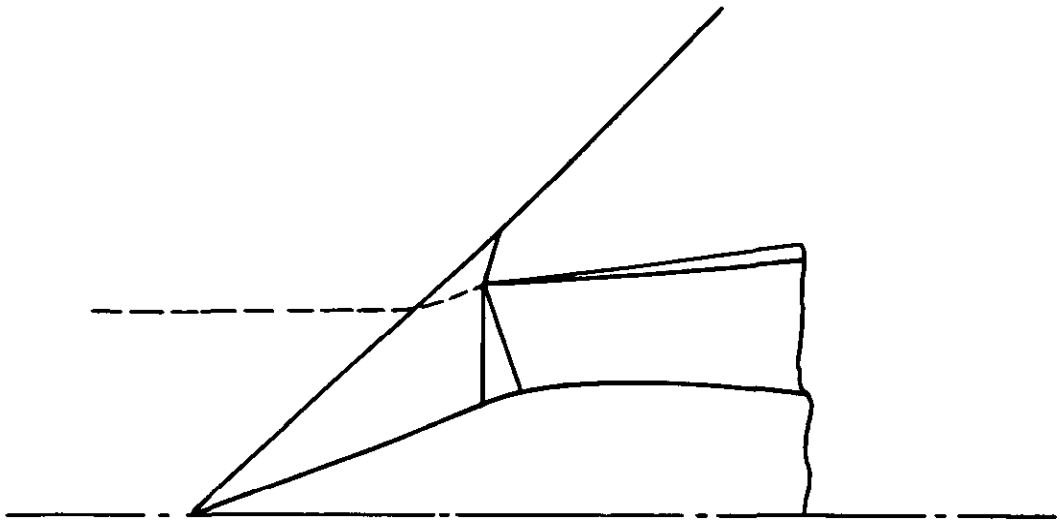

FIG. 1(a) ALL SHOCKS ATTACHED

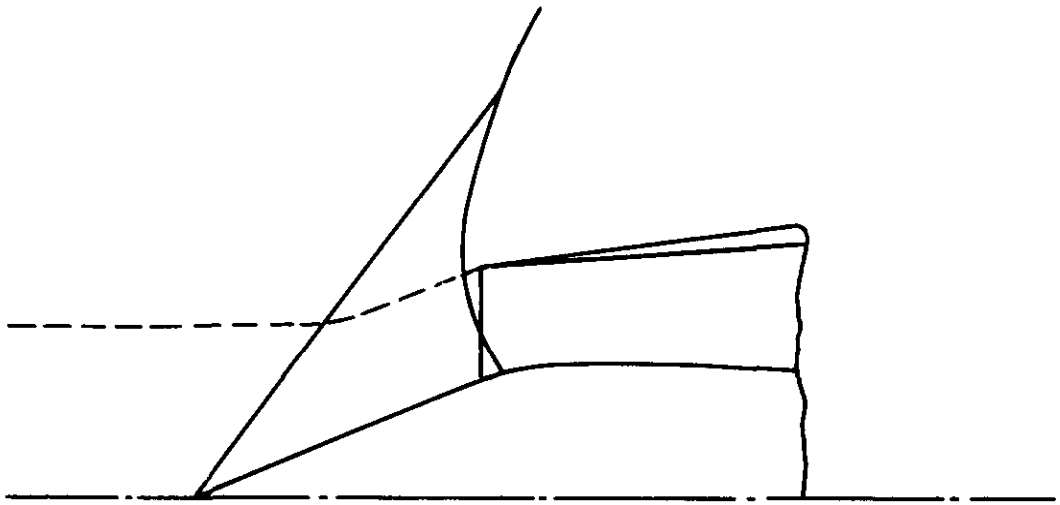

FIG. 1(b) COWL LIP SHOCK DETACHED

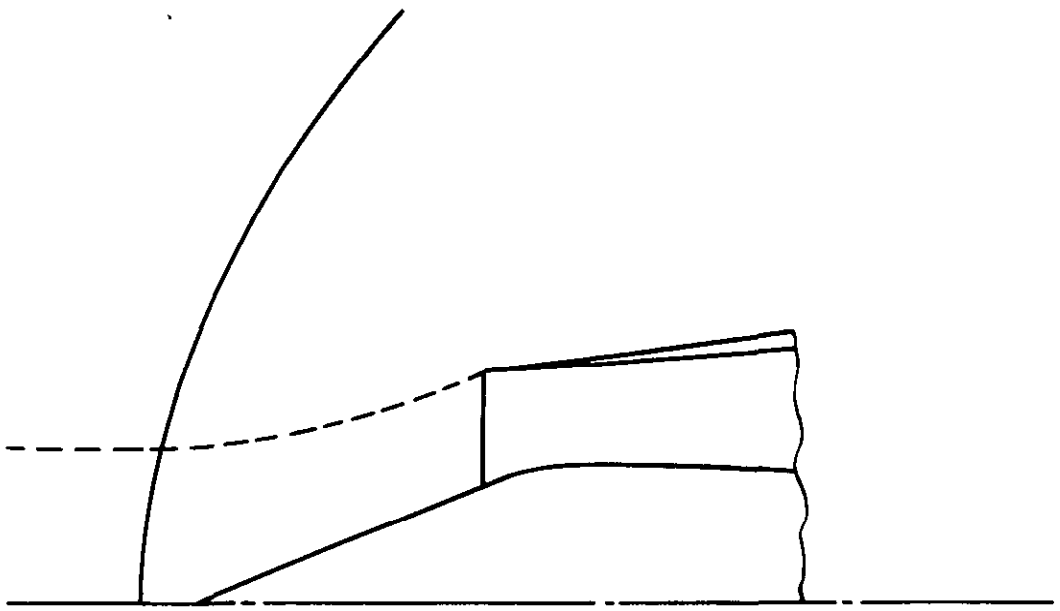

FIG. 1(c) CENTREBODY SHOCK WAVE DETACHED

FIG. 1 FLOW PATTERNS ABOUT A CENTRE BODY INTAKE

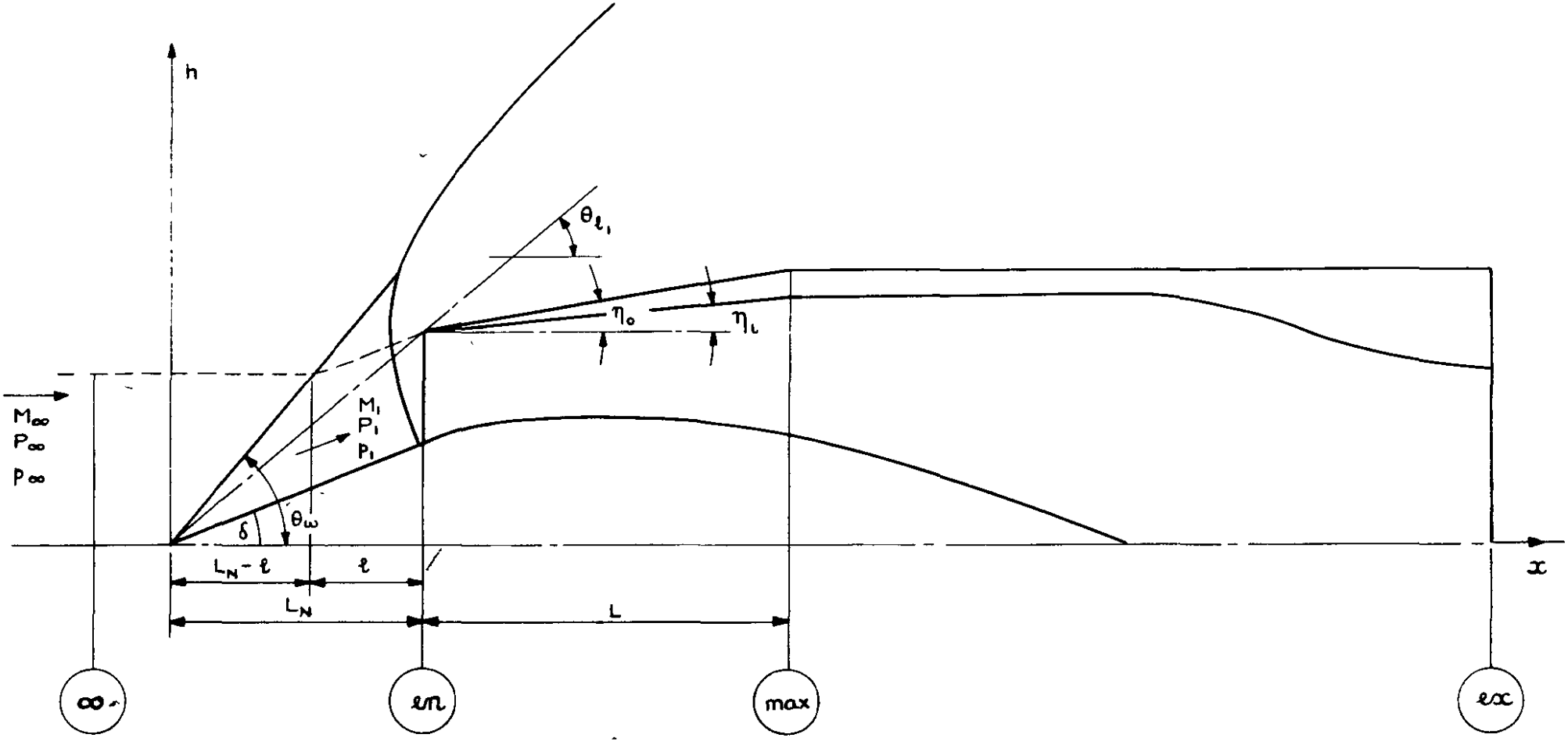

FIG. 2 NOTATION

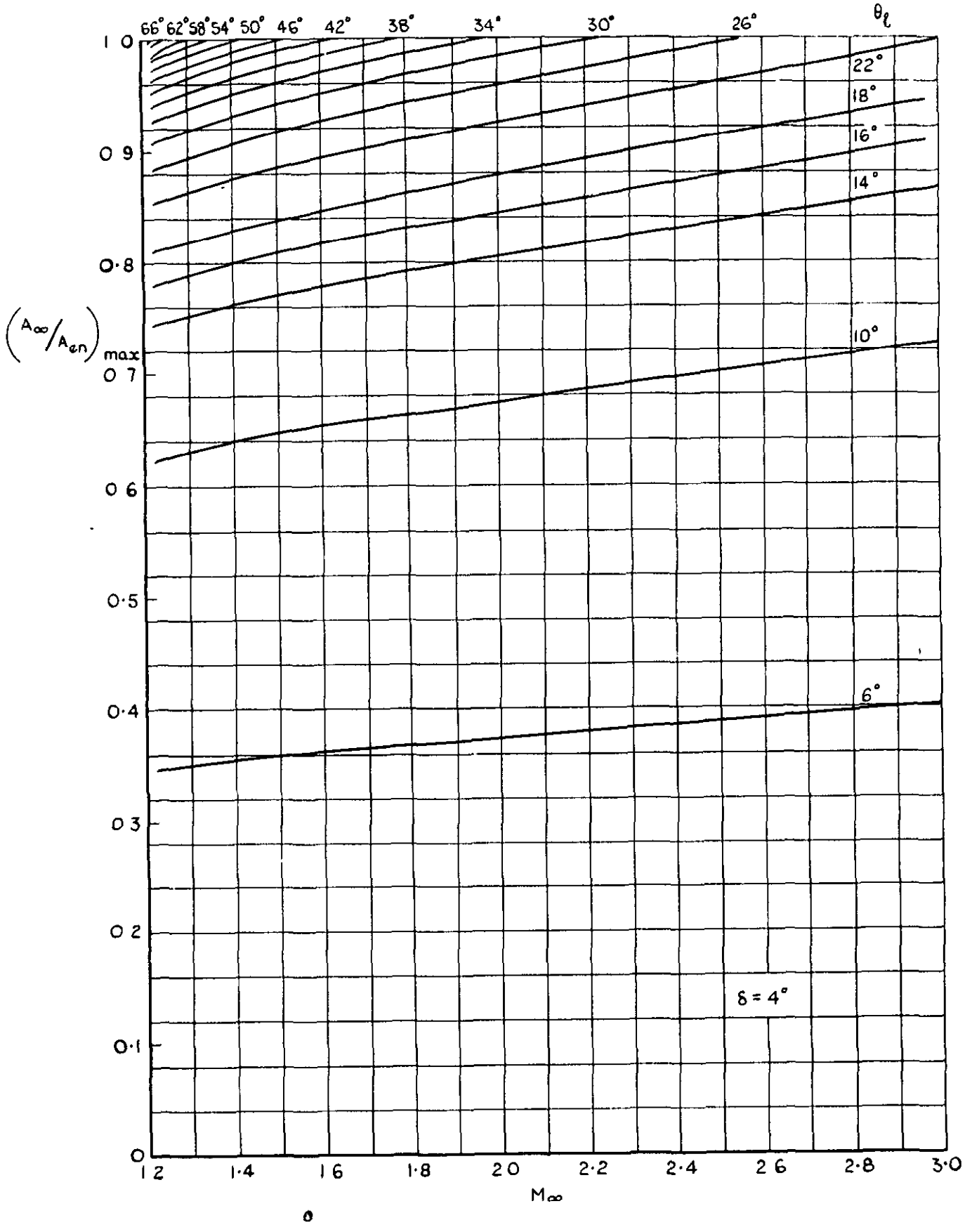

FIG. 3 VARIATION WITH MACH No. OF $\left(\frac{A_\infty}{A_{en}}\right)_{max}$ FOR $\delta = 4^\circ$

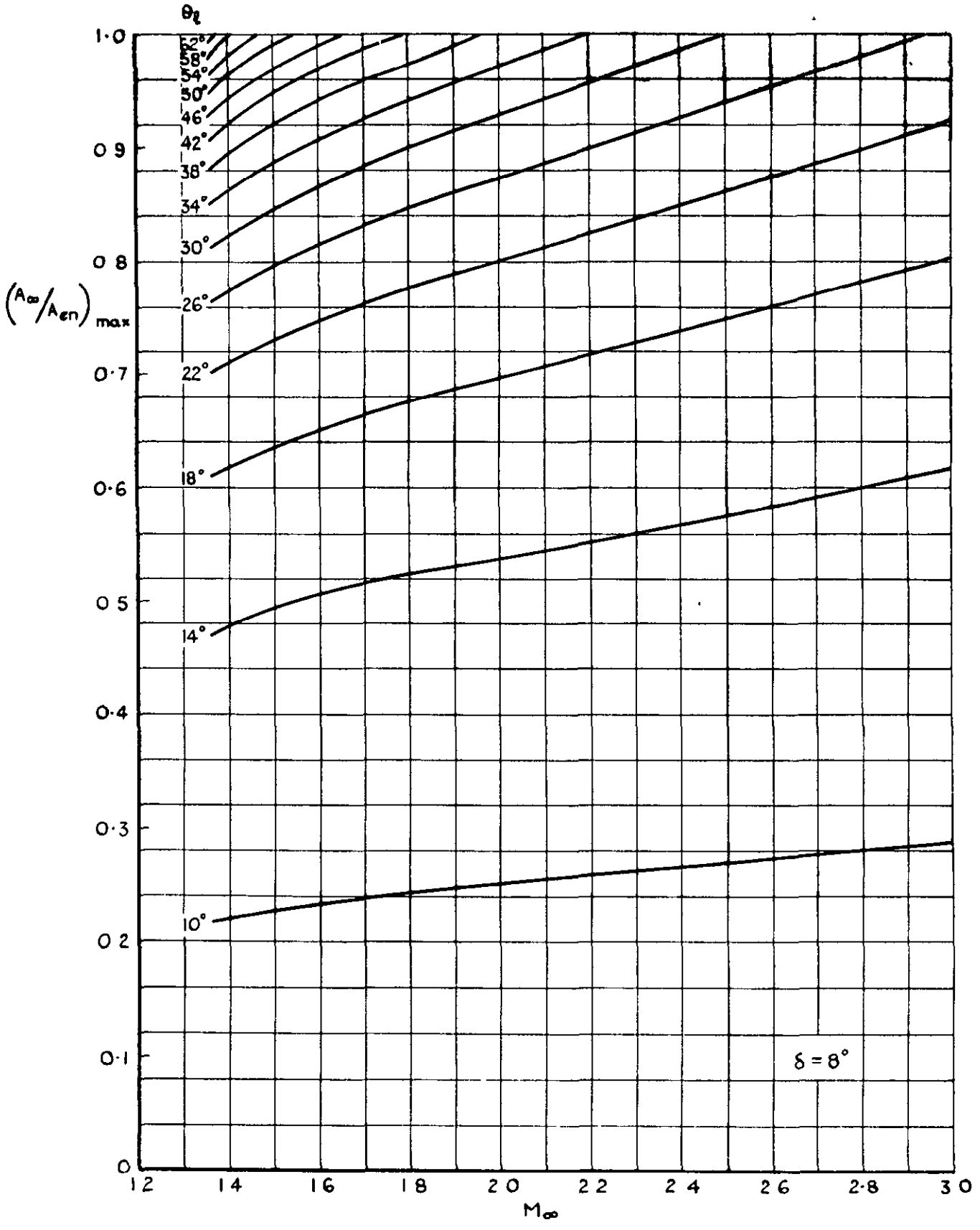

FIG. 3 (CONT'D) VARIATION WITH MACH No. OF $\left(\frac{A_\infty}{A_{en}}\right)_{max}$ FOR $\delta = 8^\circ$

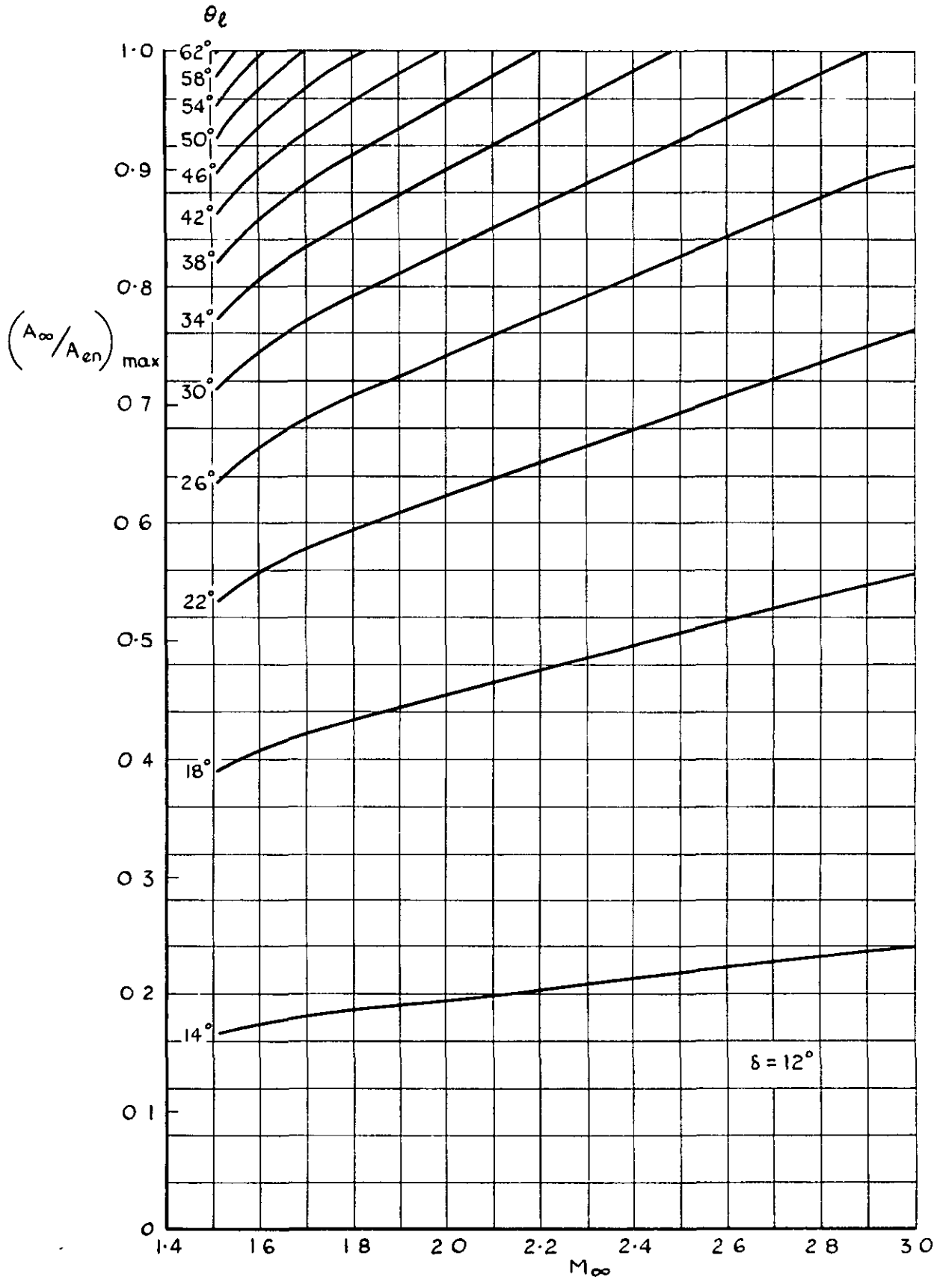

FIG. 3 (CONT'D) VARIATION WITH MACH No OF $\left(\frac{A_\infty}{A_{en}}\right)_{max}$ FOR $\delta = 12°$

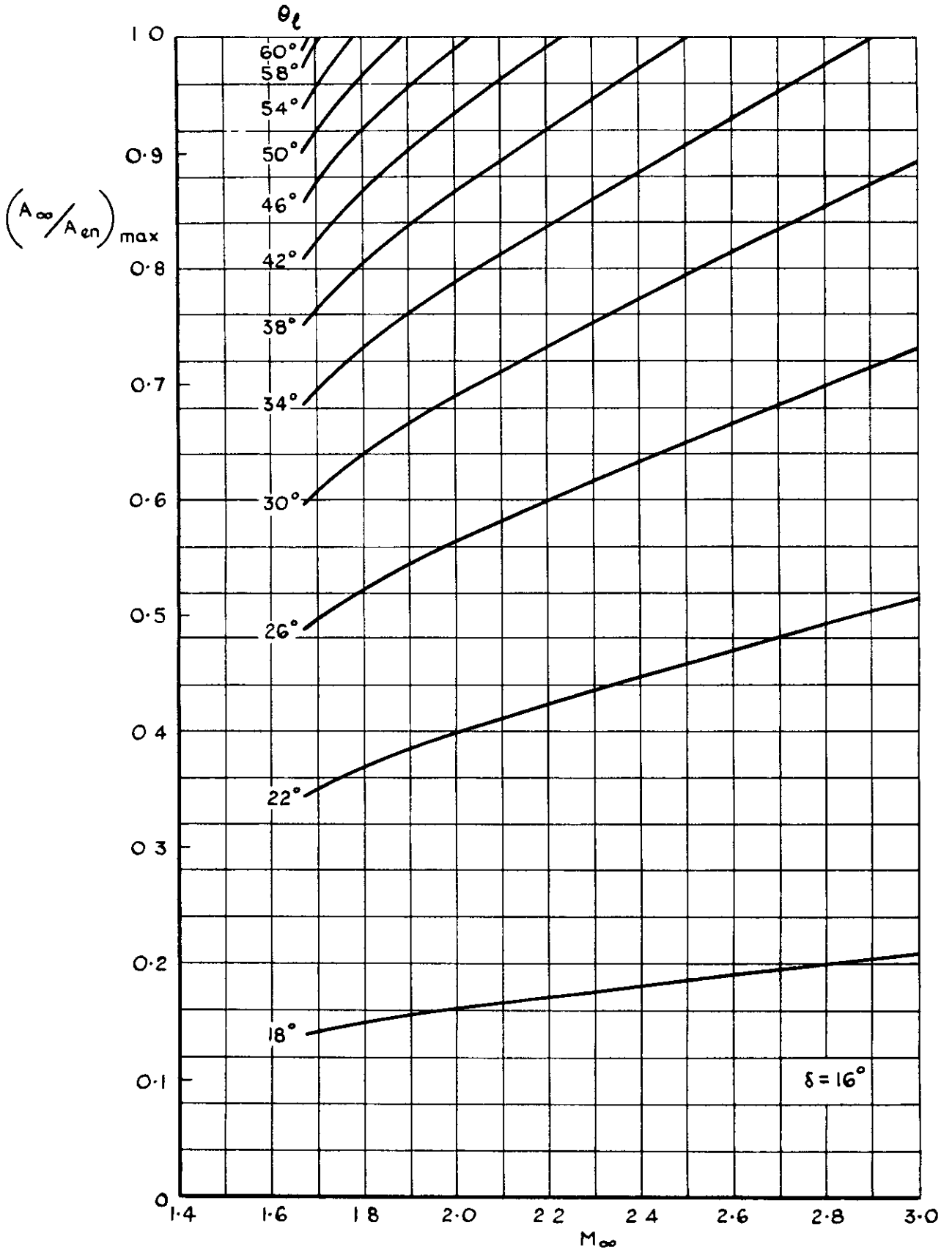

FIG. 3 (CONT'D) VARIATION WITH MACH No. OF $\left(\frac{A_\infty}{A_{en}}\right)_{max}$ FOR $\delta = 16°$

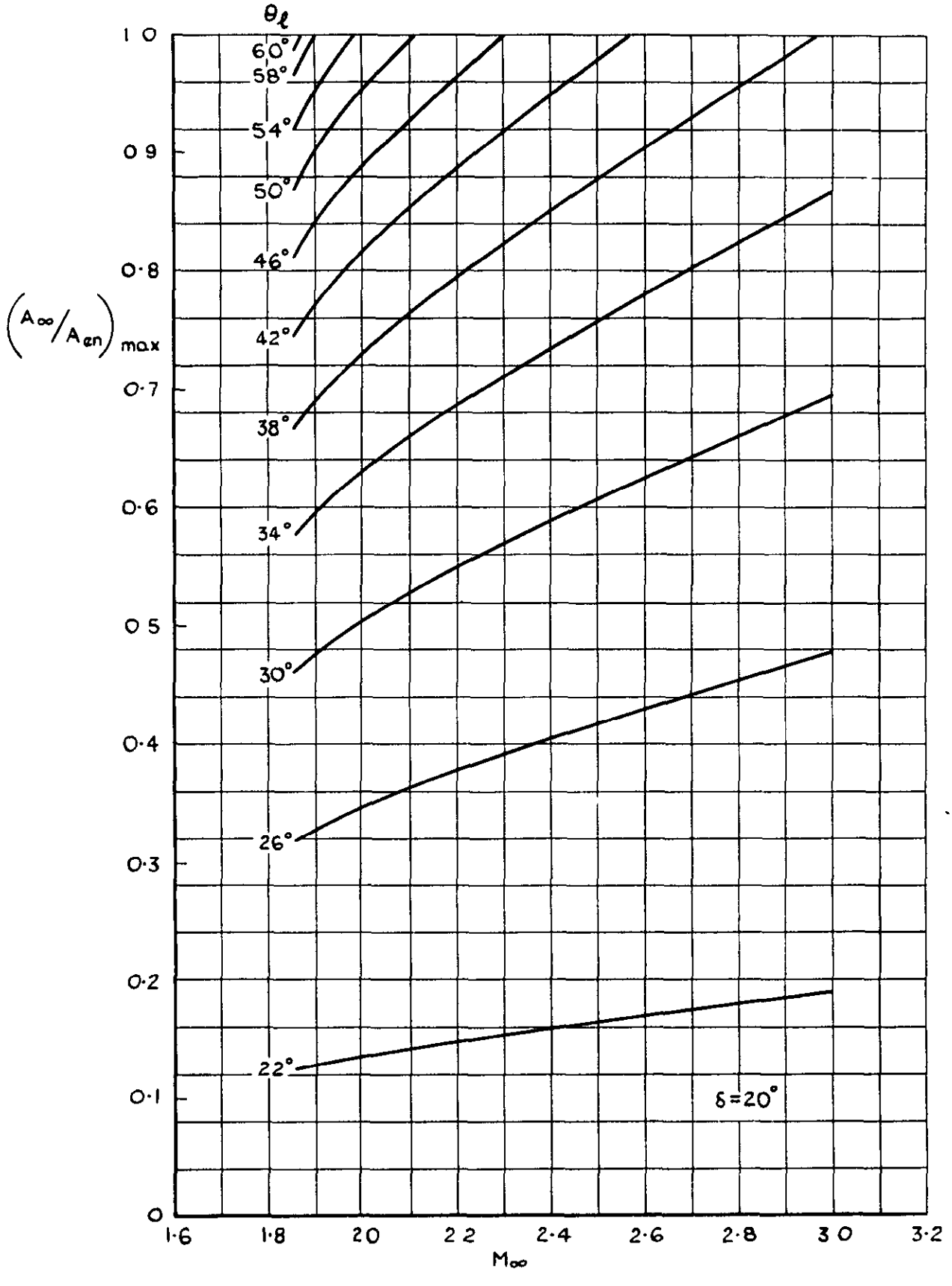

FIG. 3 (CONT'D) VARIATION WITH MACH No. OF $\left(\frac{A_\infty}{A_{en}}\right)_{max}$ FOR $\delta=20°$

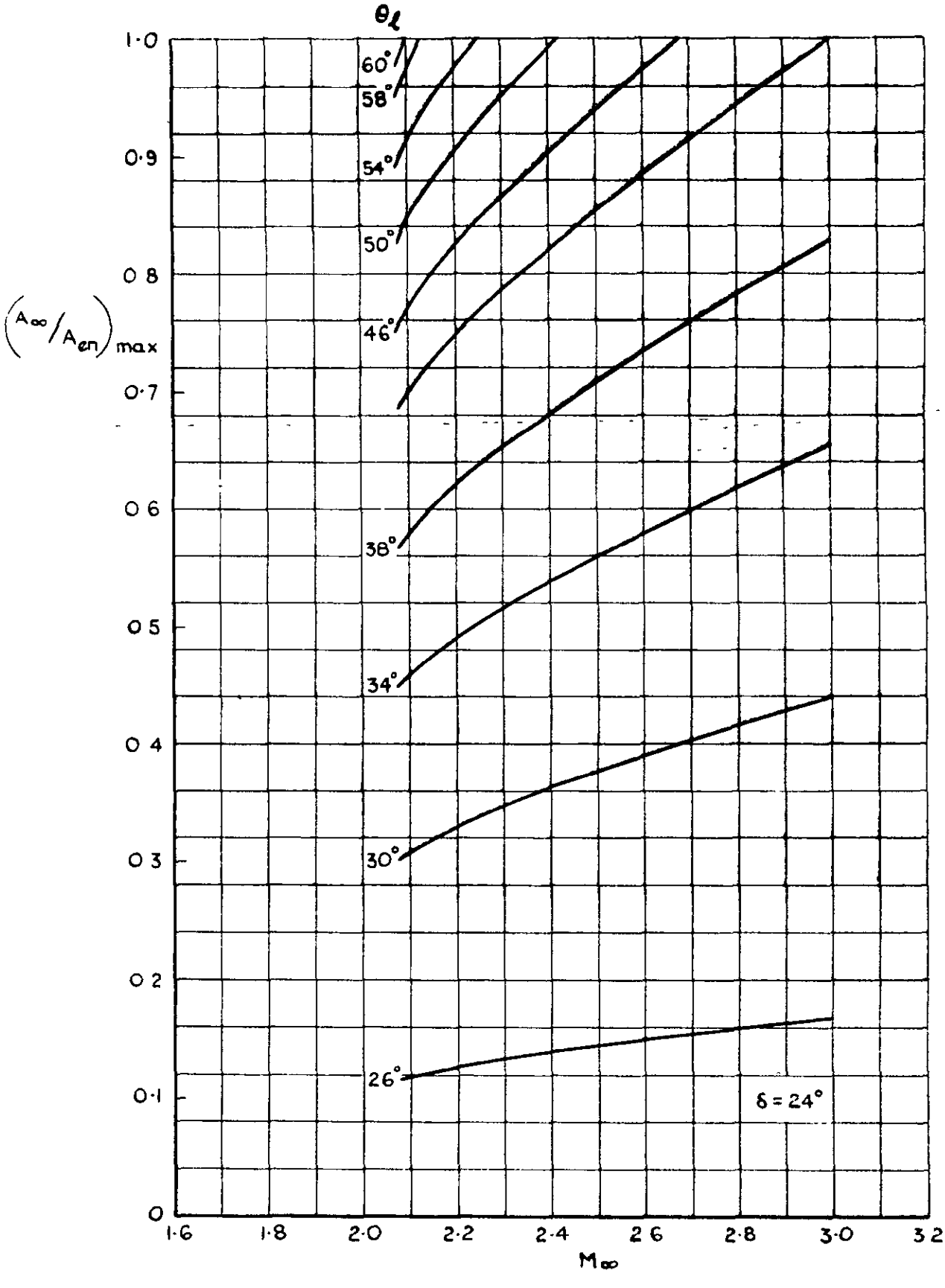

FIG. 3 (CONCL'D) VARIATION WITH MACH No. OF $\left(\frac{A\infty}{Aen}\right)_{max}$ FOR $\delta = 24^\circ$

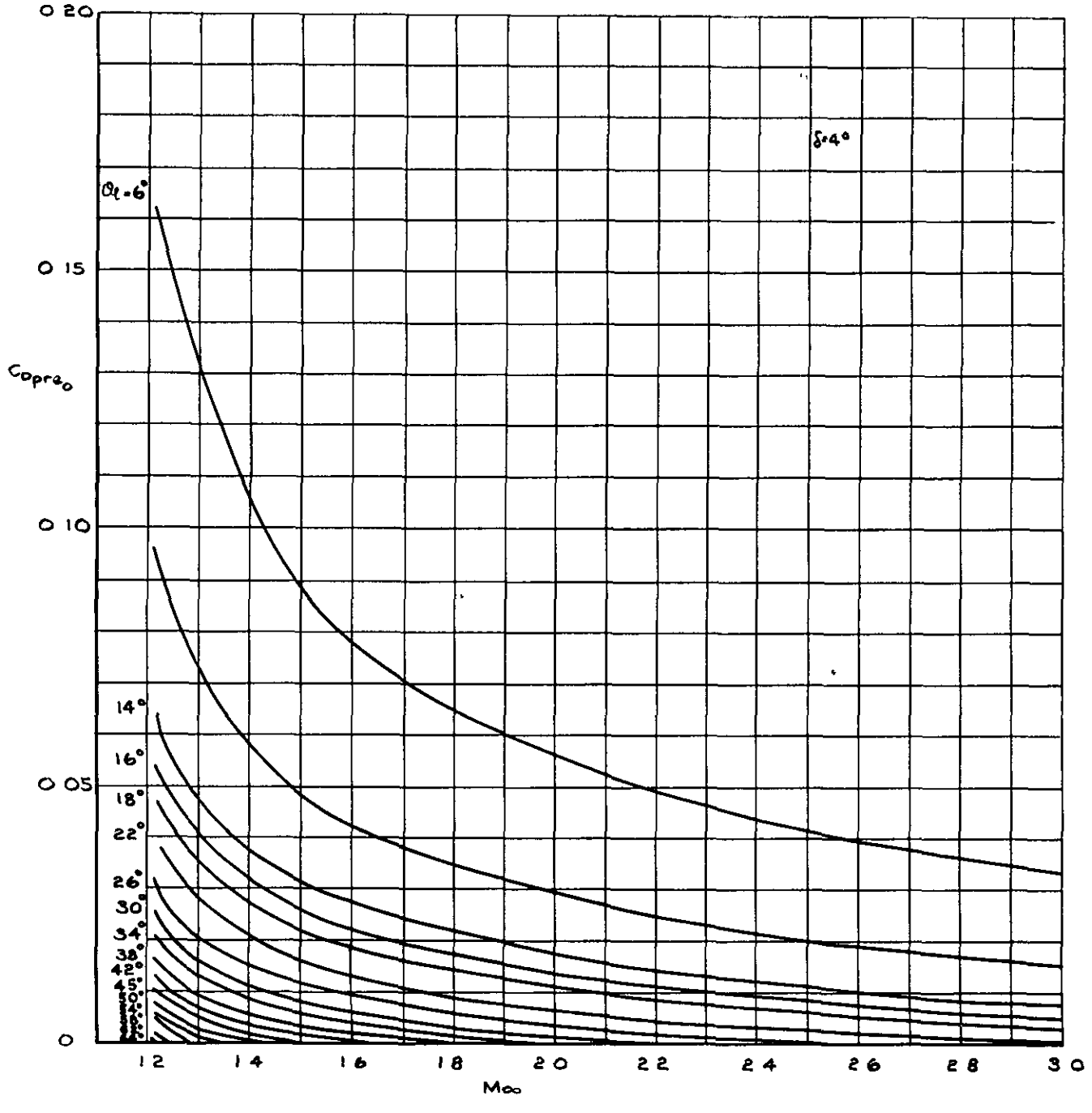

FIG.4 VARIATION WITH MACH No. OF $C_{D_{pre_0}}$ FOR $\delta = 4^\circ$

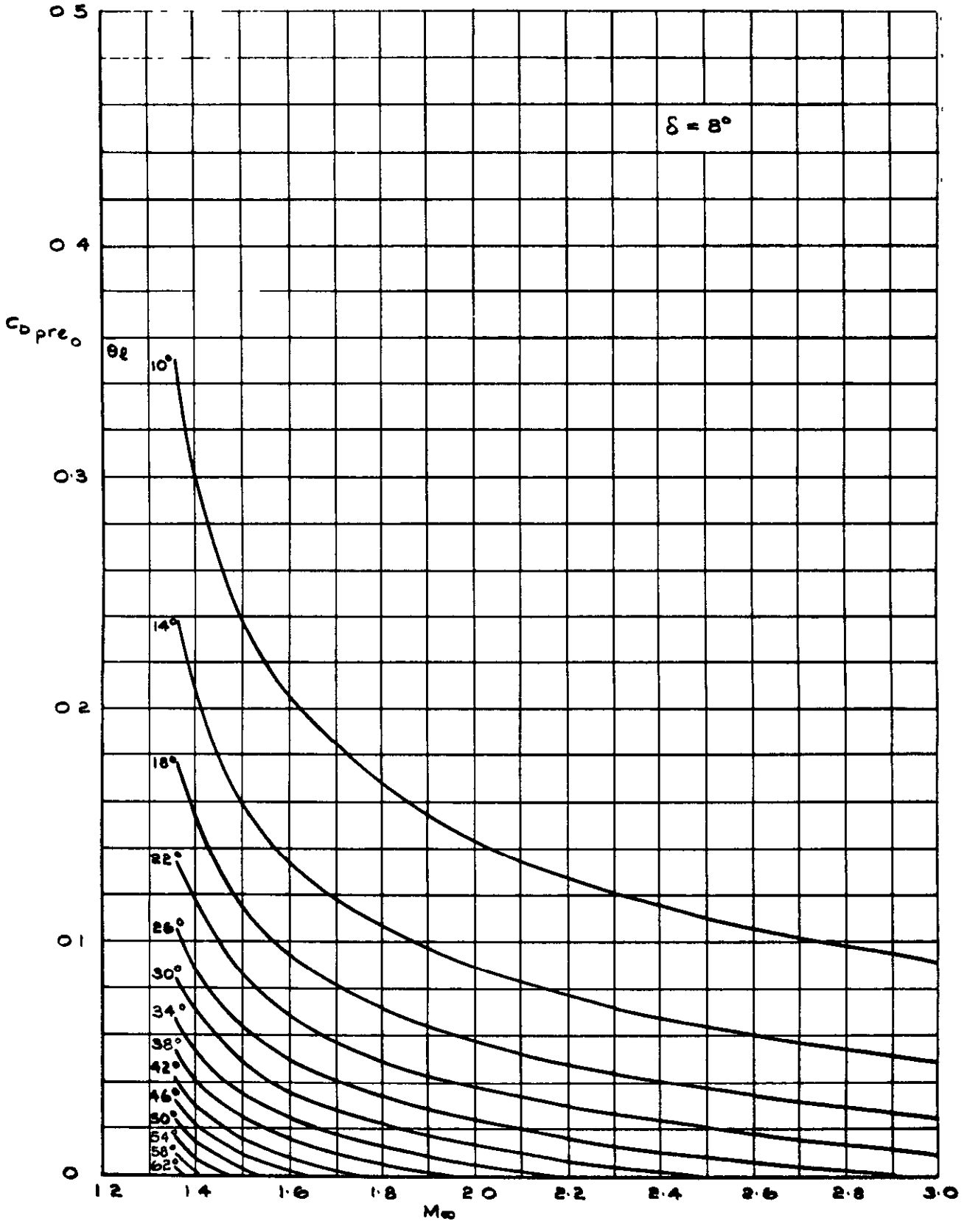

FIG.4. (CONT'D) VARIATION WITH MACH No. OF $C_{D_{cowl_o}}$ FOR $\delta = 8°$

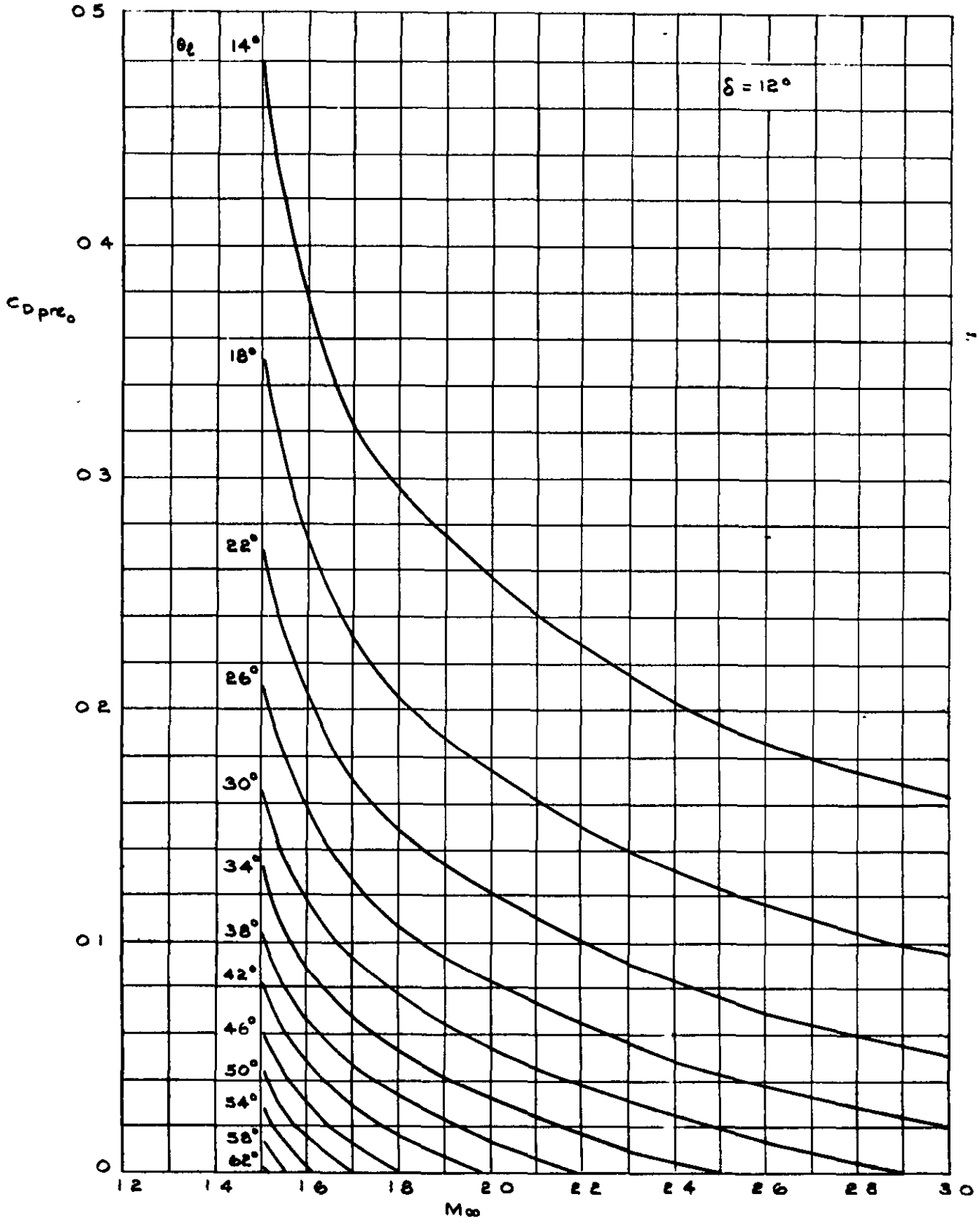

FIG 4 (CONT'D) VARIATION WITH MACH No. OF $C_{D_{pre_o}}$ FOR $\delta = 12°$

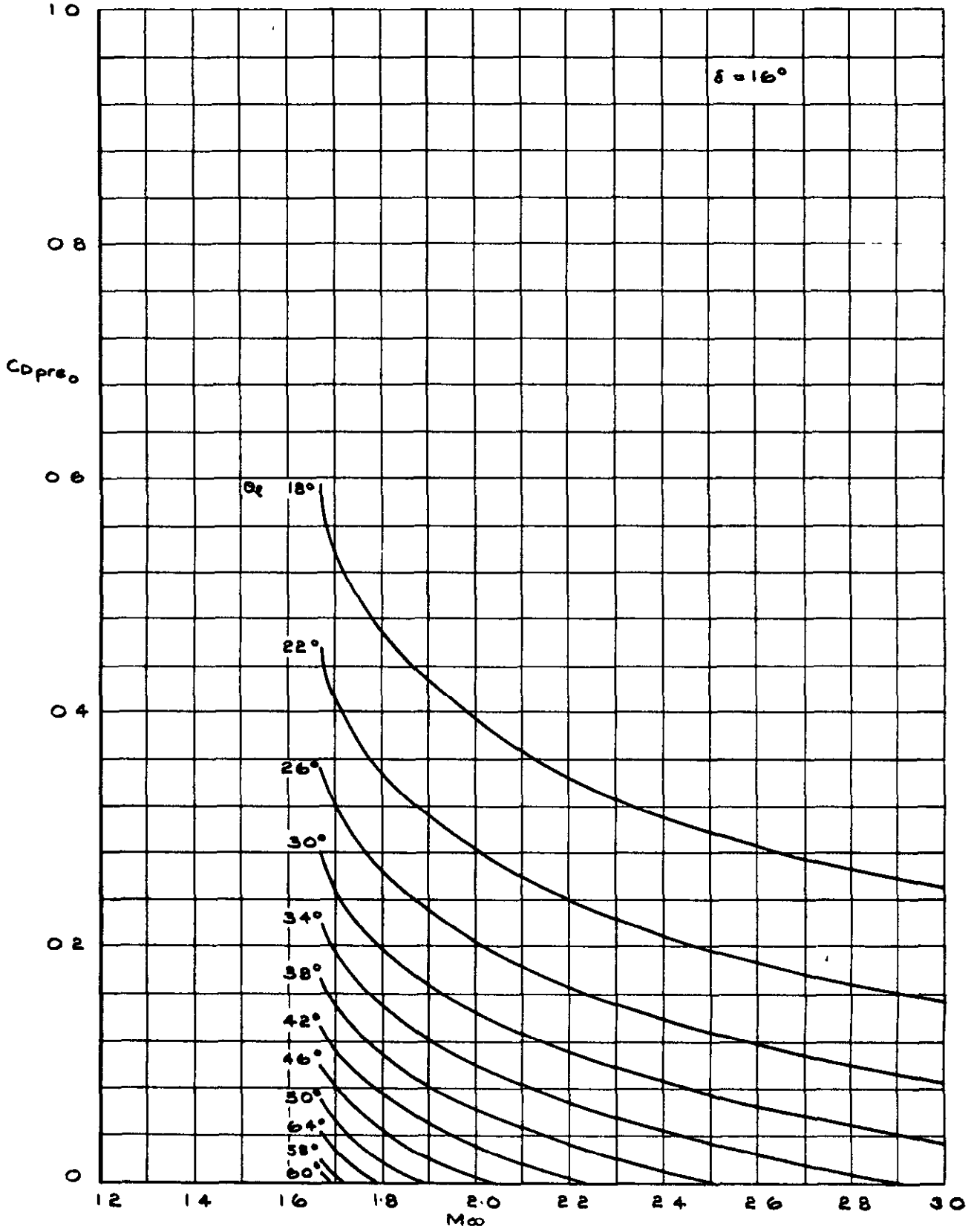

FIG. 4. (CONT'D) VARIATION WITH MACH No. OF $C_{D_{pre_o}}$ FOR $\delta = 16°$

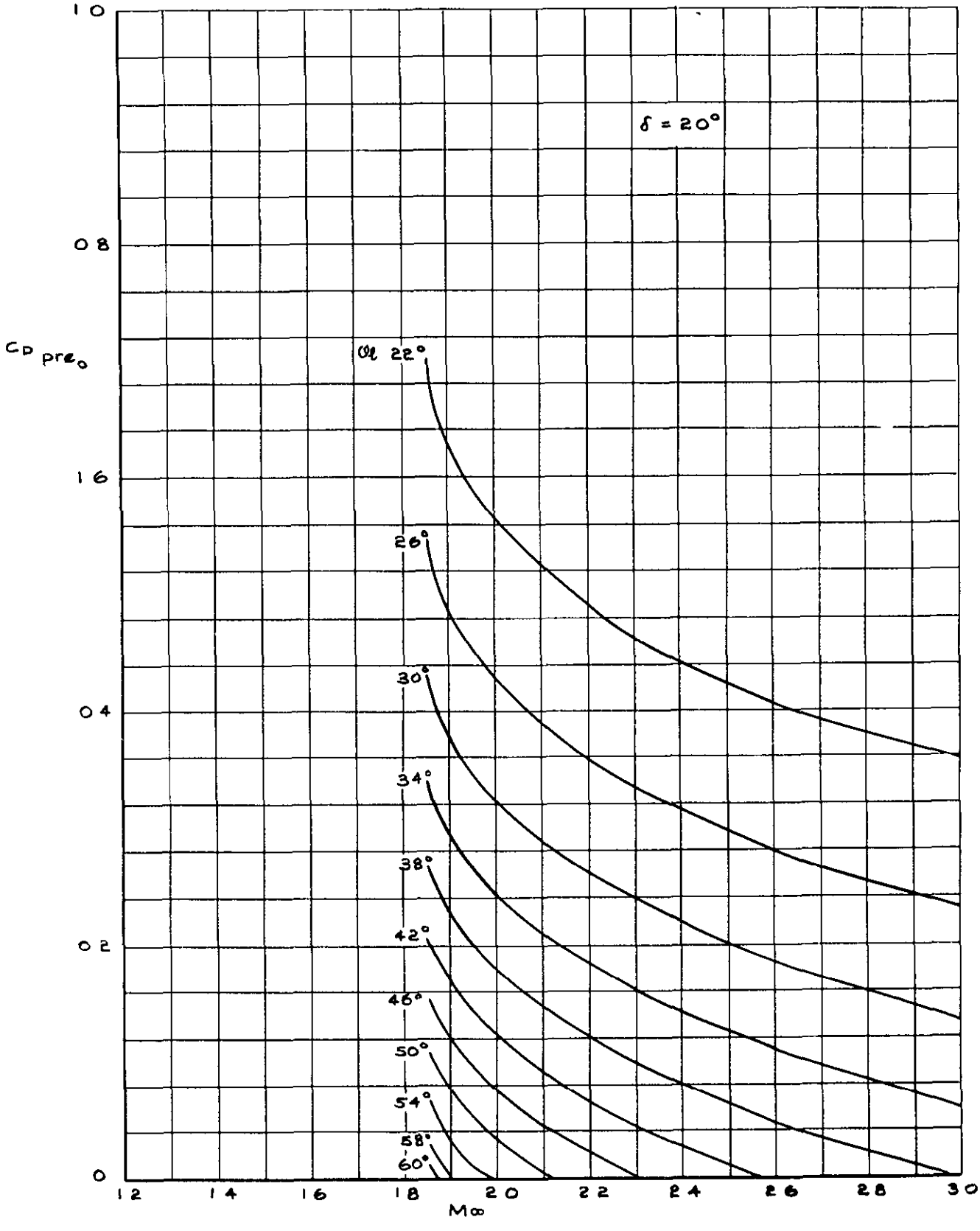

FIG. 4. CONT'D VARIATION WITH MACH No. OF $C_{D_{pre_o}}$ FOR $\delta = 20°$

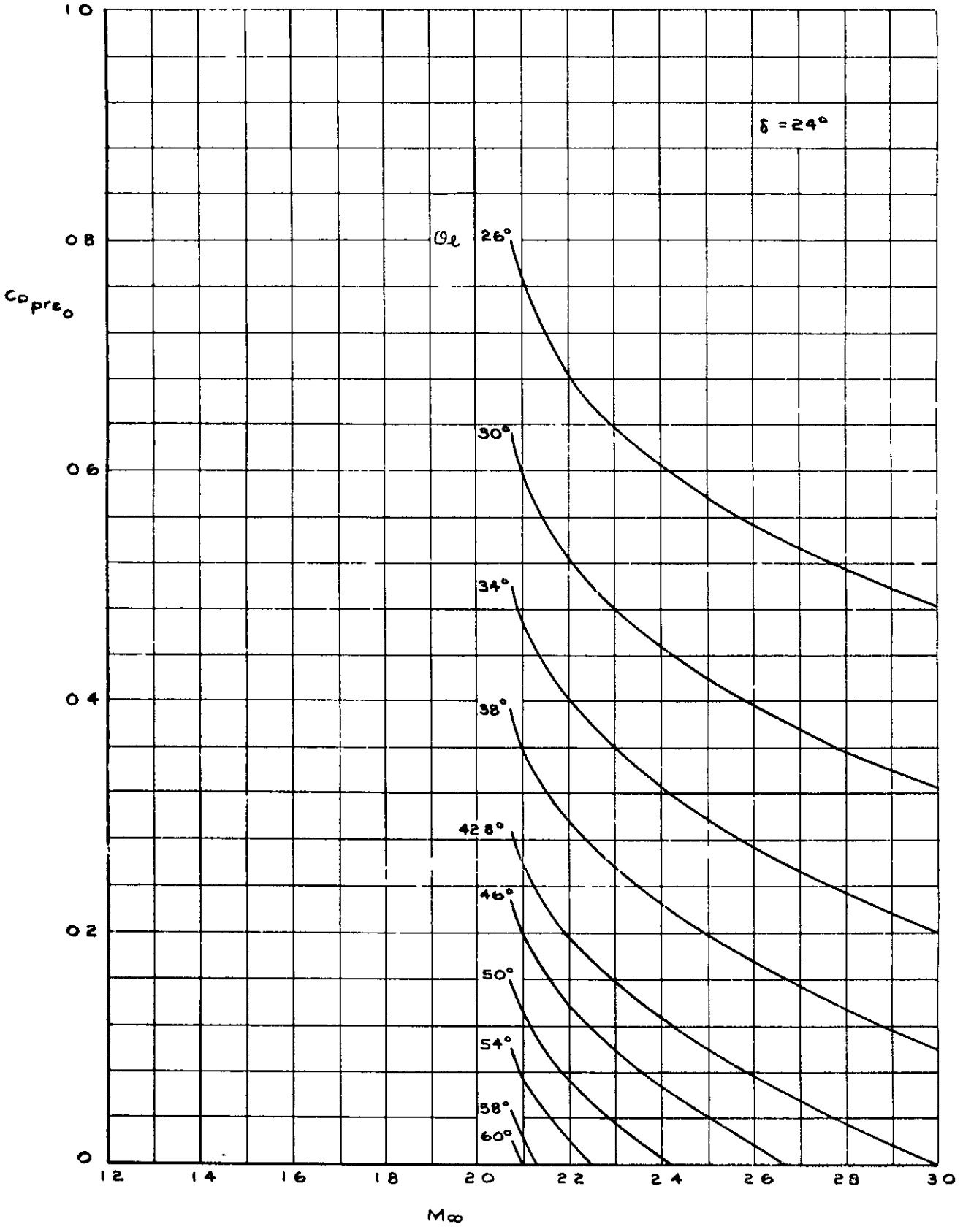

FIG 4.(CONCL'D)VARIATION WITH MACH No.OF $C_{D_{pre_o}}$ FOR $\delta=24°$

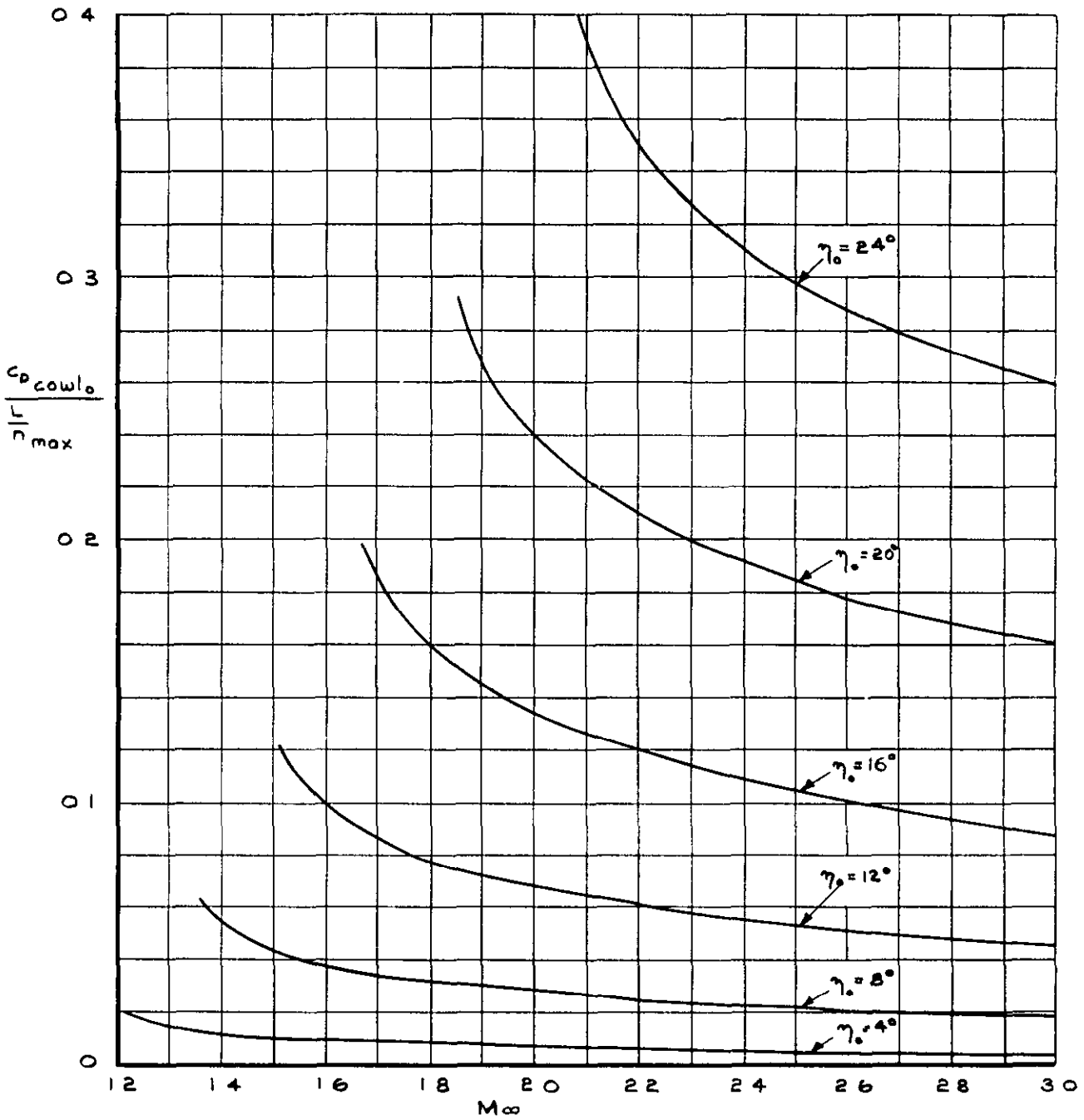

FIG.5. VARIATION OF COWL DRAG WITH MACH. NUMBER FOR STRAIGHT LINE COWL PROFILES-PRE-ENTRY FLOW NEGLECTED

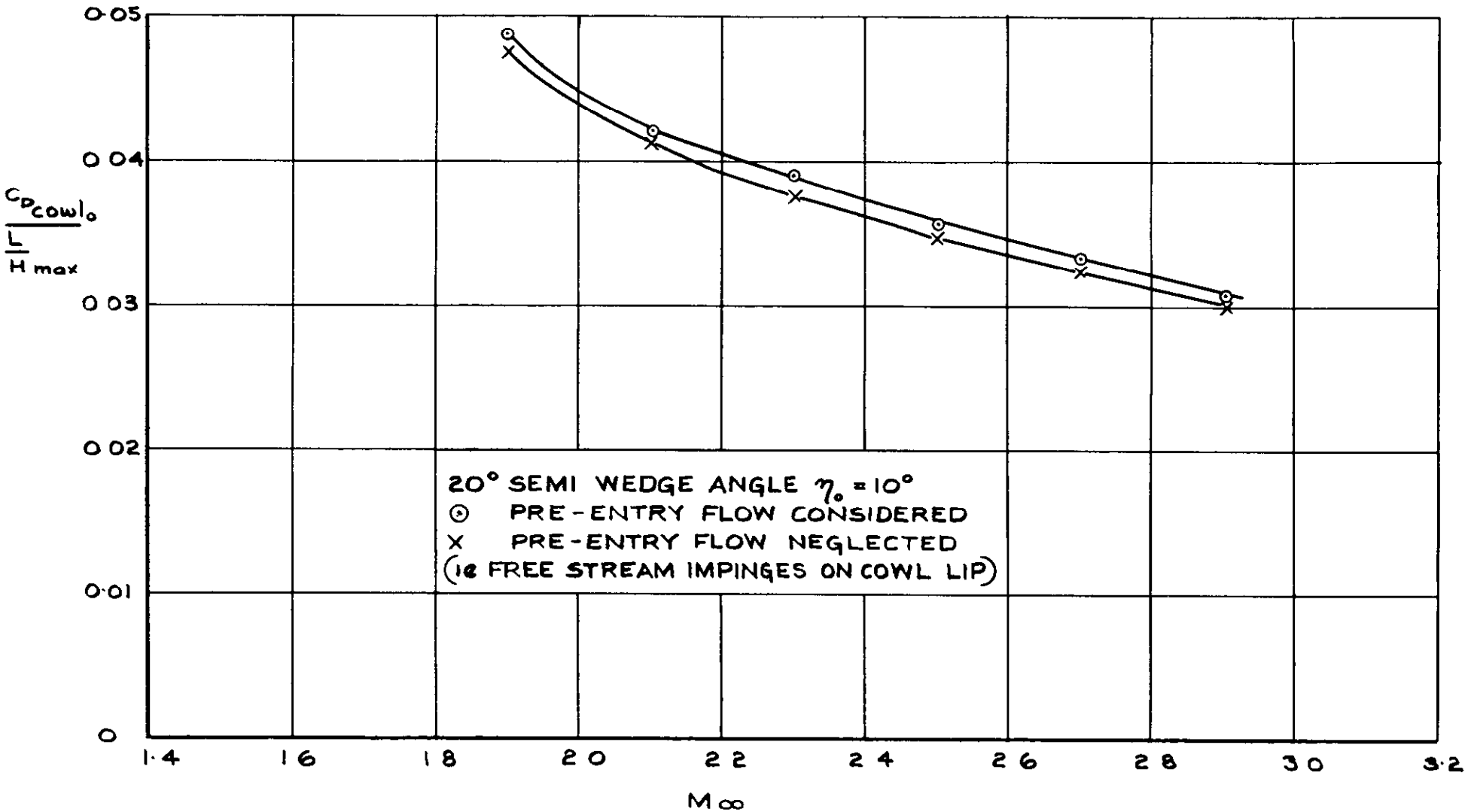

FIG. 6 VARIATION OF WAVE DRAG FOR A STRAIGHT LINE COWL WITH AND WITHOUT CONSIDERATION OF THE PRE-ENTRY FLOW

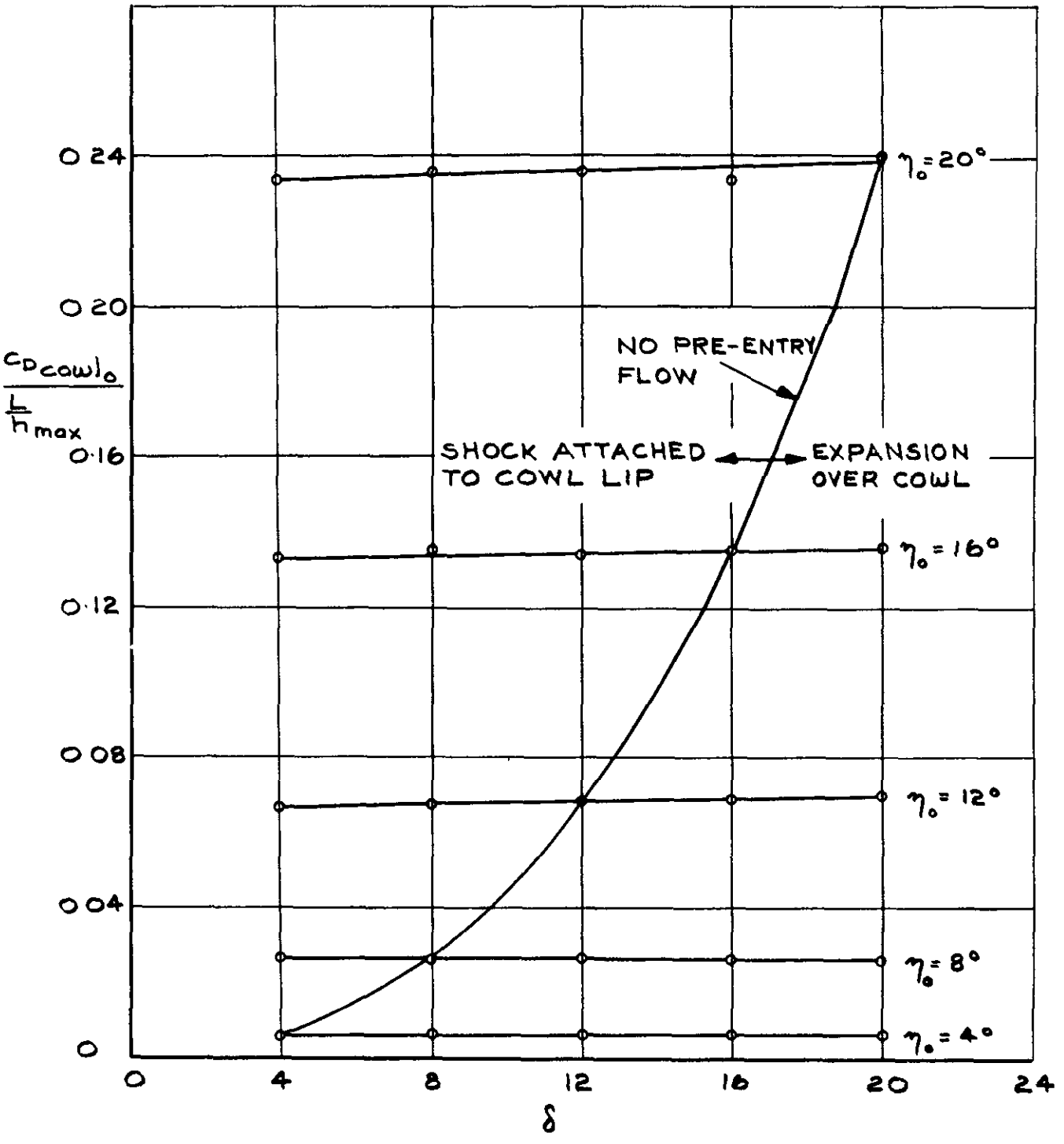

FIG. 7 VARIATION OF WAVE DRAG FOR A STRAIGHT LINE COWL WITH AND WITHOUT CONSIDERATION OF THE PRE-ENTRY FLOW, TWO DIMENSIONAL CENTRE BODY INTAKE AT $M_\infty = 2{\cdot}0$

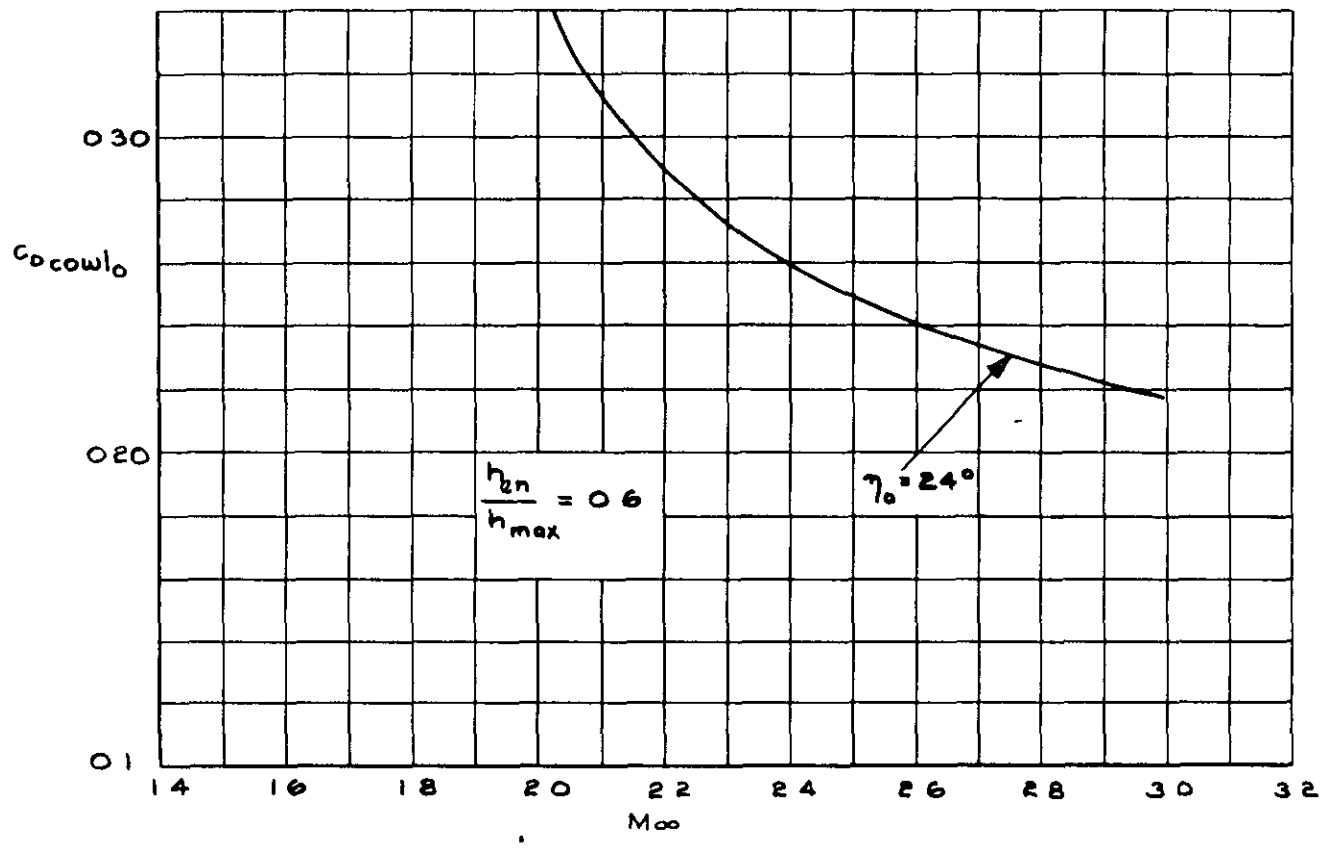

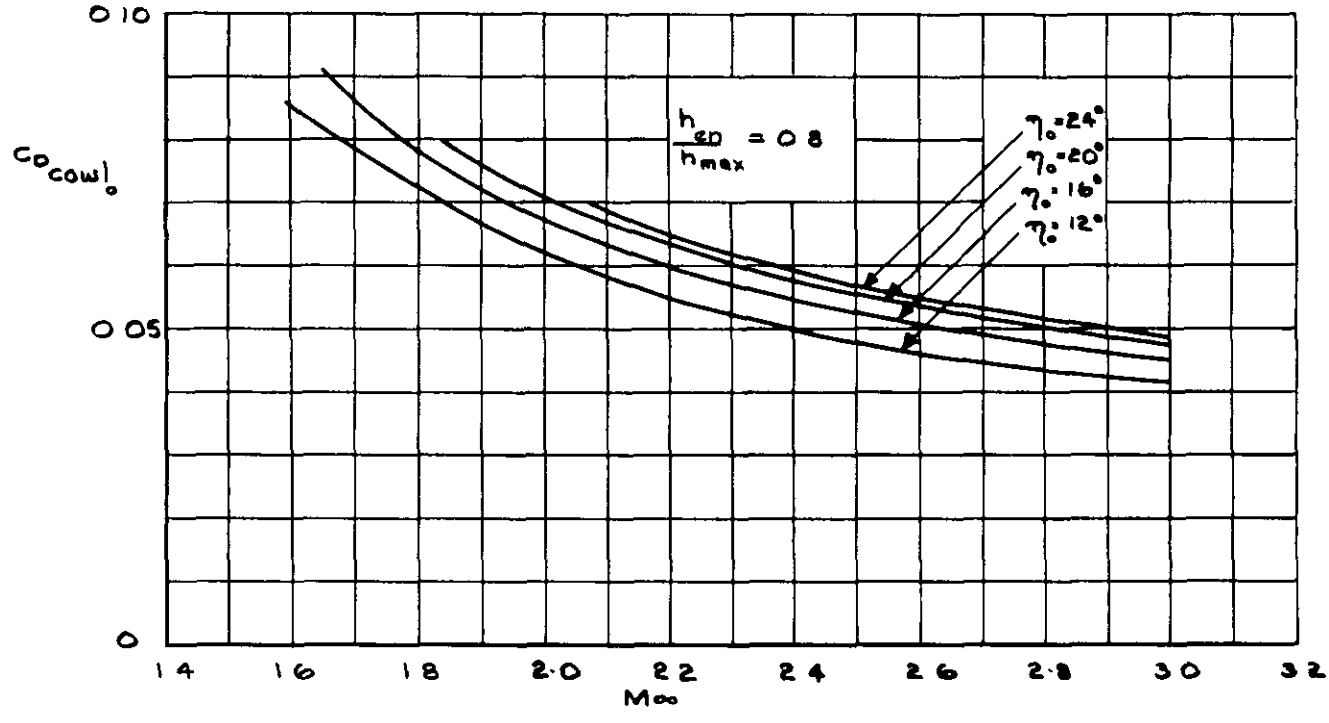

FIG.8. VARIATION OF $C_{D_{cowl_0}}$ WITH MACH No FOR TWO DIMENSIONAL ELLIPTICAL COWL PROFILES WITH $\frac{L}{H_{max}} = 1.0$

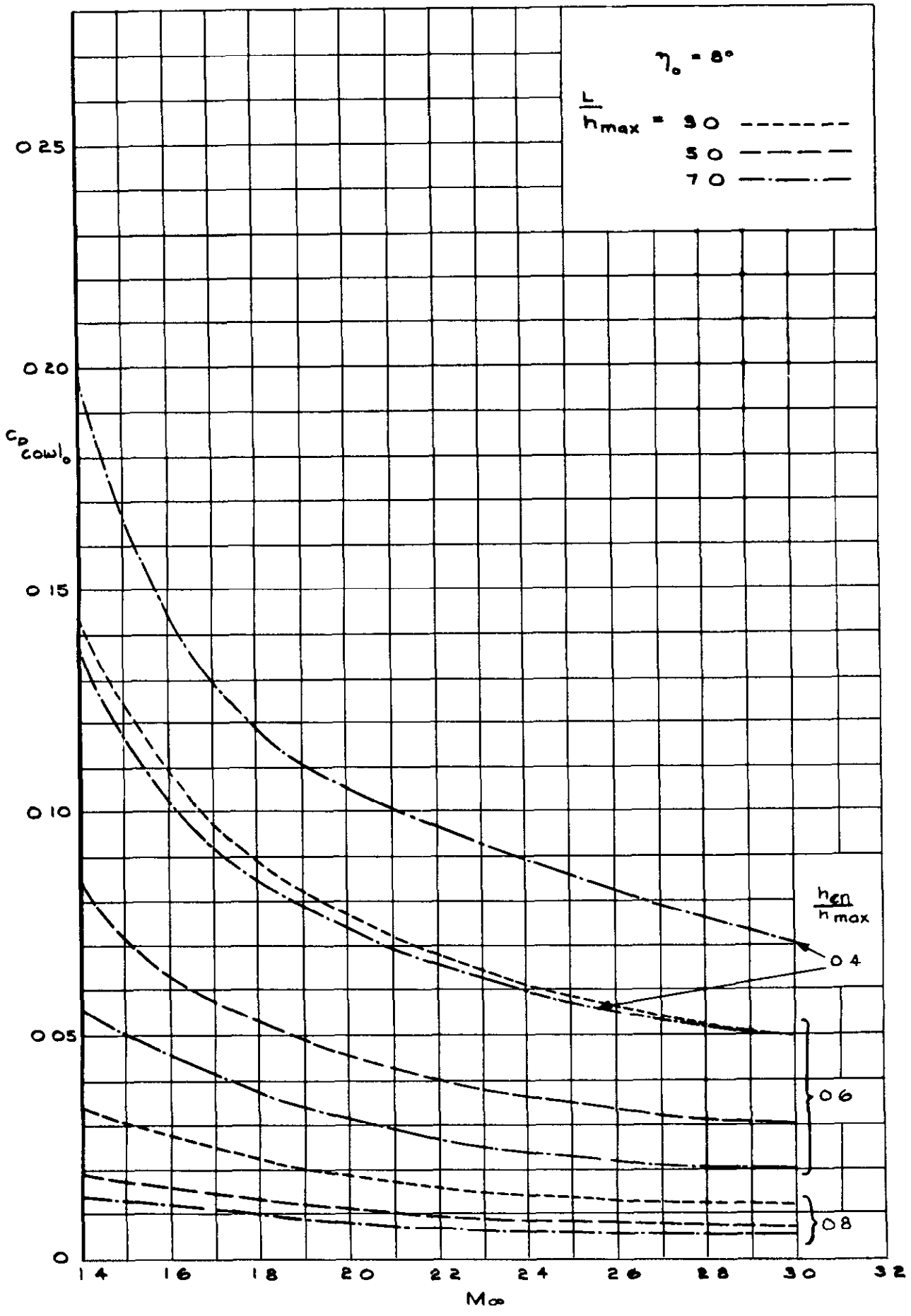

FIG.8 (CONT'D) VARIATION OF $C_{D_{cowl_0}}$ WITH MACH No FOR TWO DIMENSIONAL ELLIPTICAL COWL PROFILES HAVING $\eta_0 = 8°$

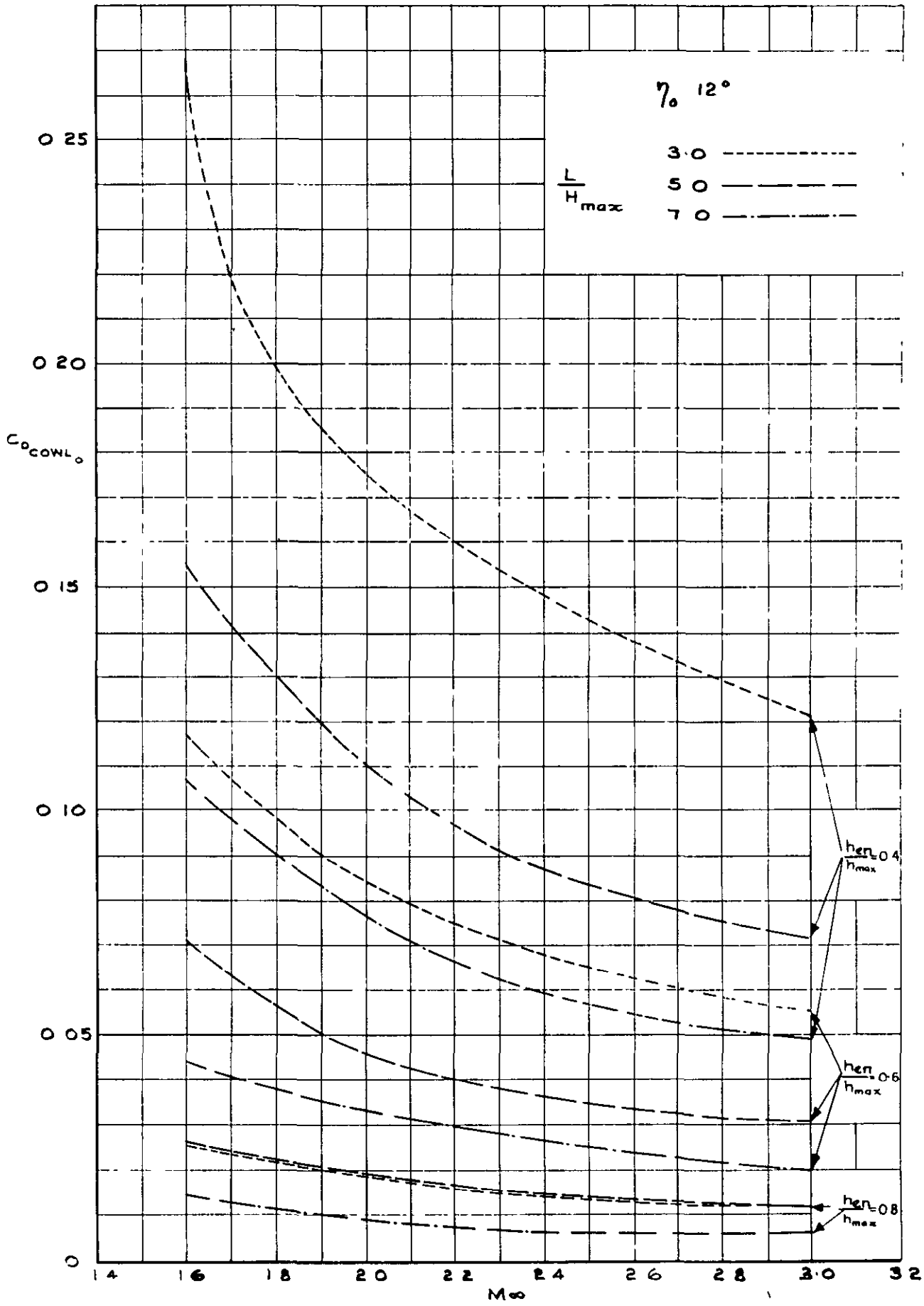

FIG.8 (CONT'D) VARIATION OF $C_{D_{cowl_0}}$ WITH MACH No FOR TWO DIMENSIONAL ELLIPTICAL COWL PROFILES HAVING η_0=12°

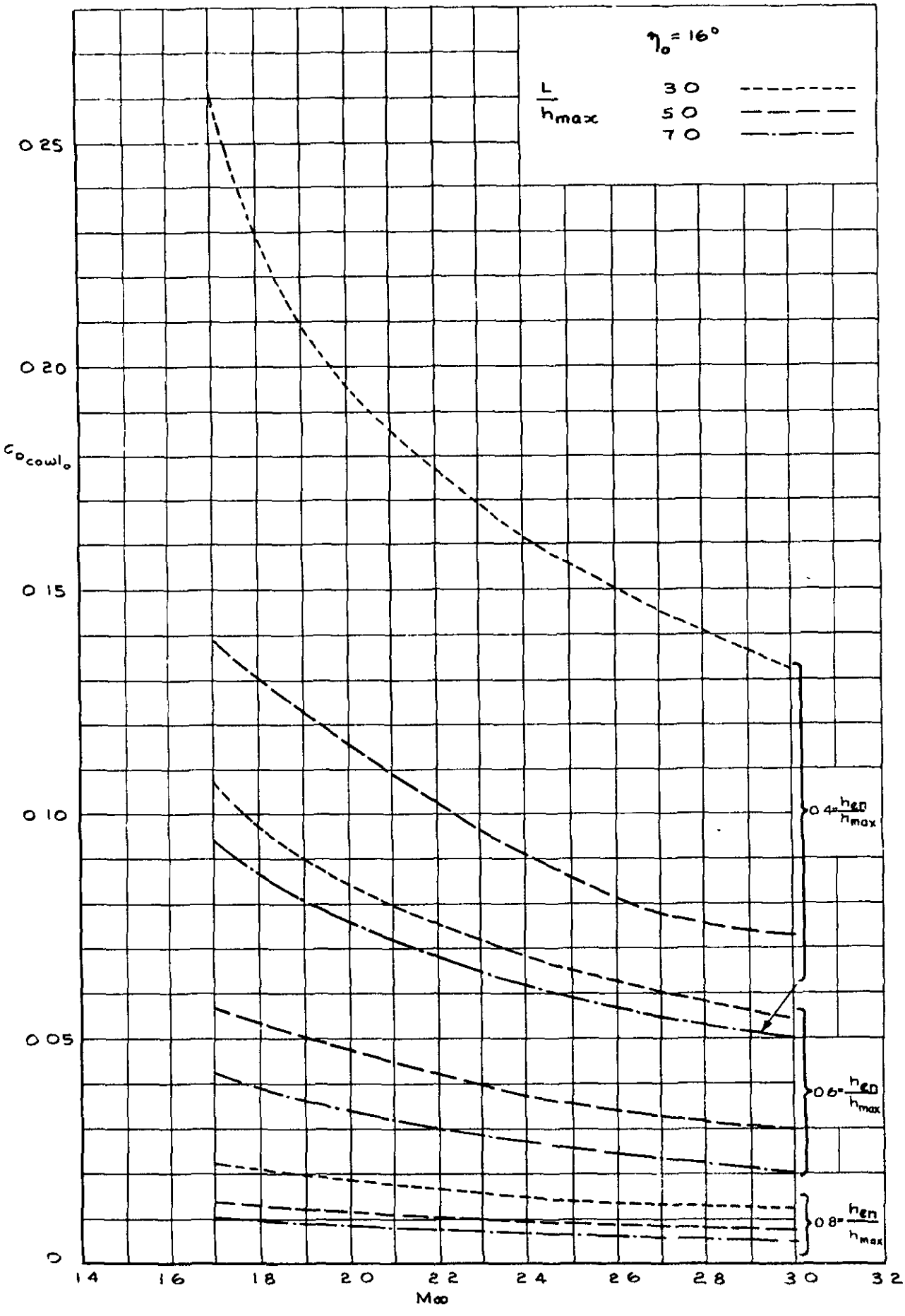

FIG 8 (CONT'D) VARIATION OF $C_{D_{cowl_o}}$ WITH MACH No FOR TWO DIMENSIONAL ELLIPTICAL COWL PROFILES HAVING $\eta_o = 16°$

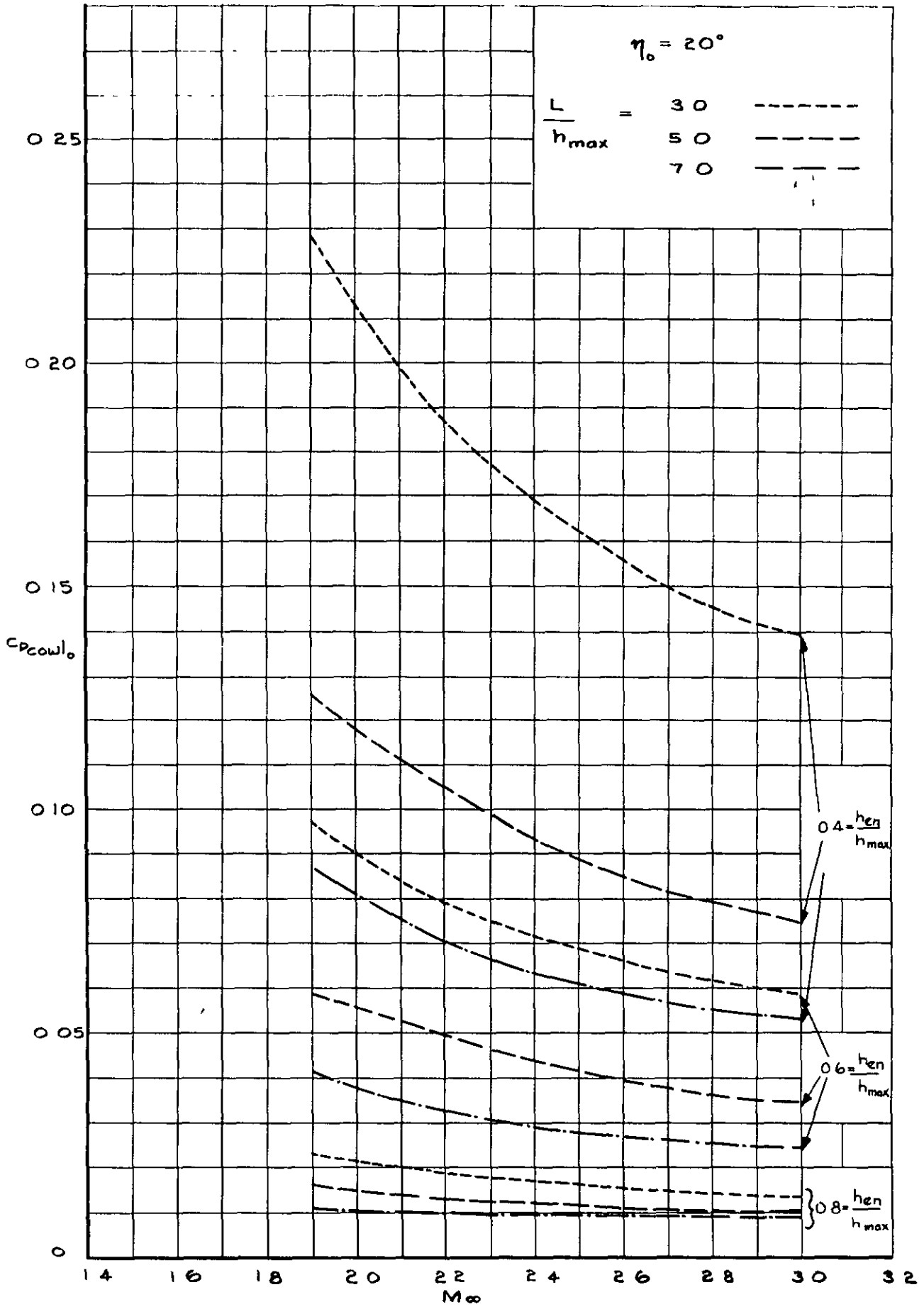

FIG. 8 (CONT'D) VARIATION OF $C_{D_{cowl_o}}$ WITH MACH No FOR TWO DIMENSIONAL ELLIPTICAL COWL PROFILES HAVING $\eta_o = 20°$

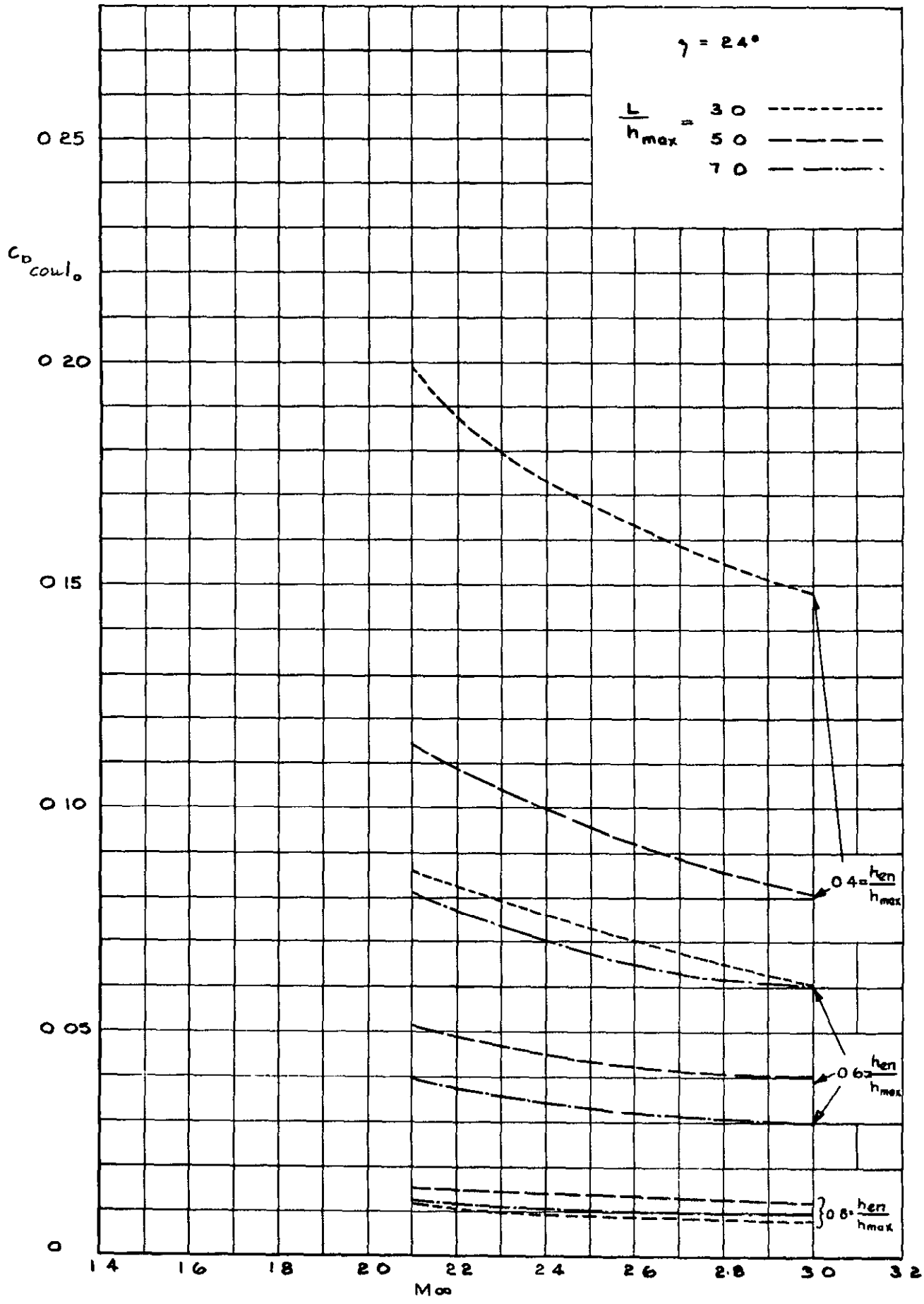

FIG.8 (CONCL'D) VARIATION OF $C_{D_{cowl_o}}$ WITH MACH No. FOR TWO DIMENSIONAL ELLIPTICAL COWL PROFILES HAVING $\gamma_o = 24°$

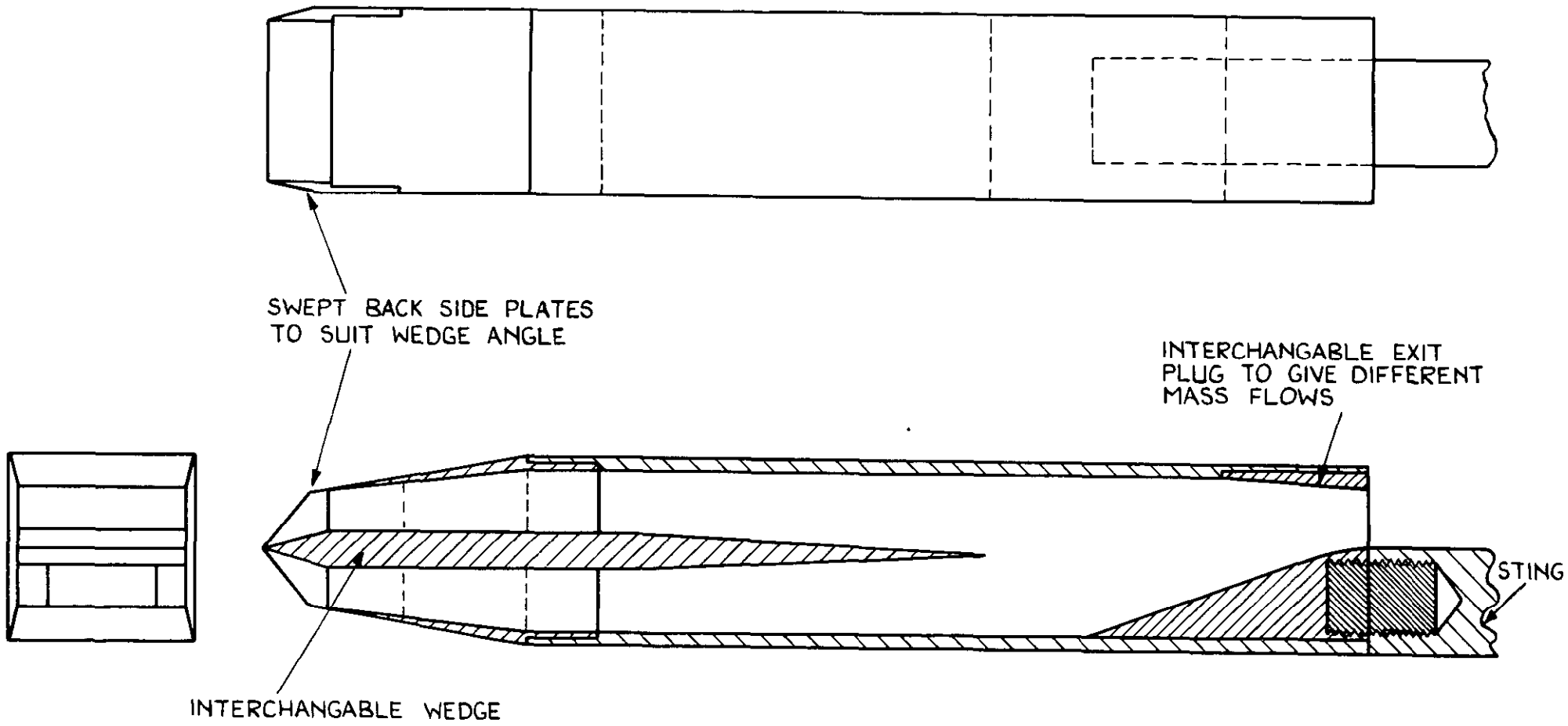

SCALE :- FULL SIZE

FIG. 9 TWO DIMENSIONAL INTAKE MODEL USED FOR DRAG AND PRESSURE RECOVERY MEASUREMENTS

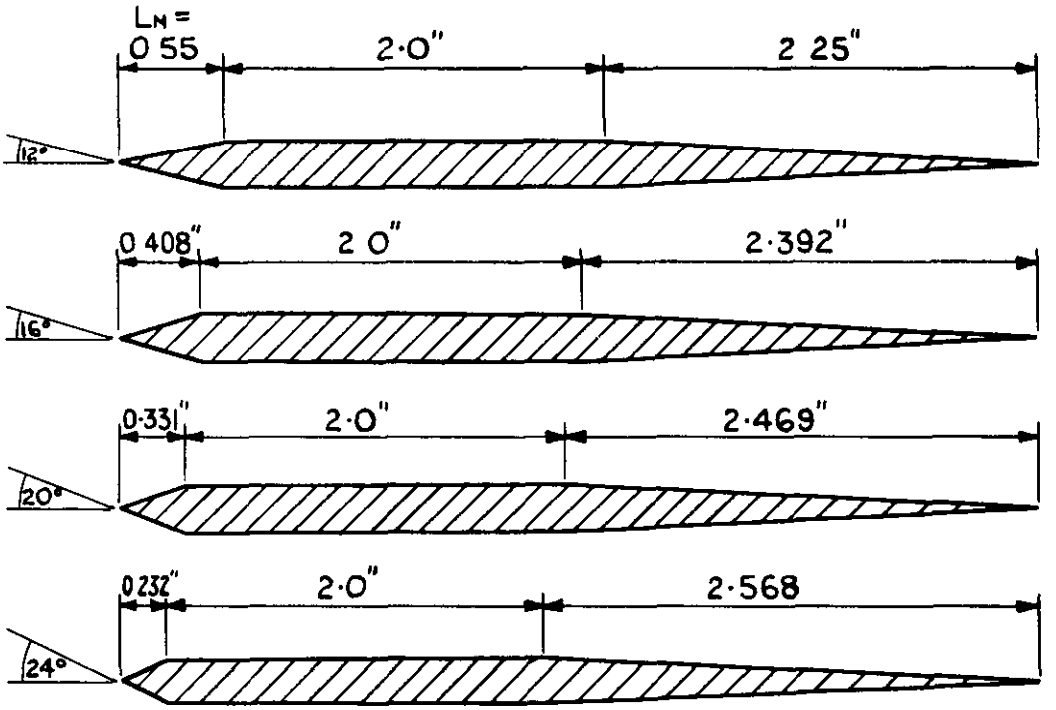

FIG. 10 WEDGE CENTREBODY DIMENSIONS

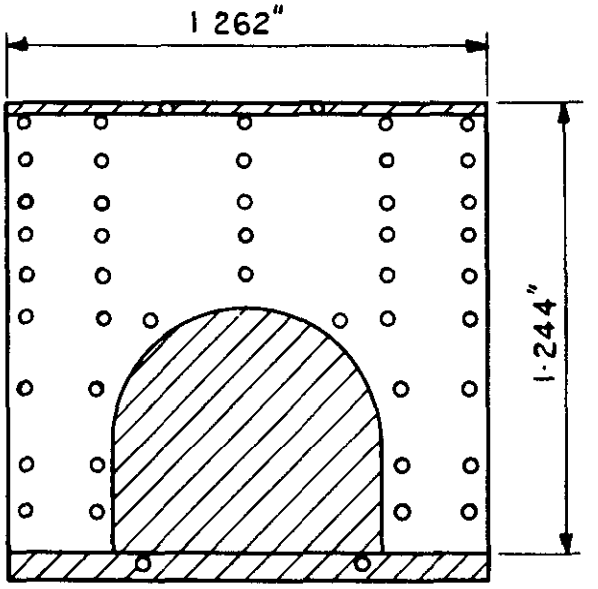

SCALE : 2 × FULL SIZE

FIG. 11 APPROXIMATE LOCATION OF PITOT TUBES IN EXIT PLANE

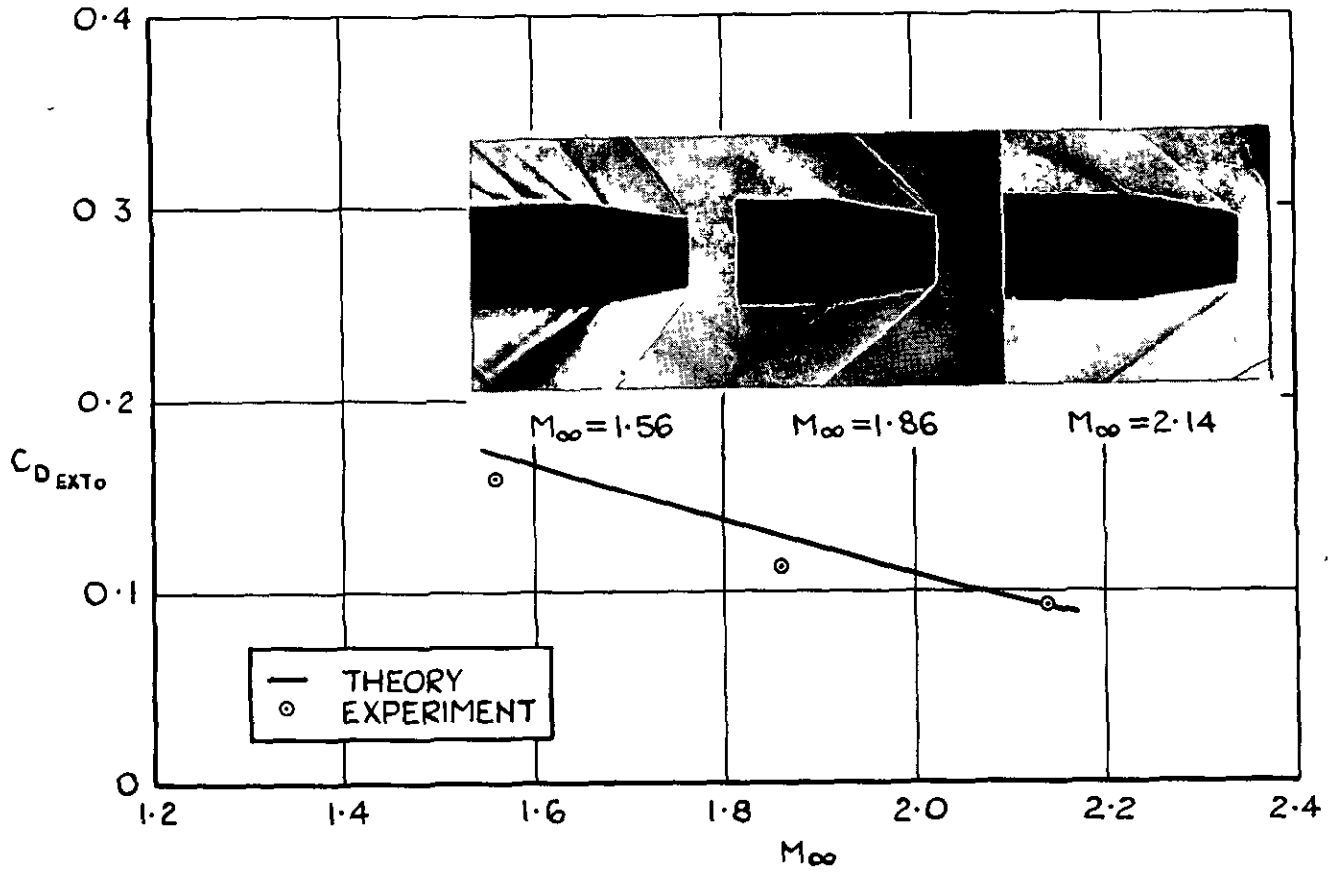

FIG. 12 (a)

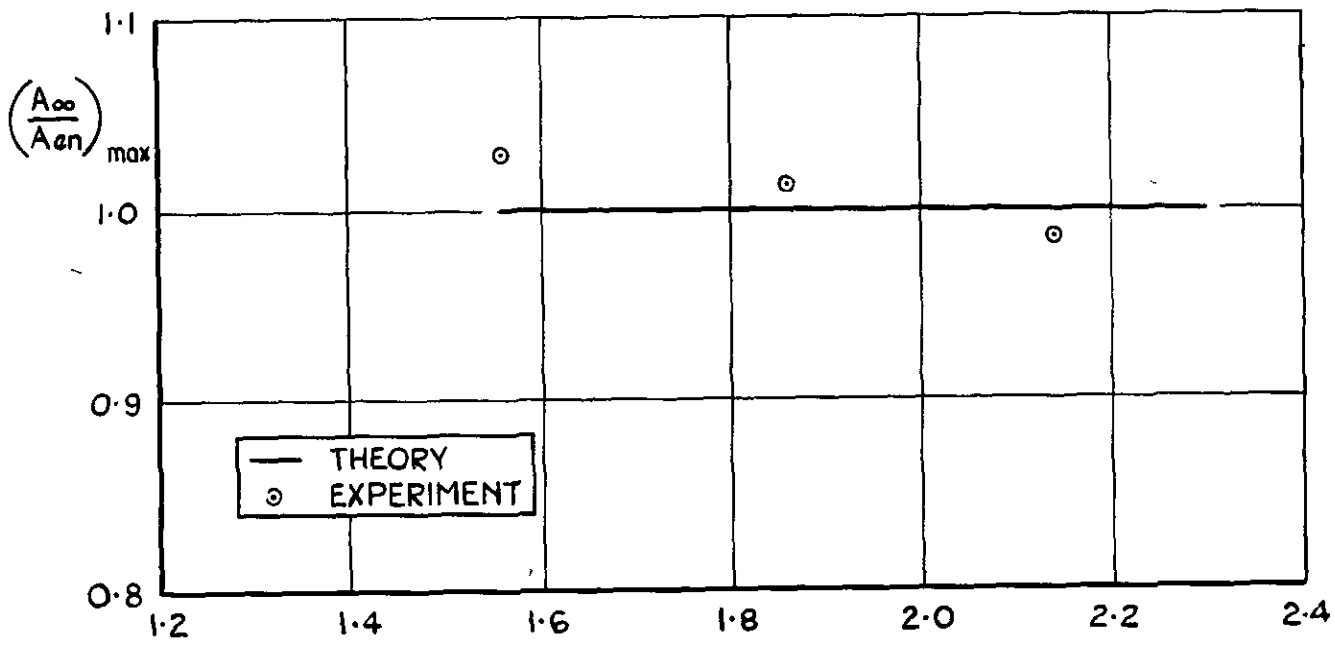

FIG. 12 (b)

FIG. 12 COMPARISON BETWEEN THE THEORETICAL AND MEASURED VALUES OF $C_{D_{EXTo}}$ AND $\frac{A_\infty}{A_{en}}$ FOR PITOT TYPE INTAKE AT FULL MASS FLOW

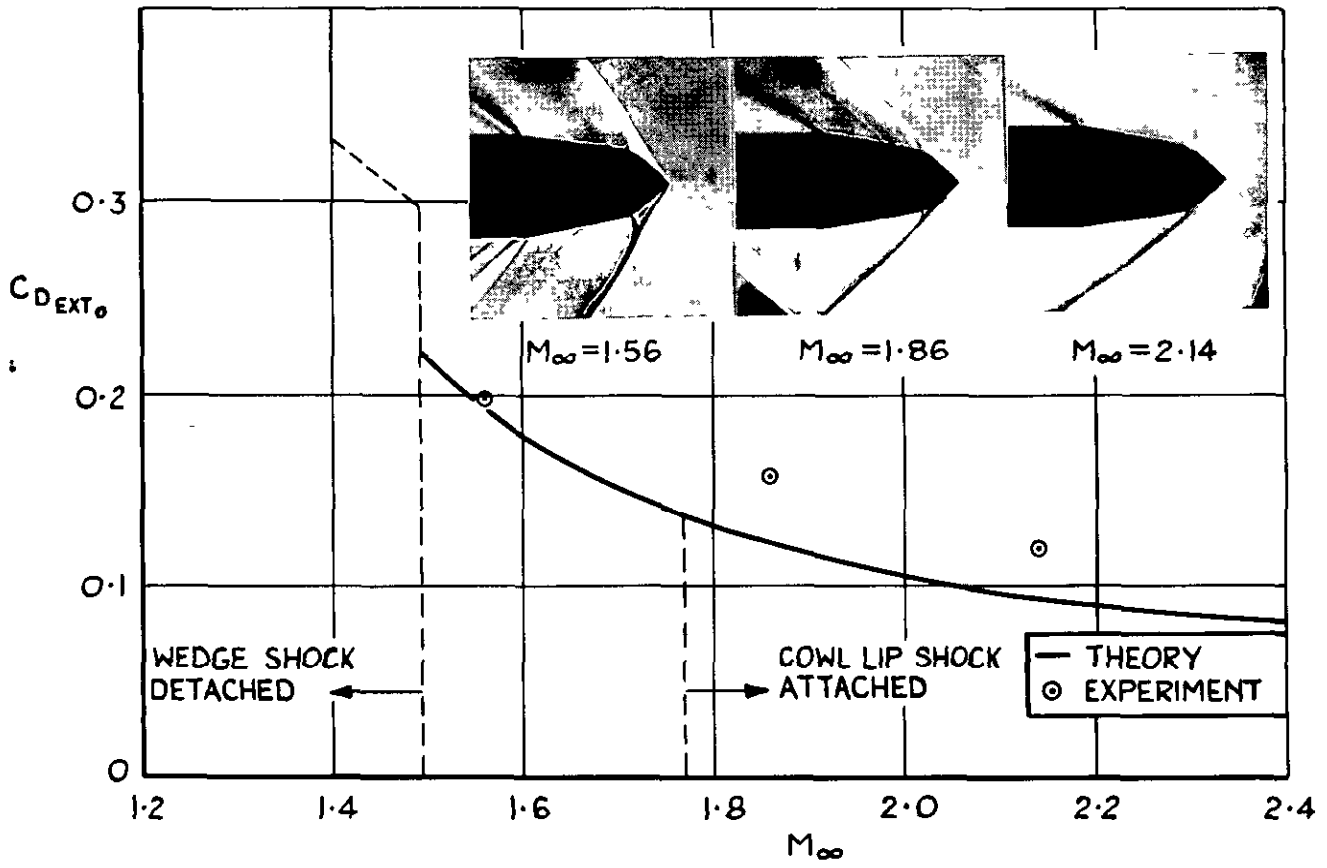

FIG. 13 (a)

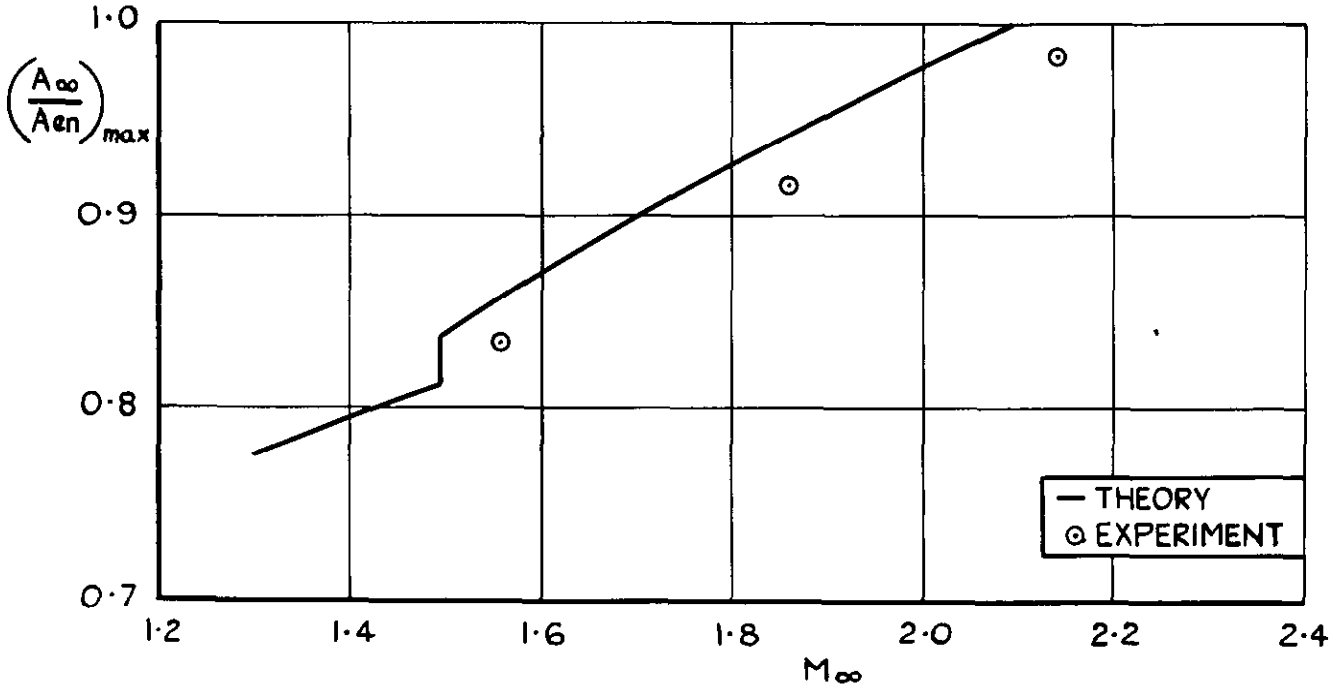

FIG. 13 (b)

FIG. 13 COMPARISON BETWEEN THE THEORETICAL AND MEASURED VALUES OF $C_{D_{EXT_o}}$ AND $\frac{A_\infty}{A_{en}}$ FOR 12° WEDGE CENTREBODY INTAKE AT FULL MASS FLOW

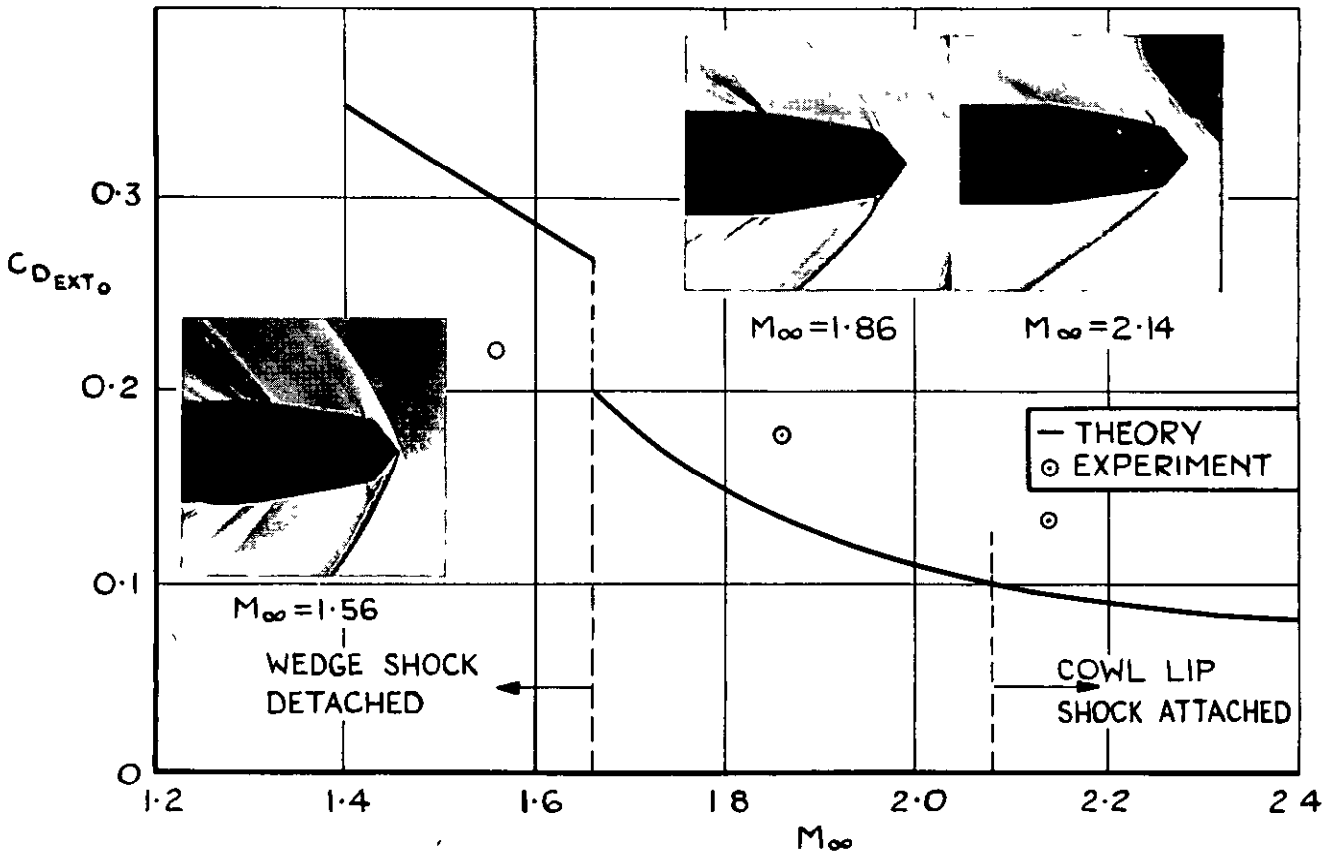

FIG. 14 (a)

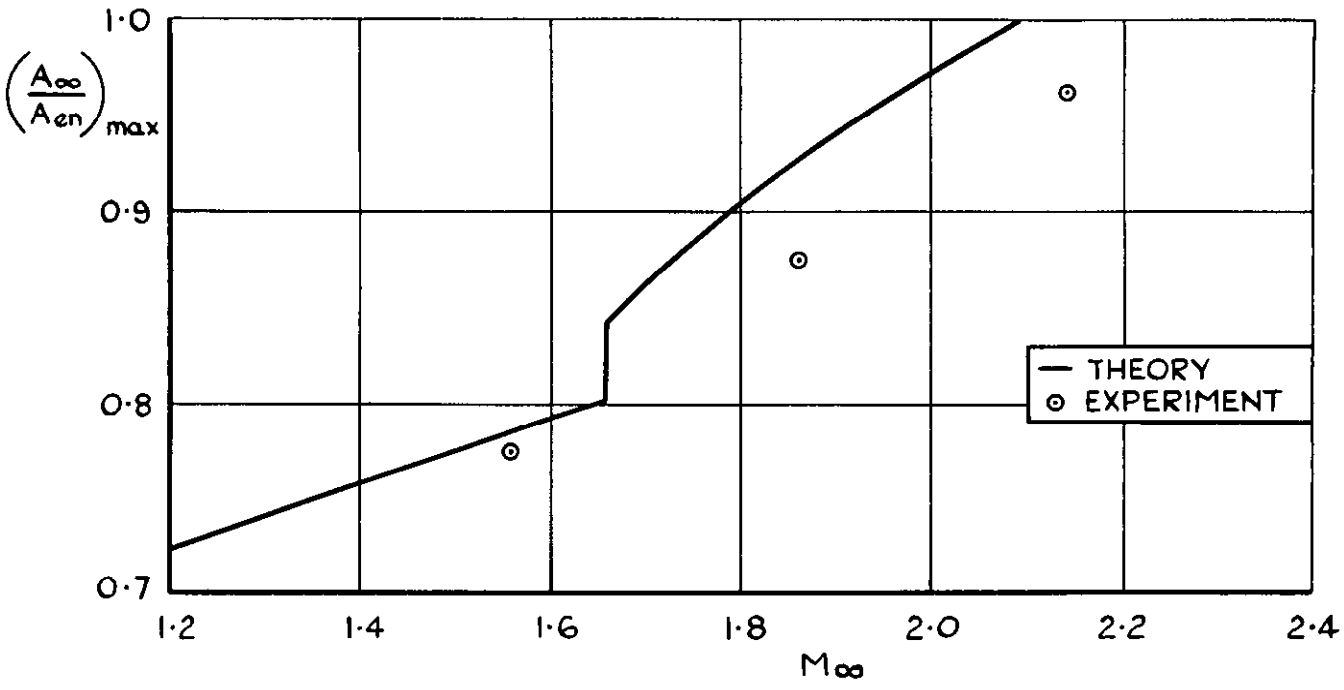

FIG. 14 (b)

FIG. 14 COMPARISON BETWEEN THE THEORETICAL AND MEASURED VALUES OF $C_{D_{EXT_o}}$ AND $\frac{A_\infty}{A_{en}}$ FOR 16° WEDGE CENTREBODY INTAKE AT FULL MASS FLOW

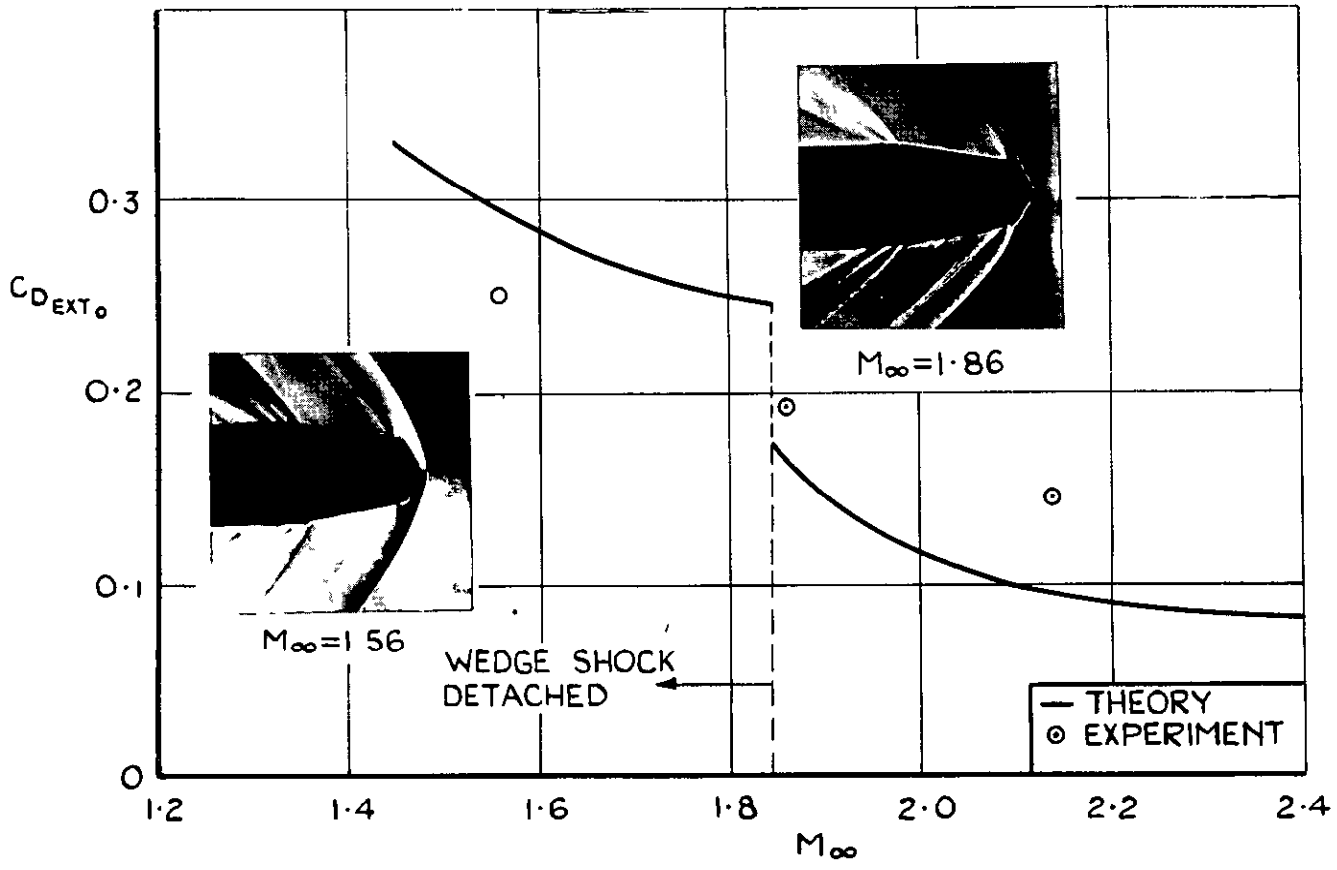

FIG. 15 (a)

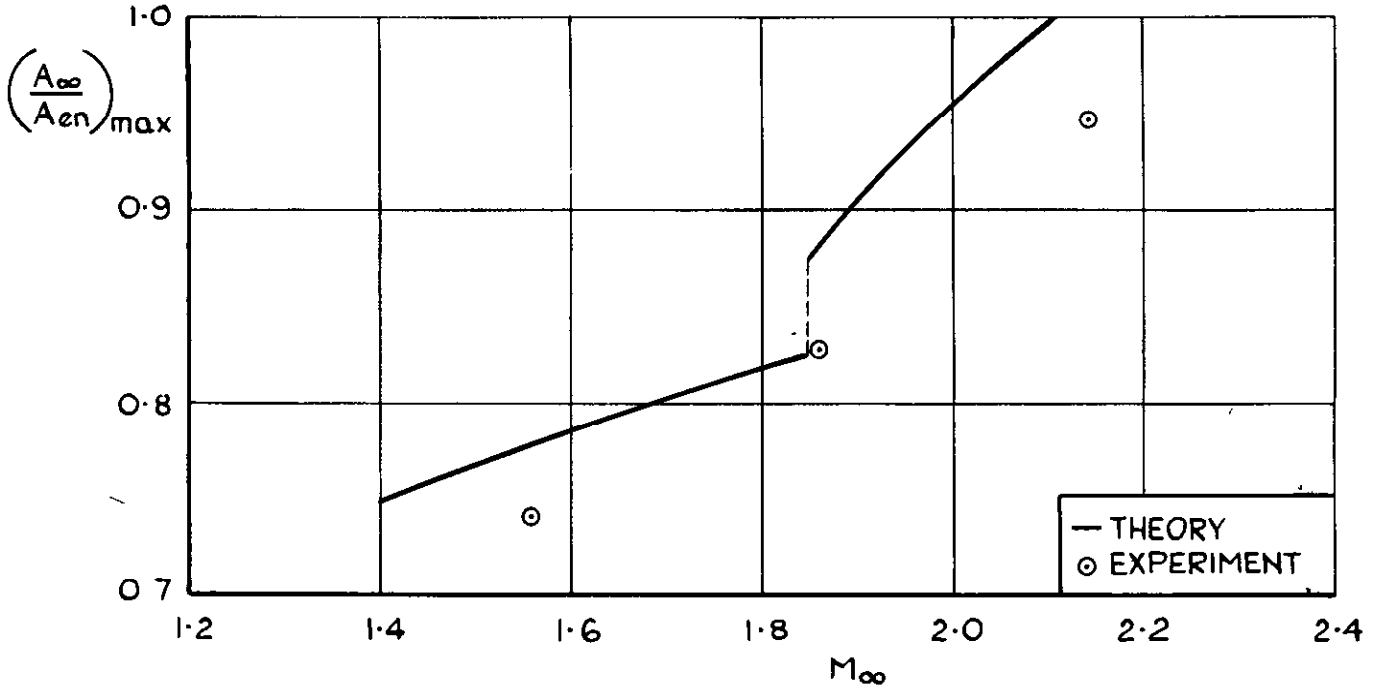

FIG. 15 (b)

FIG 15 COMPARISON BETWEEN THE THEORETICAL AND MEASURED VALUES OF $C_{D_{EXT_o}}$ AND $\frac{A_\infty}{A_{en}}$ FOR 20° WEDGE CENTREBODY INTAKE AT FULL MASS FLOW

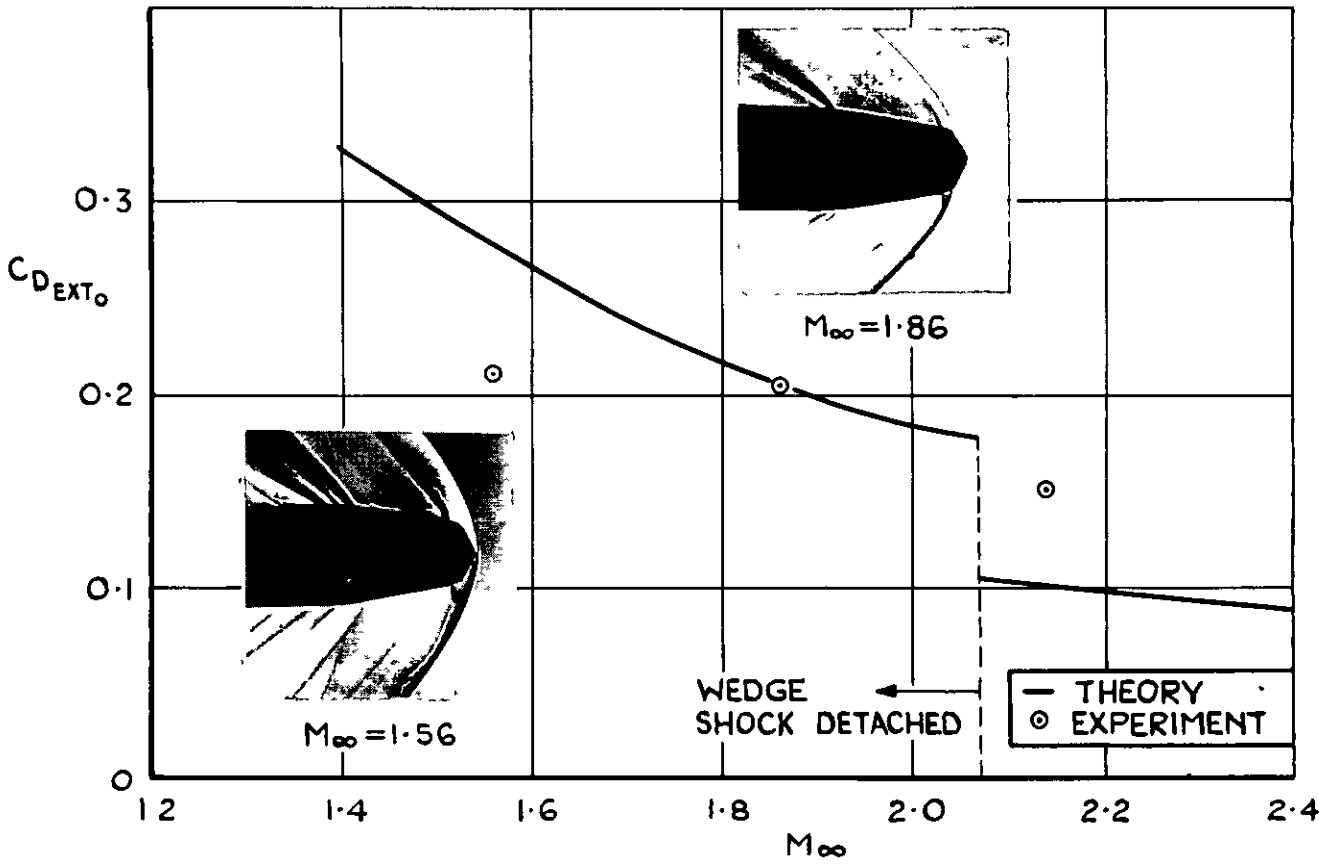

FIG. 16(a)

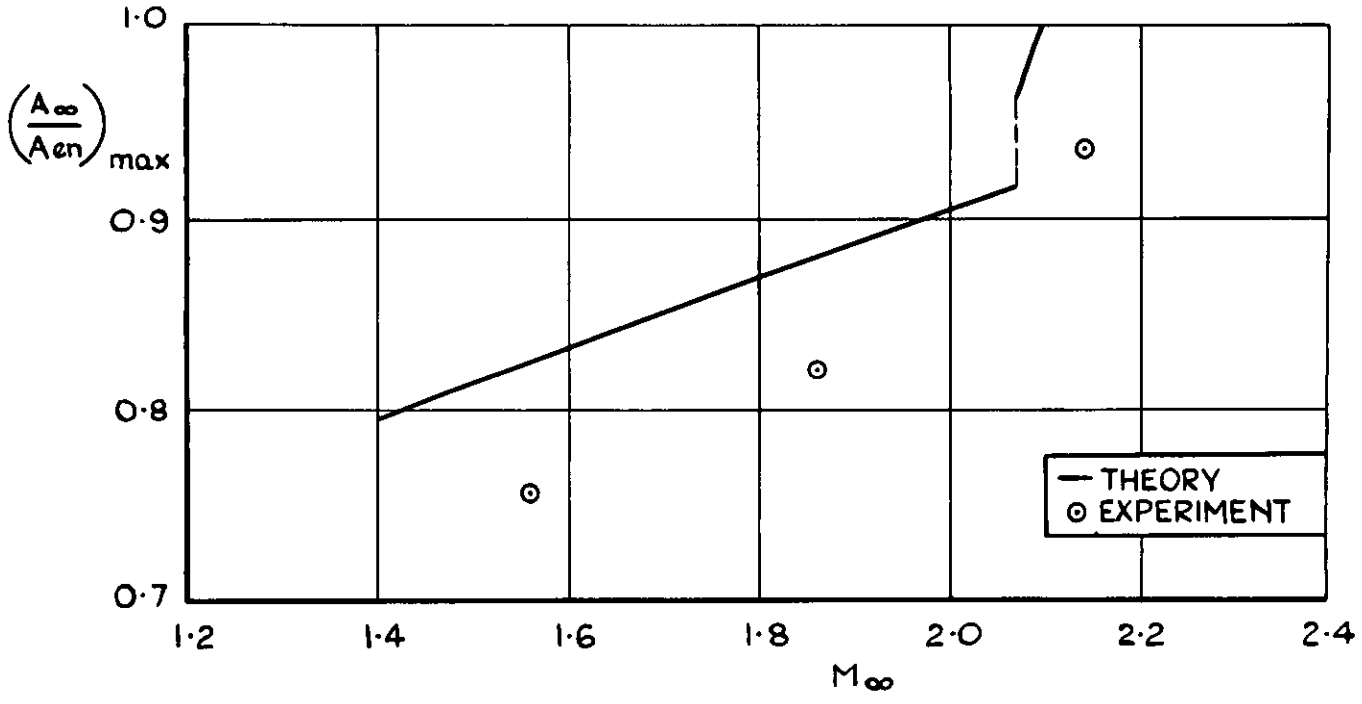

FIG. 16(b)

FIG. 16 COMPARISON BETWEEN THE THEORETICAL AND MEASURED VALUES OF $C_{D_{EXT_o}}$ AND $\frac{A_\infty}{A_{en}}$ FOR 24° WEDGE CENTREBODY INTAKE AT FULL MASS FLOW

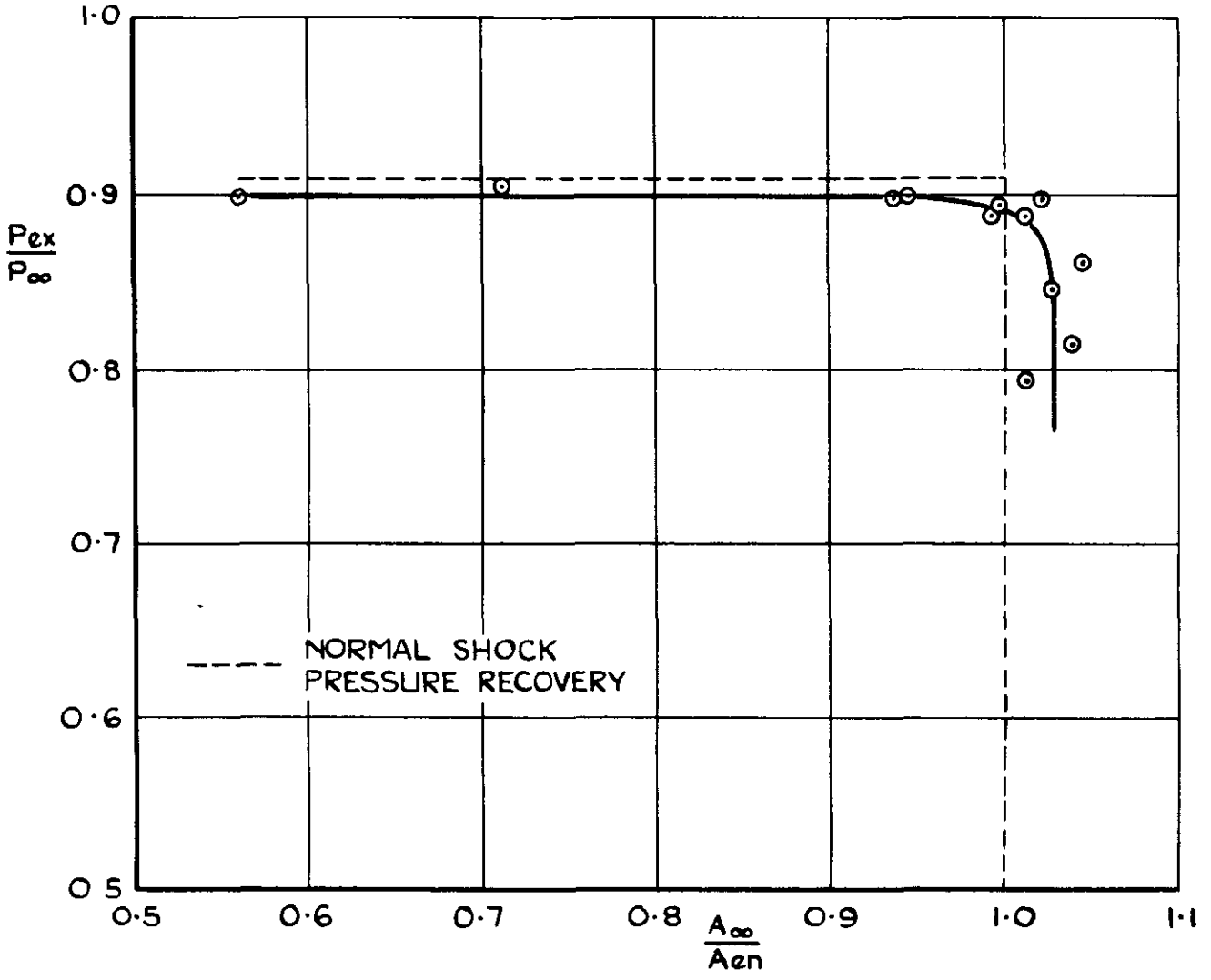

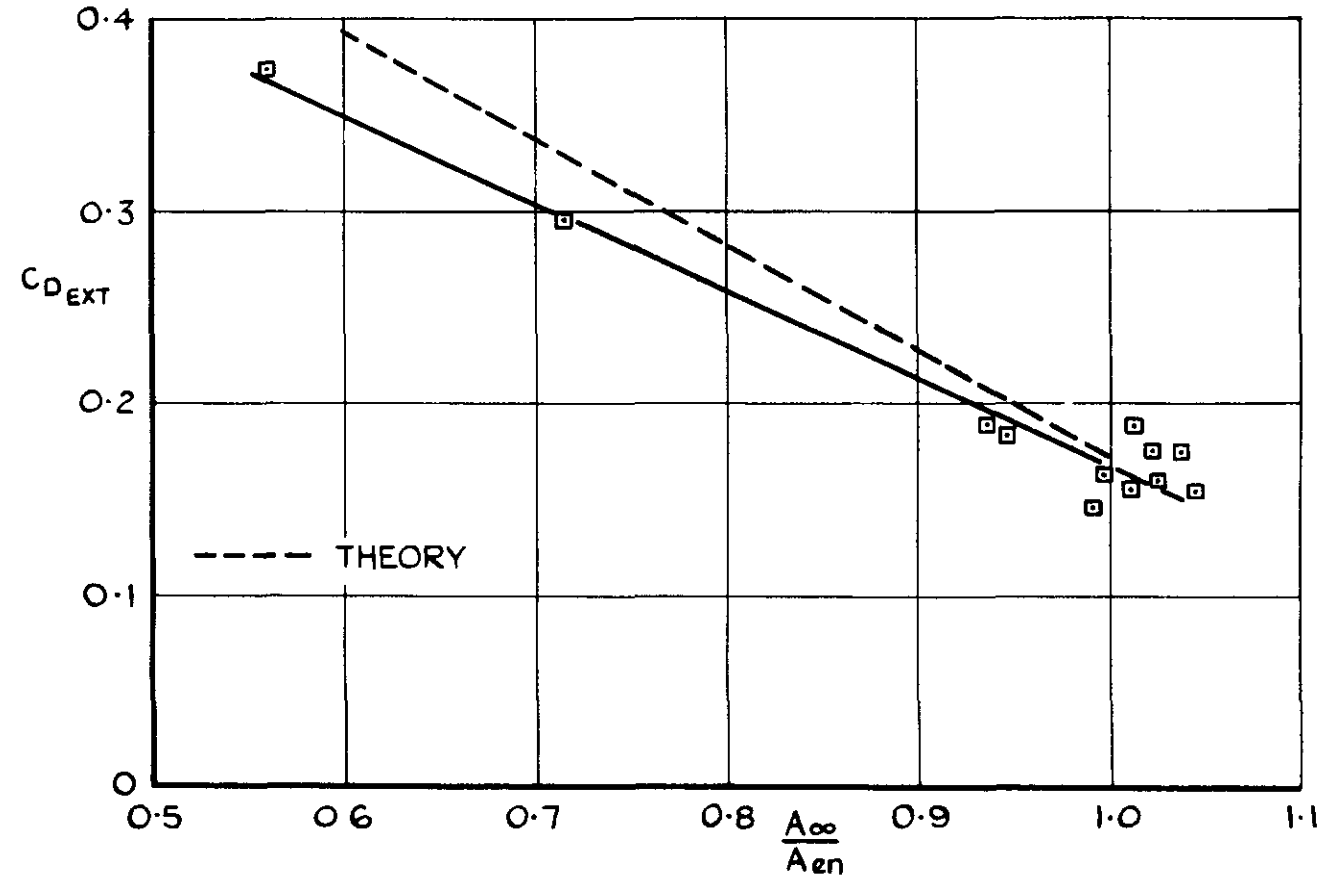

FIG. 17(a) VARIATION OF DRAG AND PRESSURE RECOVERY WITH MASS FLOW THROUGH A PITOT INTAKE AT $M_\infty = 1{\cdot}56$

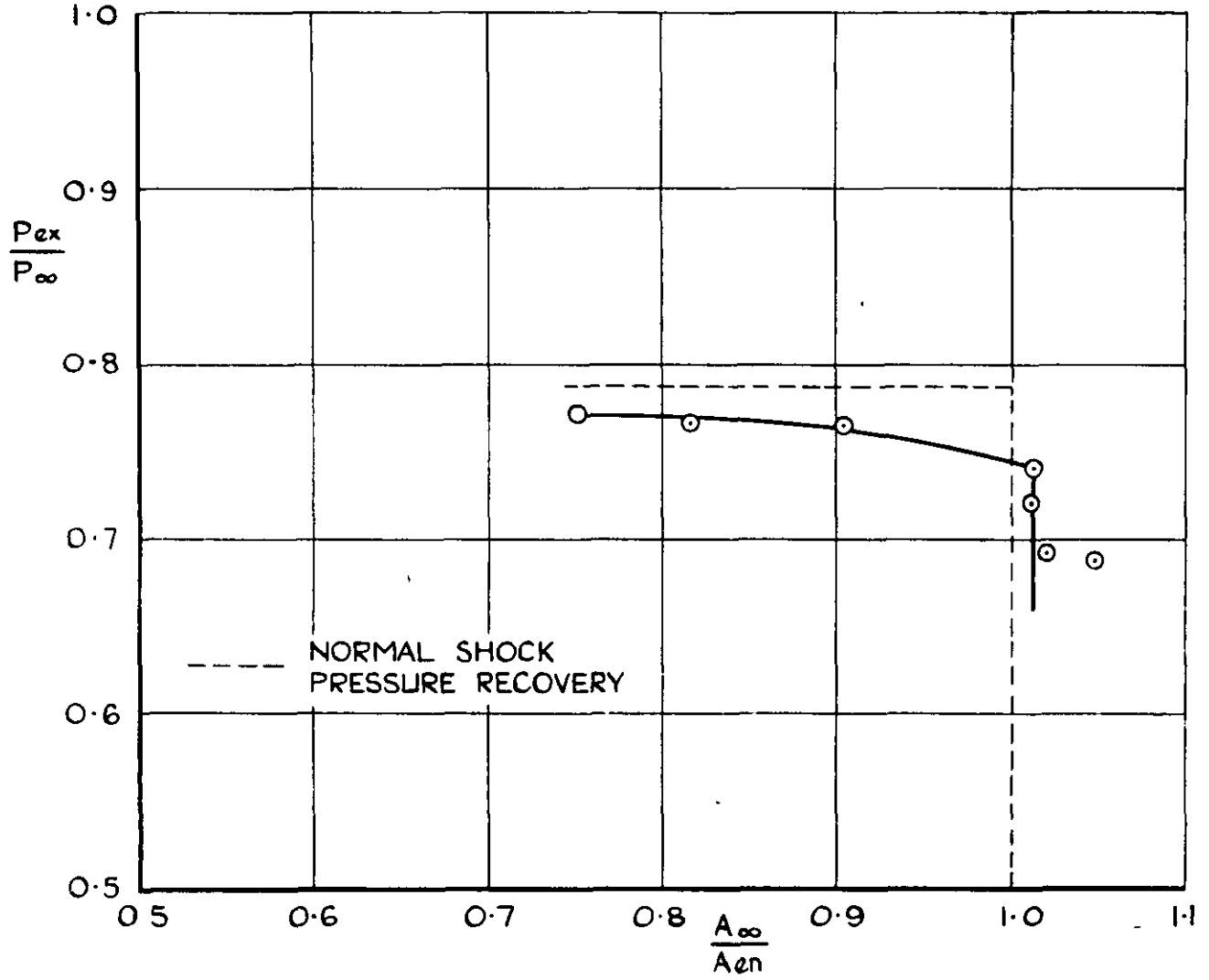

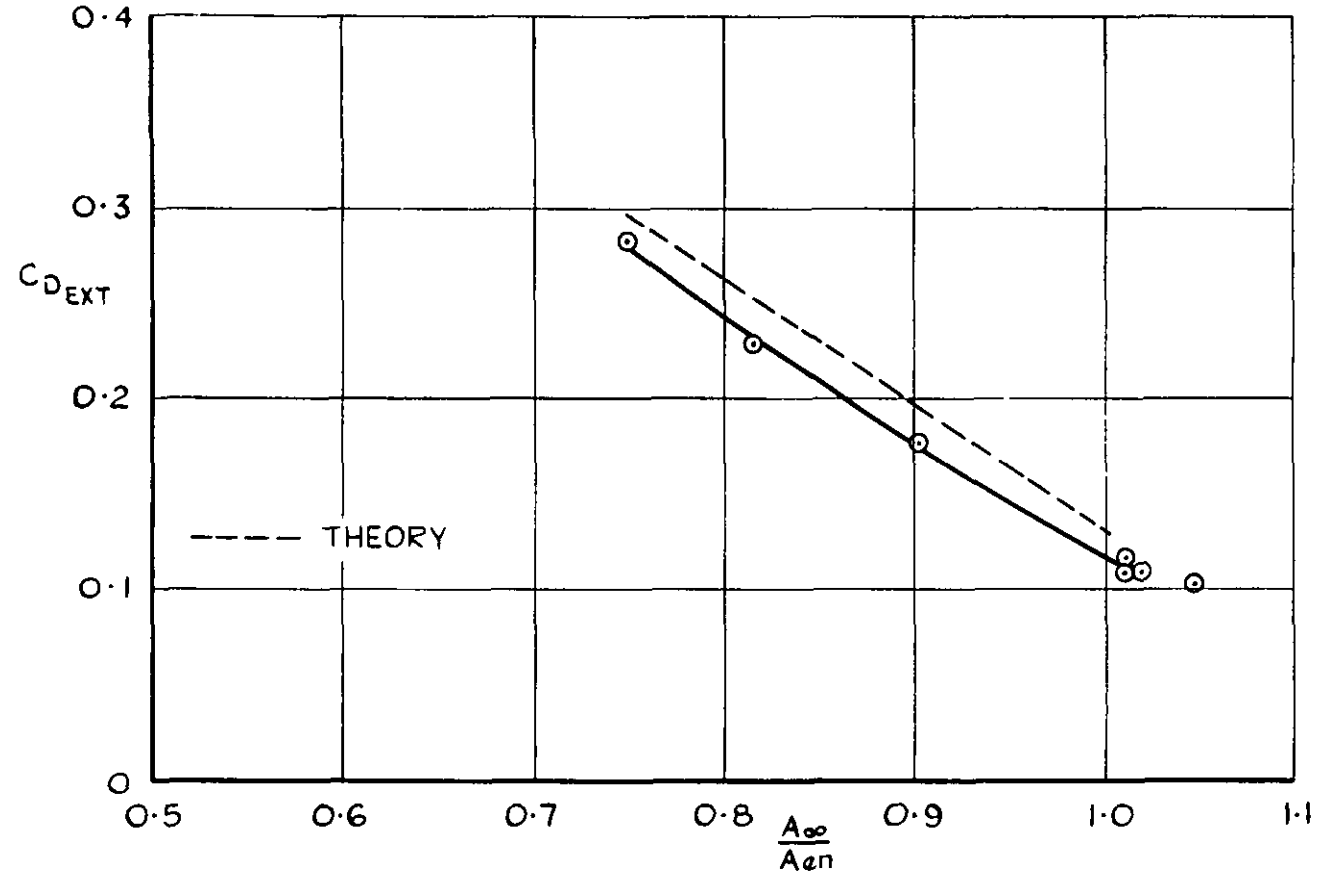

FIG. 17(b) VARIATION OF DRAG AND PRESSURE RECOVERY WITH MASS FLOW THROUGH A PITOT INTAKE AT $M_\infty = 1 \cdot 86$

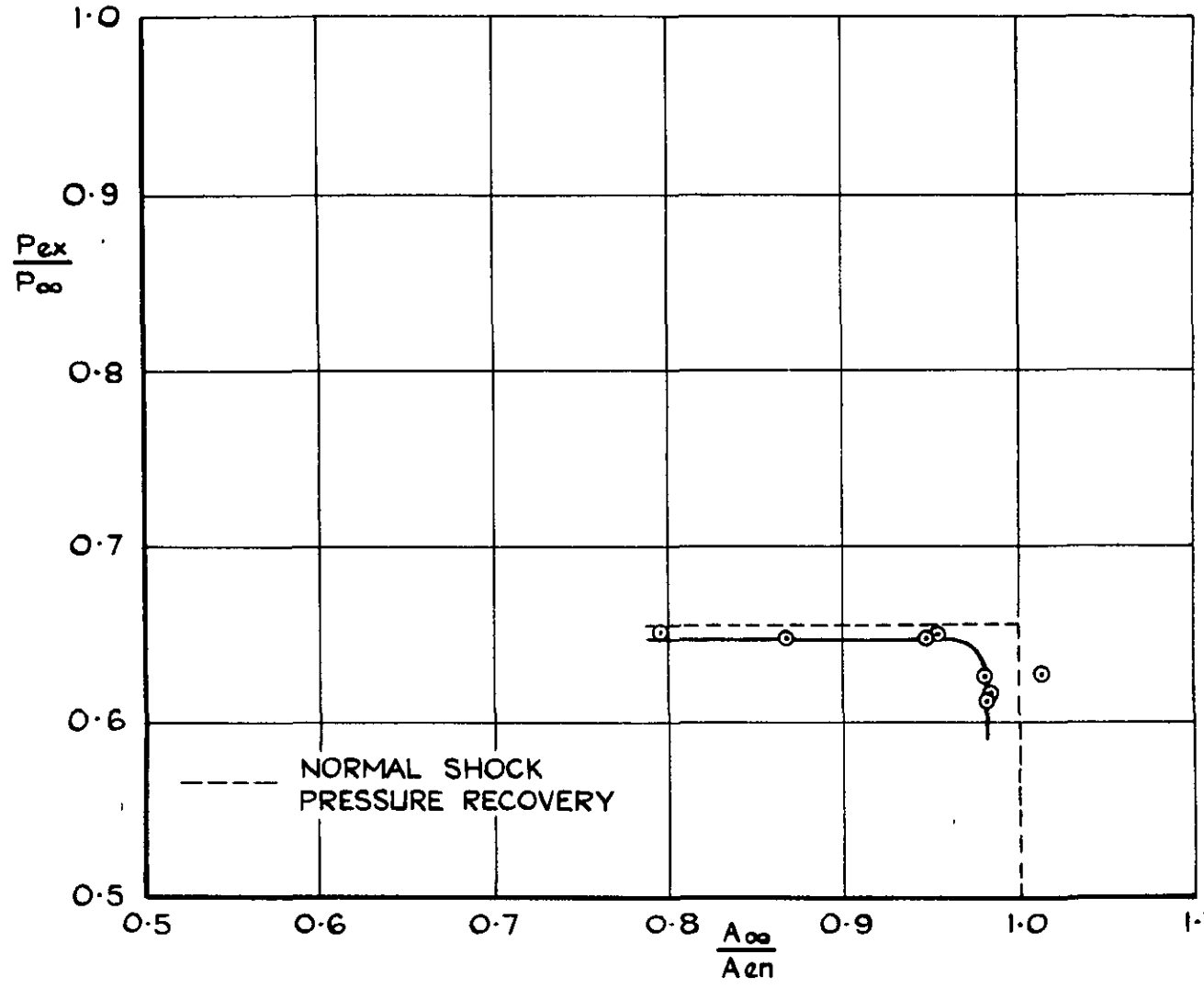

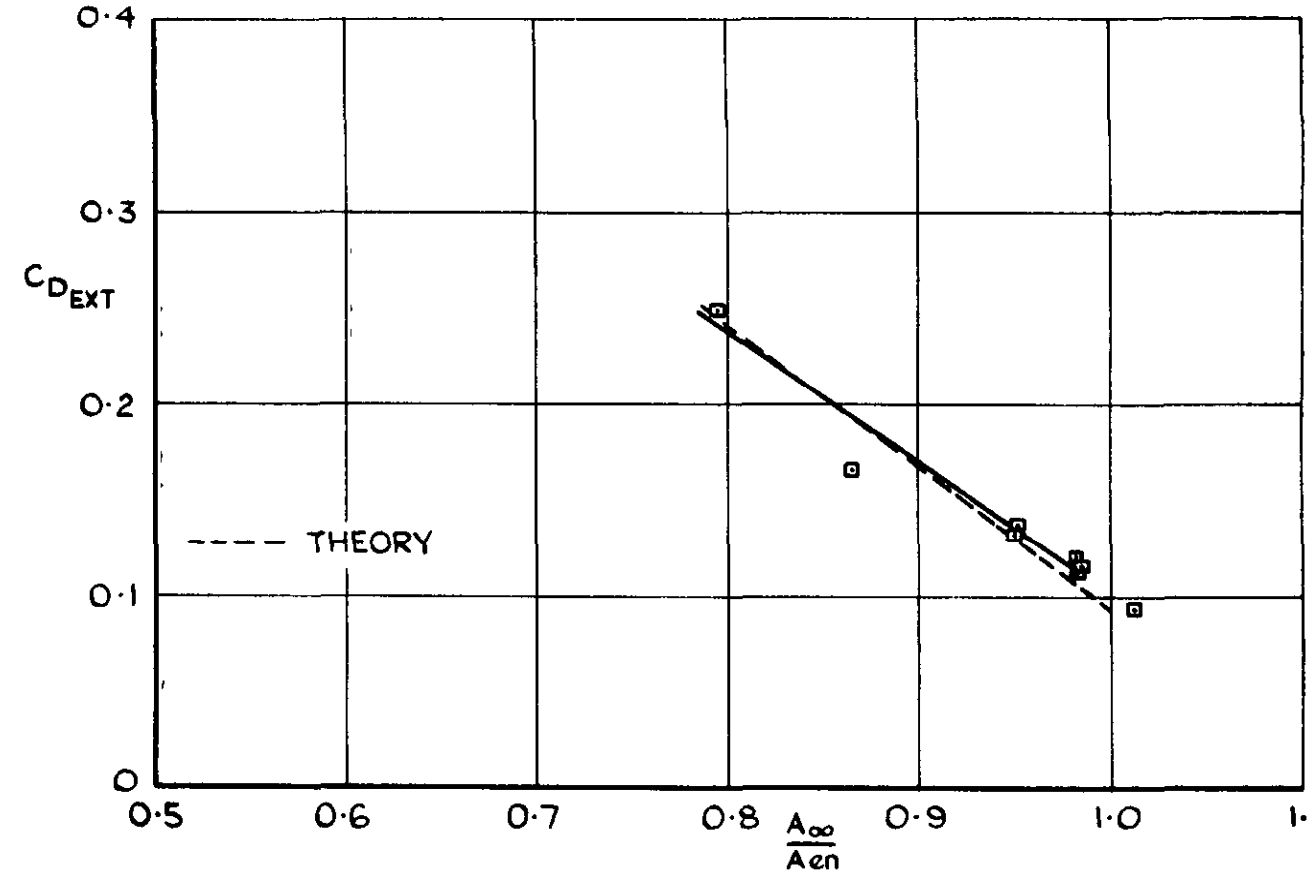

FIG. 17 (c) VARIATION OF DRAG AND PRESSURE RECOVERY WITH MASS FLOW THROUGH A PITOT INTAKE AT $M_\infty = 2 \cdot 14$

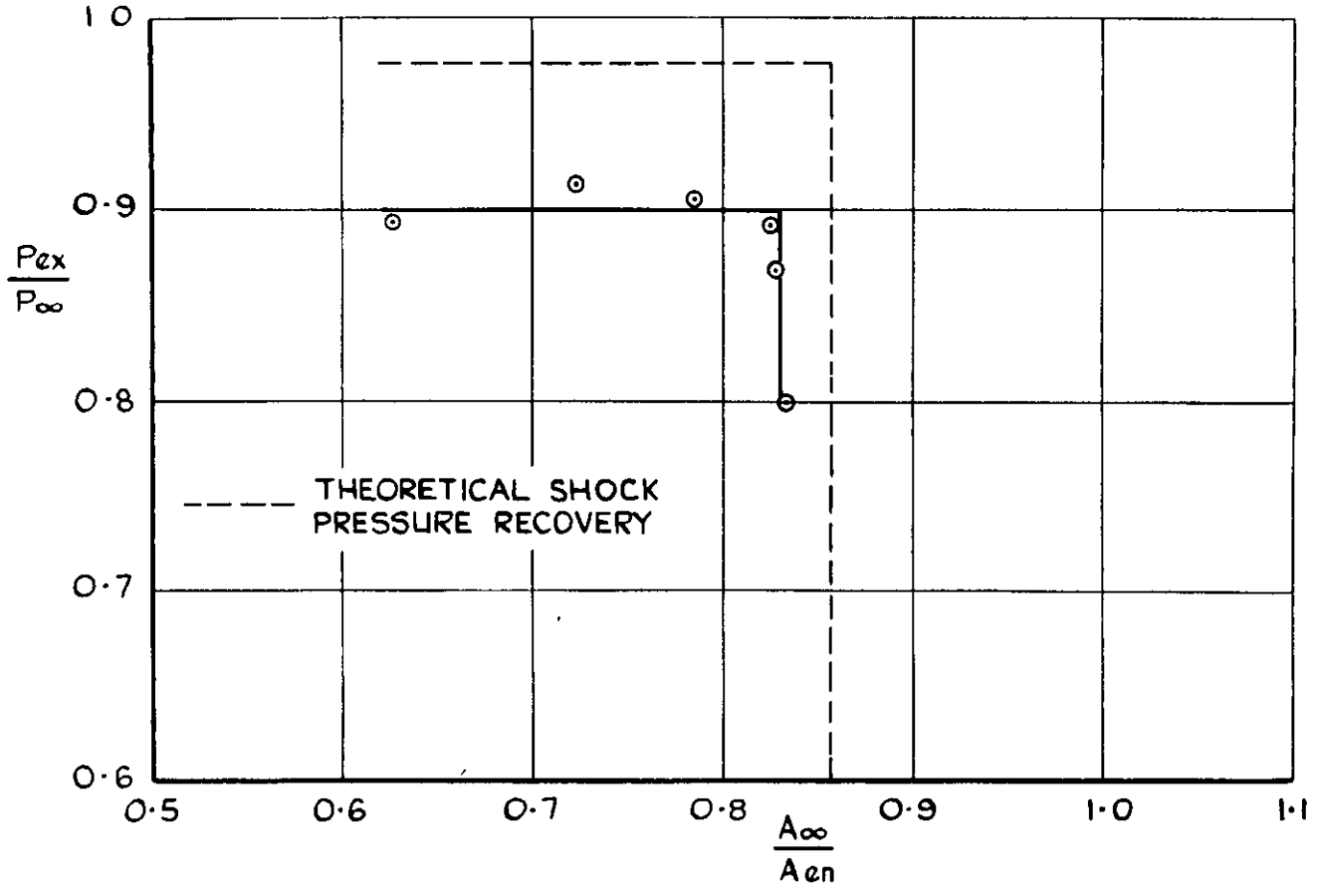

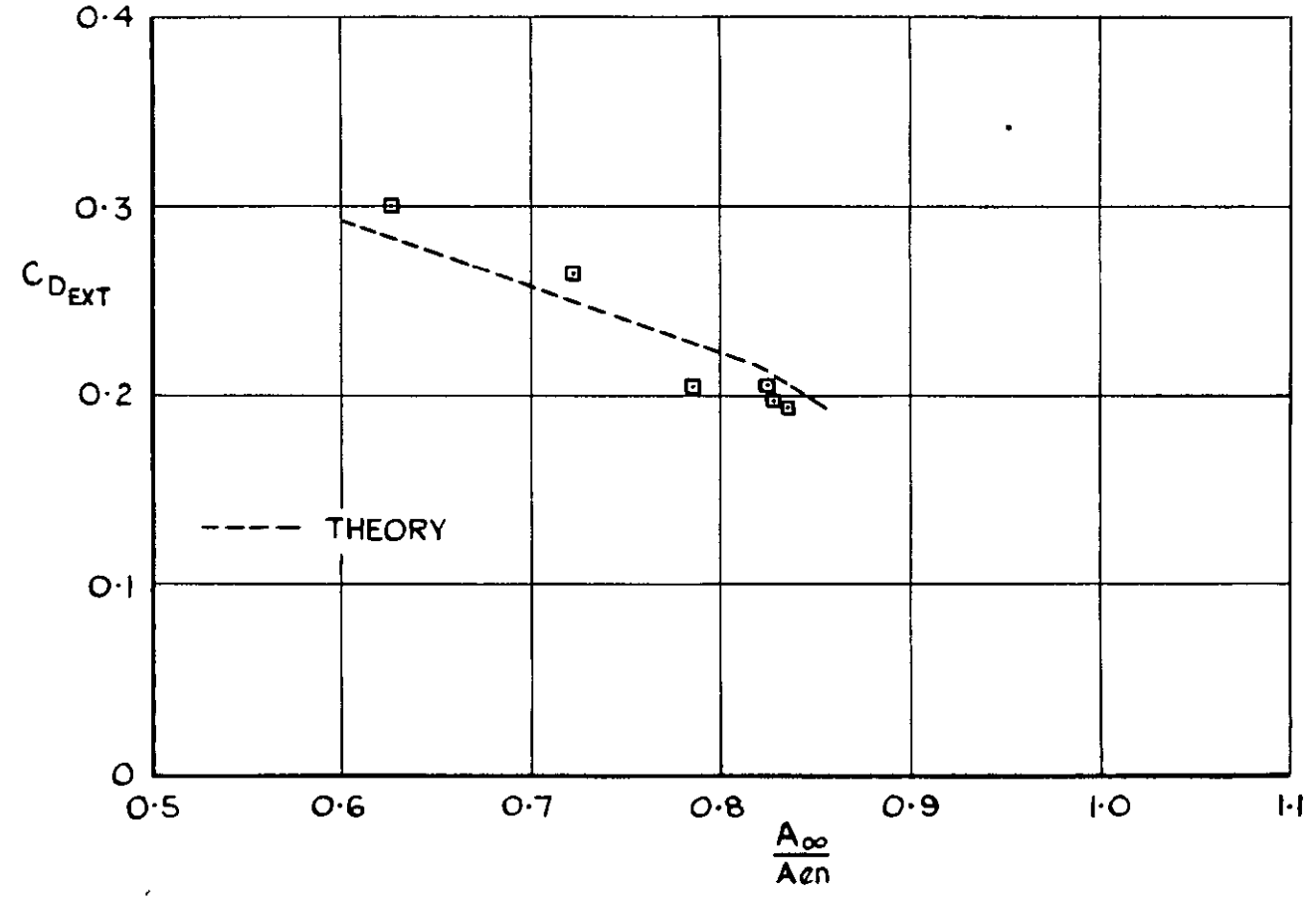

FIG. 18(a) VARIATION OF DRAG AND PRESSURE RECOVERY WITH MASS FLOW THROUGH A 12° WEDGE CENTRE BODY INTAKE AT $M_\infty = 1.56$

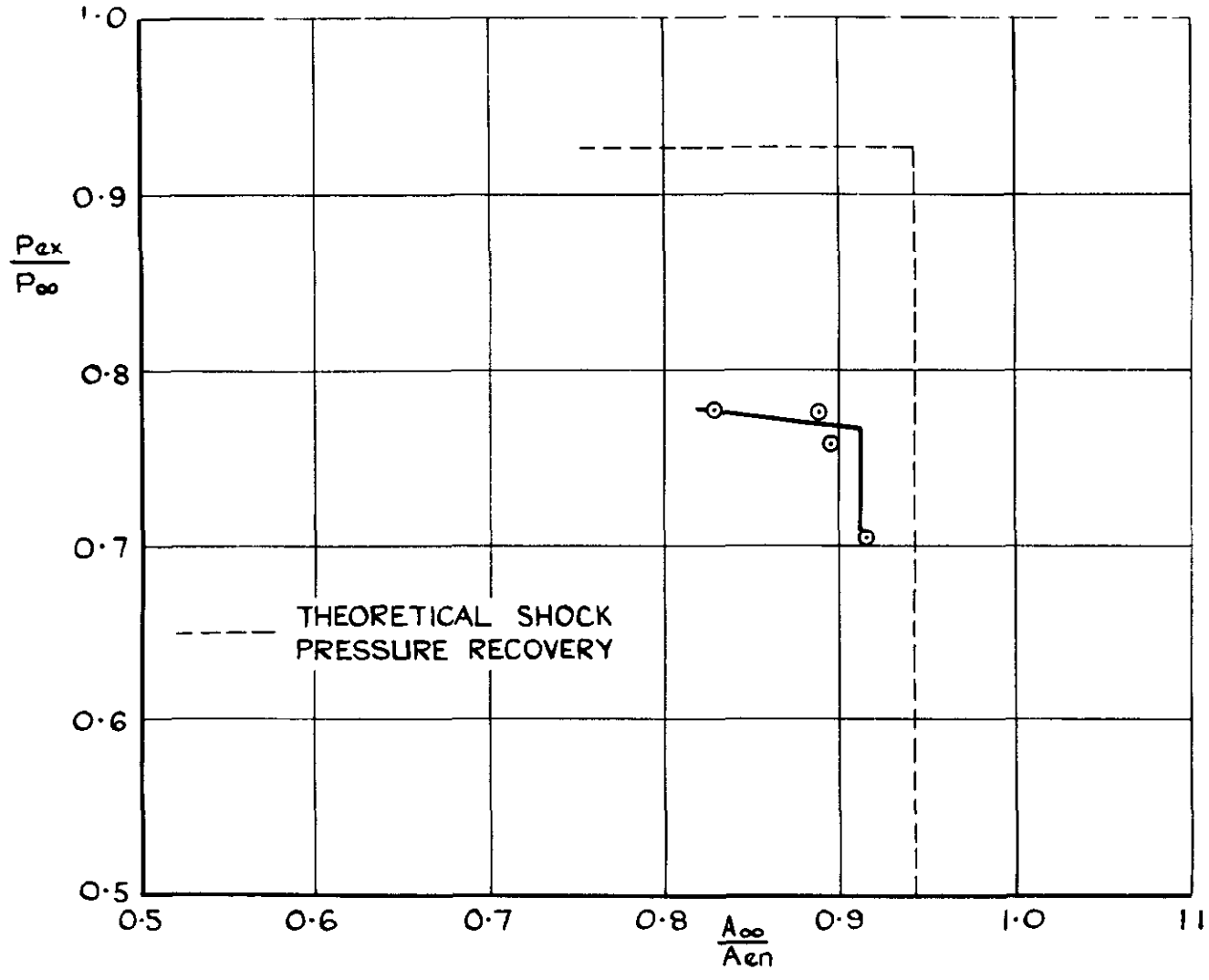

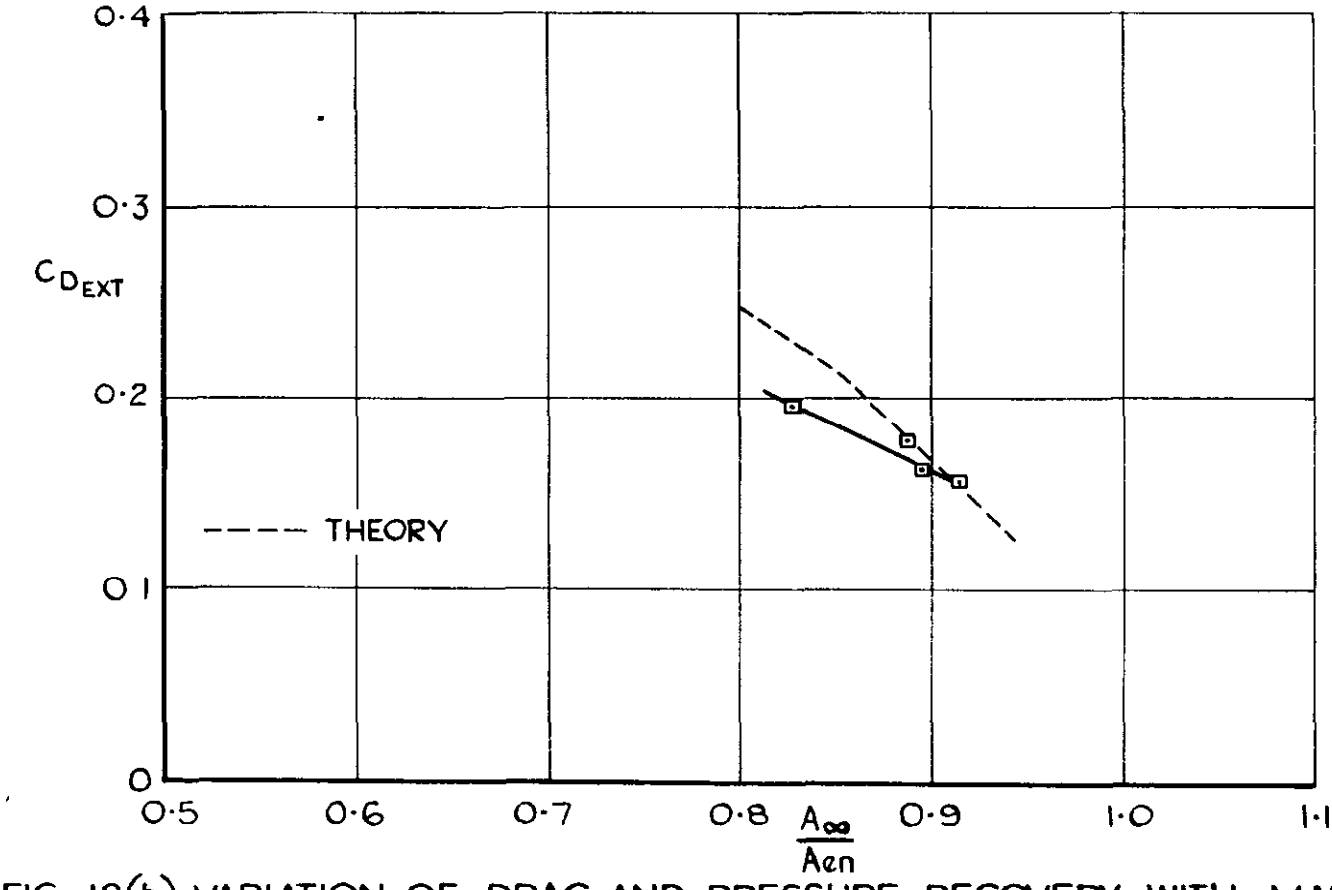

FIG. 18(b) VARIATION OF DRAG AND PRESSURE RECOVERY WITH MASS FLOW THROUGH A 12° WEDGE CENTRE BODY INTAKE AT $M_\infty = 1{\cdot}86$

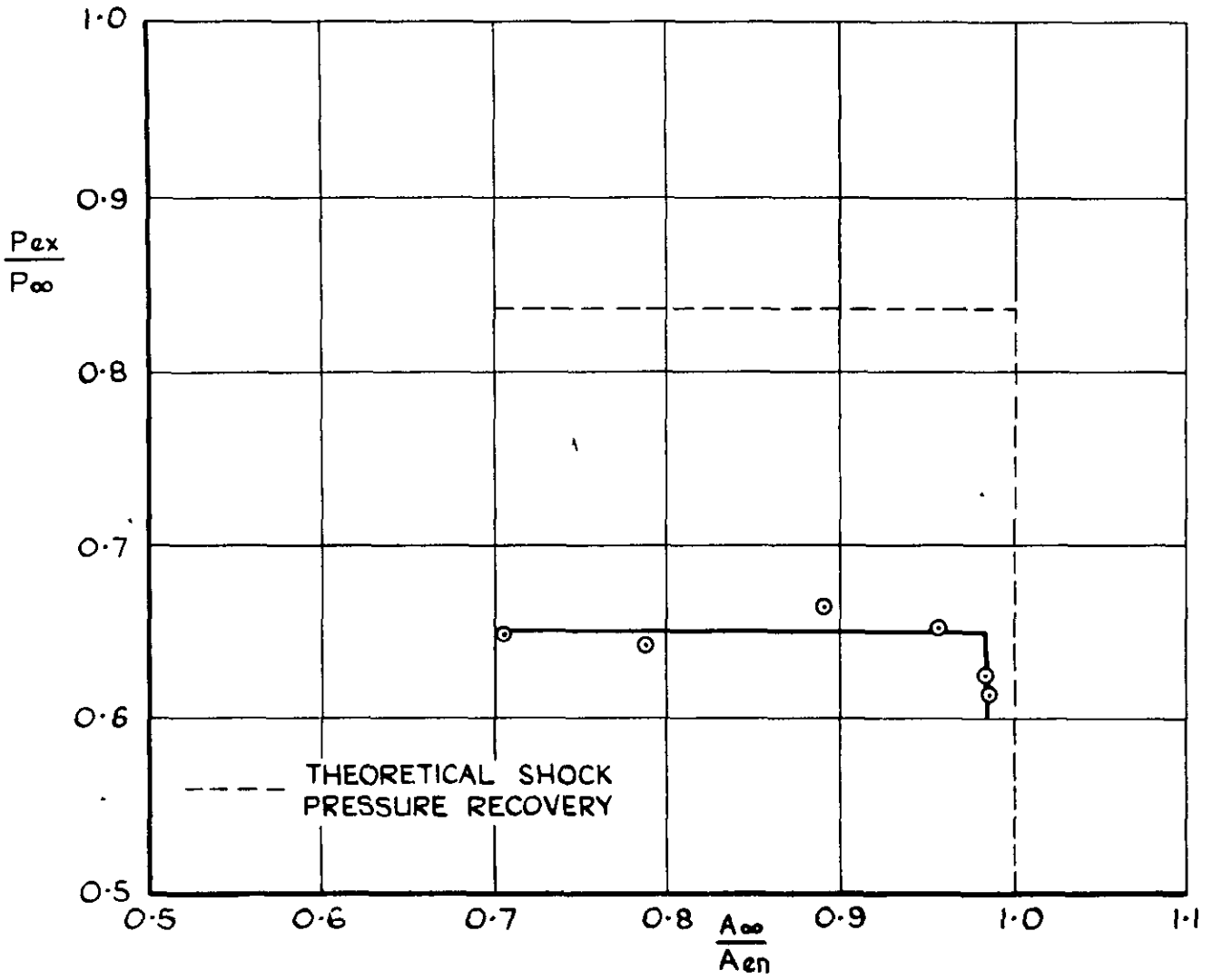

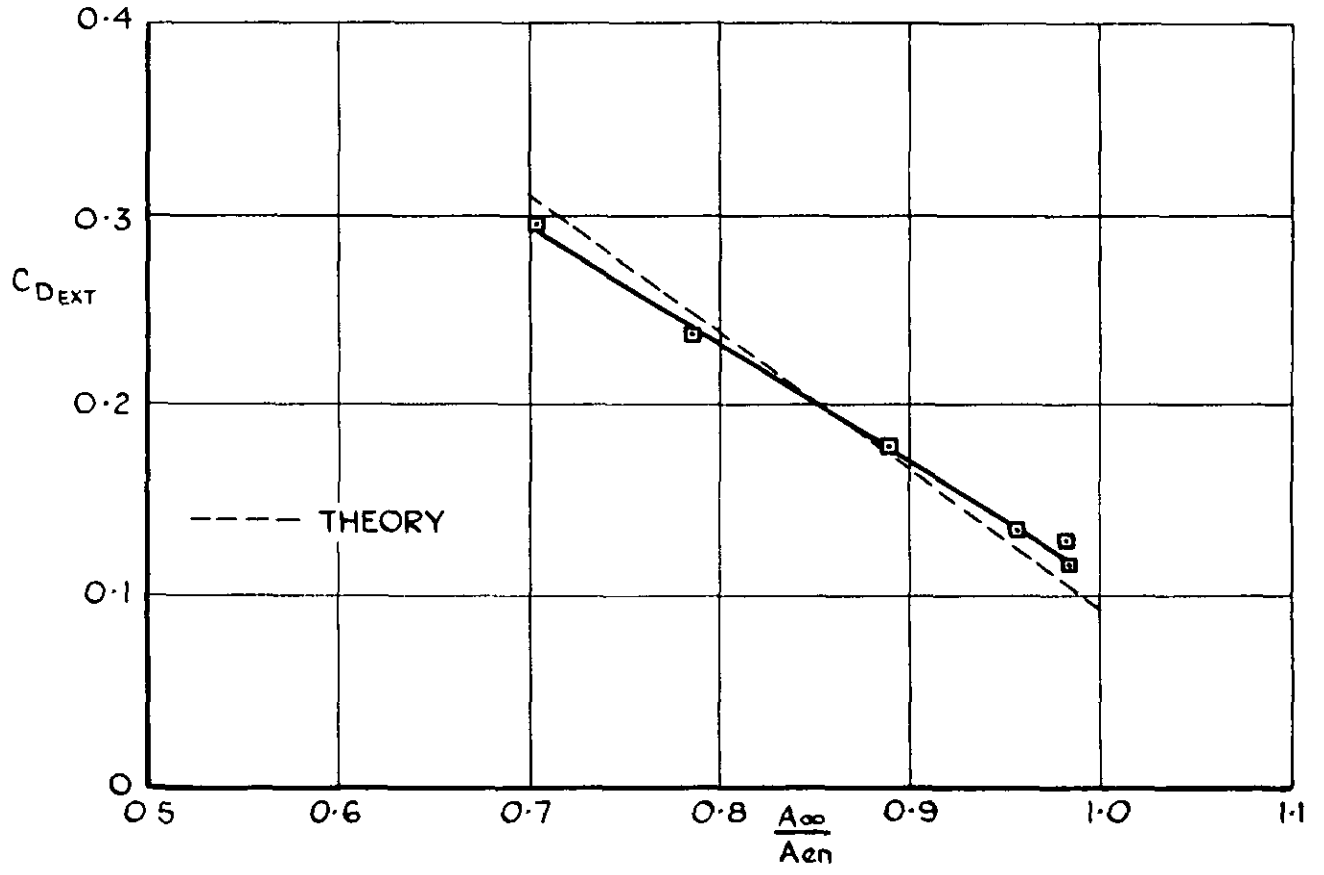

FIG. 18(c) VARIATION OF DRAG AND PRESSURE RECOVERY WITH MASS FLOW THROUGH A 12° WEDGE CENTRE BODY INTAKE AT $M_\infty = 2{\cdot}14$

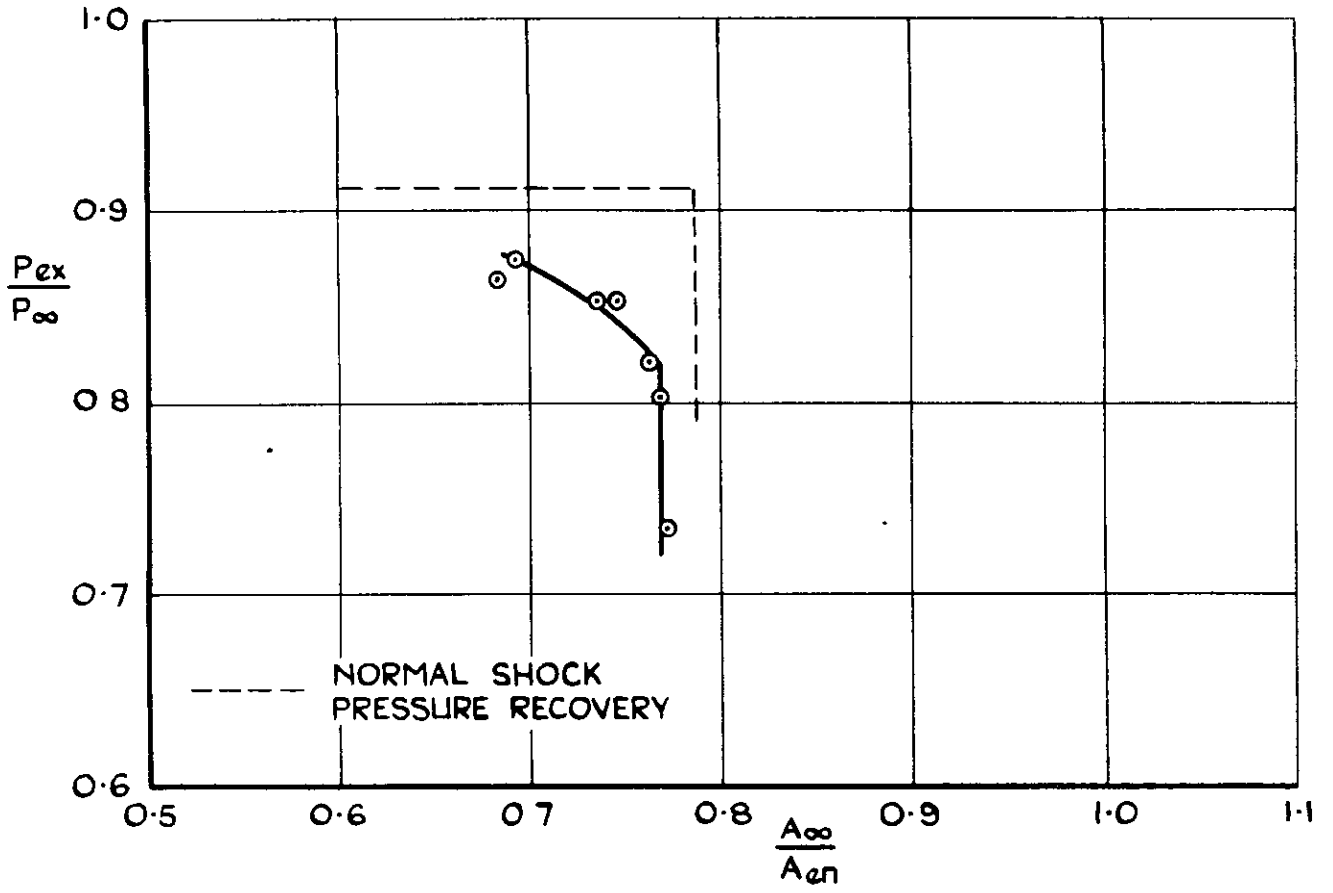

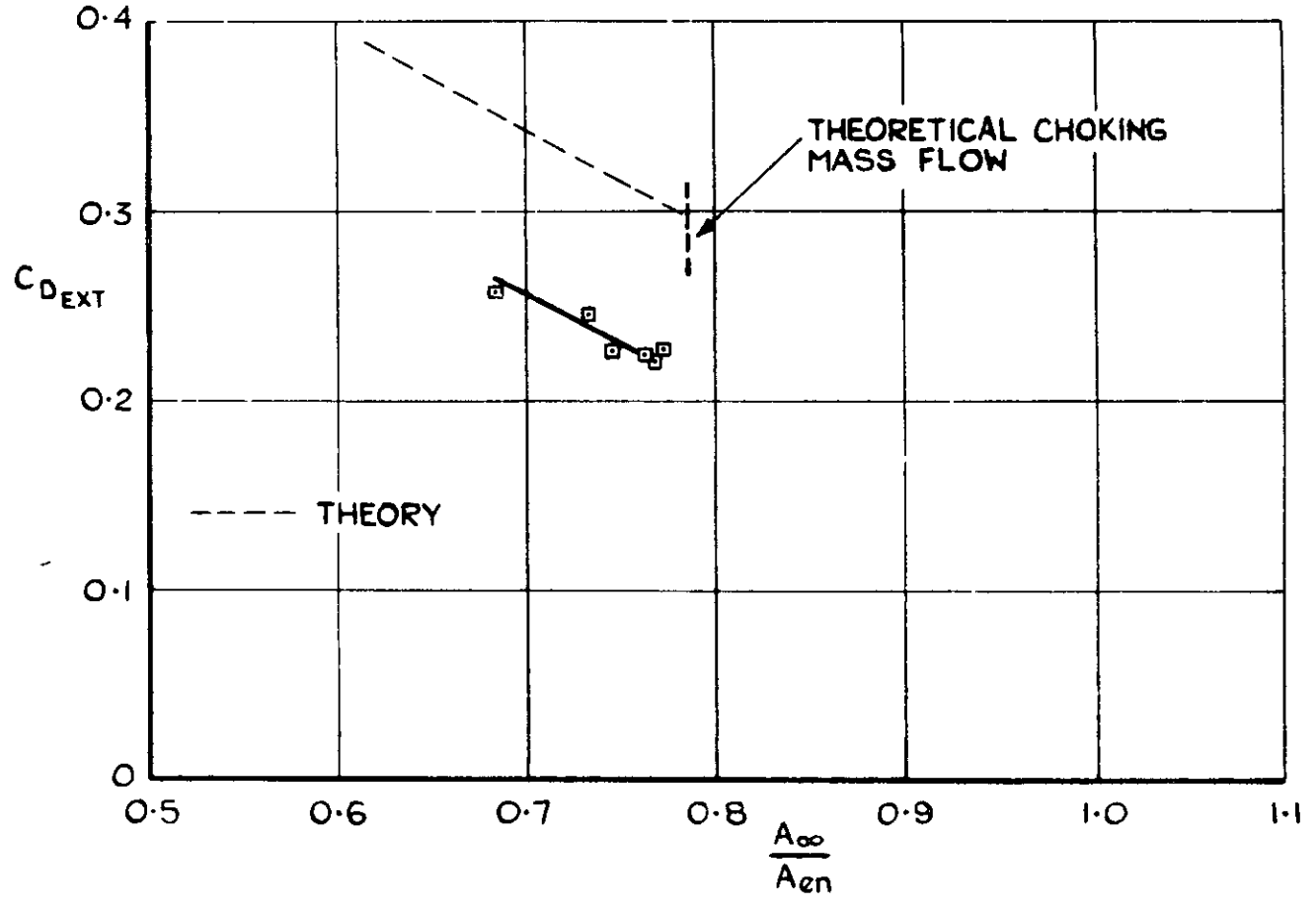

FIG. 19(a) VARIATION OF DRAG AND PRESSURE RECOVERY WITH MASS FLOW THROUGH A 16° WEDGE CENTRE BODY INTAKE AT $M_\infty = 1{\cdot}56$

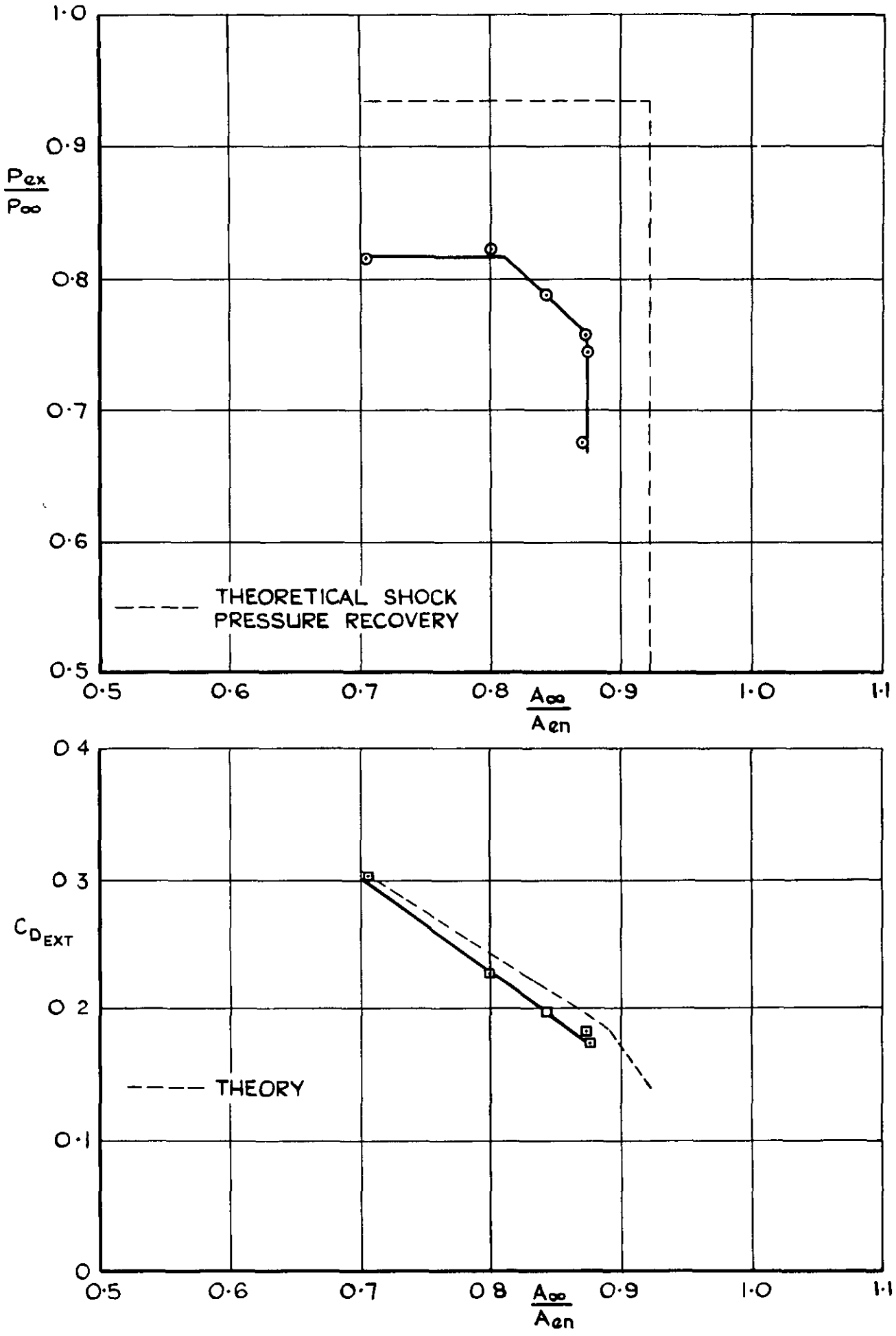

FIG. 19(b) VARIATION OF DRAG AND PRESSURE RECOVERY WITH MASS FLOW THROUGH A 16° WEDGE CENTRE BODY INTAKE AT $M_\infty = 1{\cdot}86$

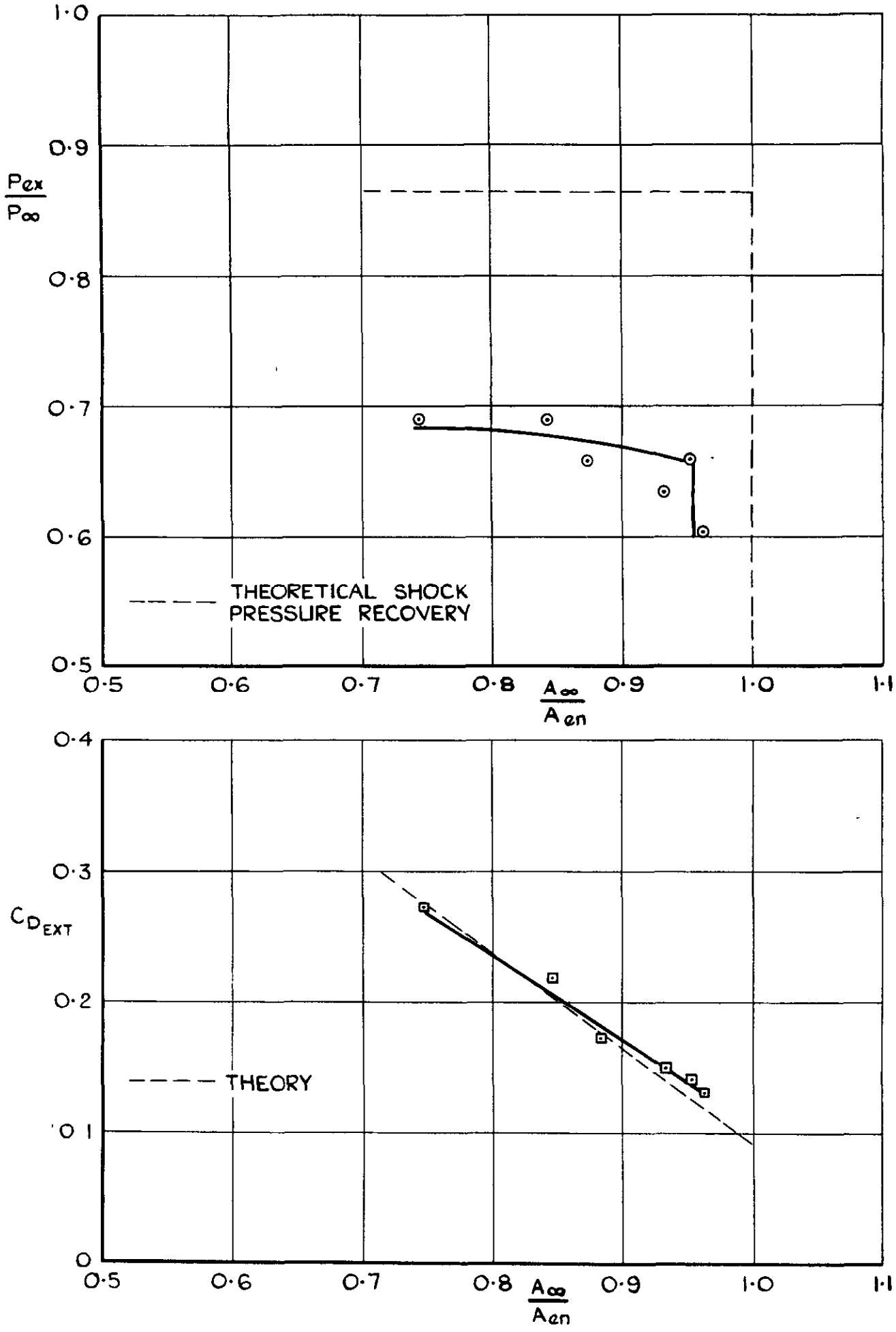

FIG. 19 (c) VARIATION OF DRAG AND PRESSURE RECOVERY WITH MASS FLOW THROUGH A 16° WEDGE CENTRE BODY INTAKE AT $M_\infty = 2{\cdot}14$

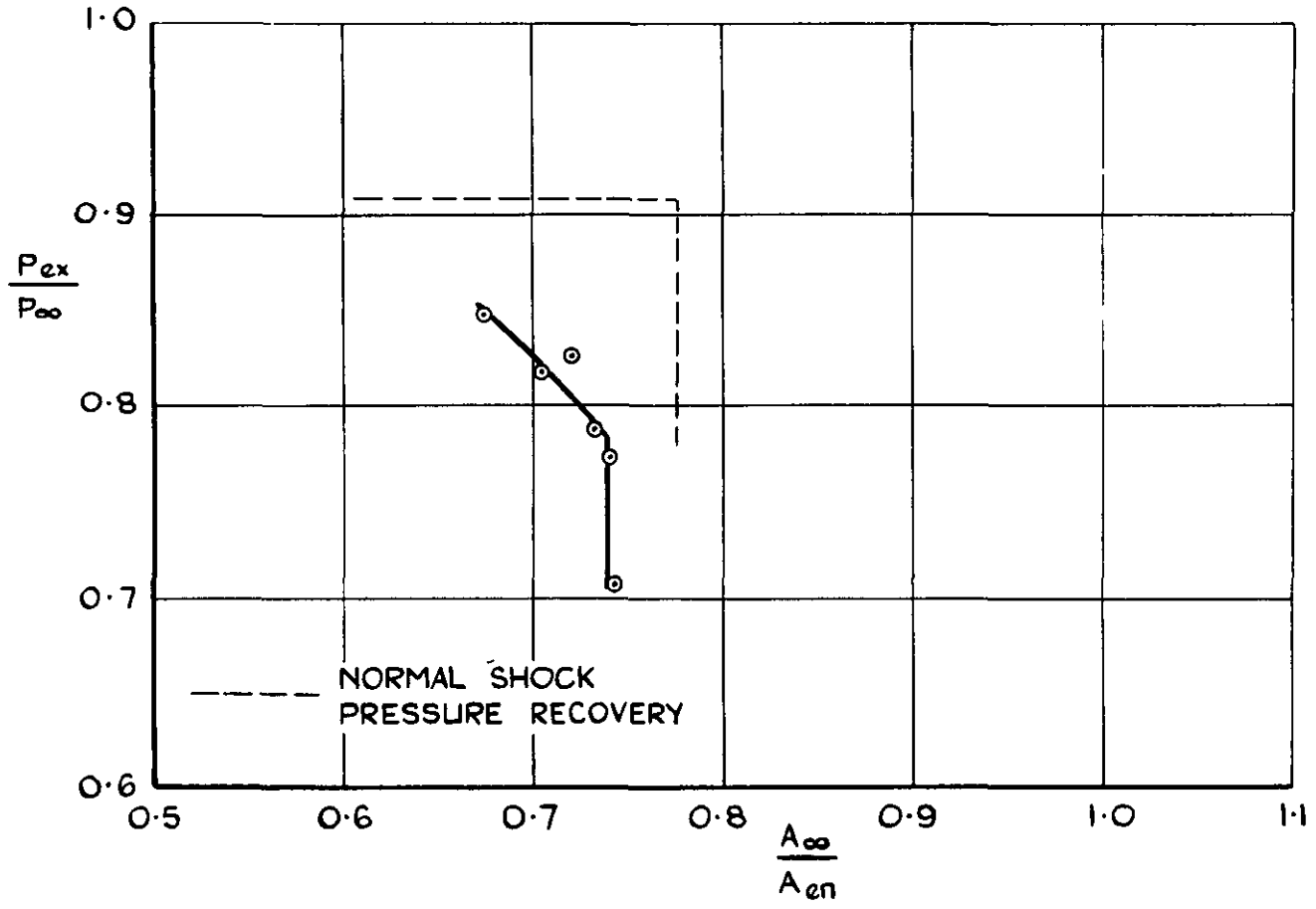

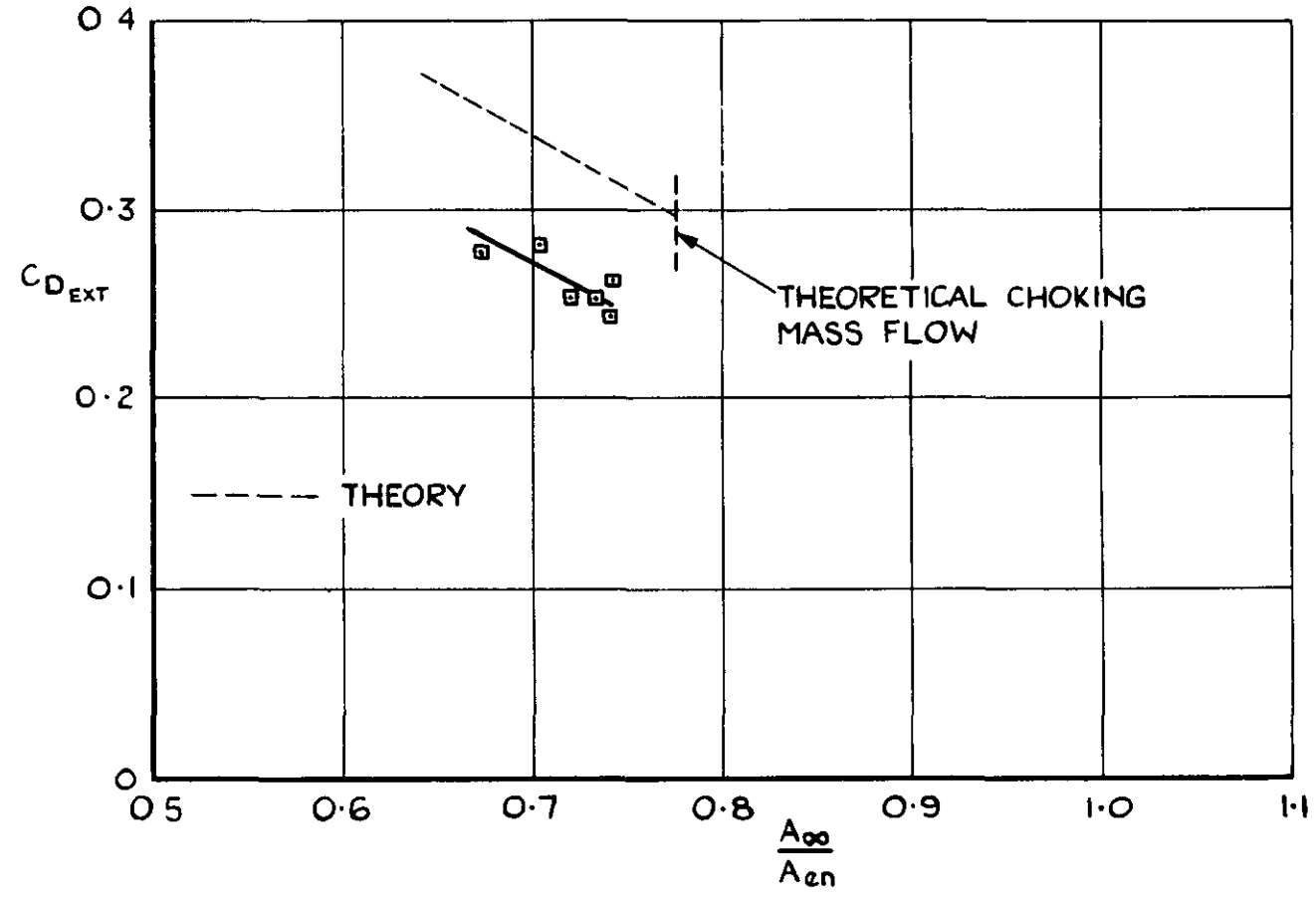

FIG. 20(a) VARIATION OF DRAG AND PRESSURE RECOVERY WITH MASS FLOW THROUGH A 20° WEDGE CENTRE BODY INTAKE AT $M_\infty = 1{\cdot}56$

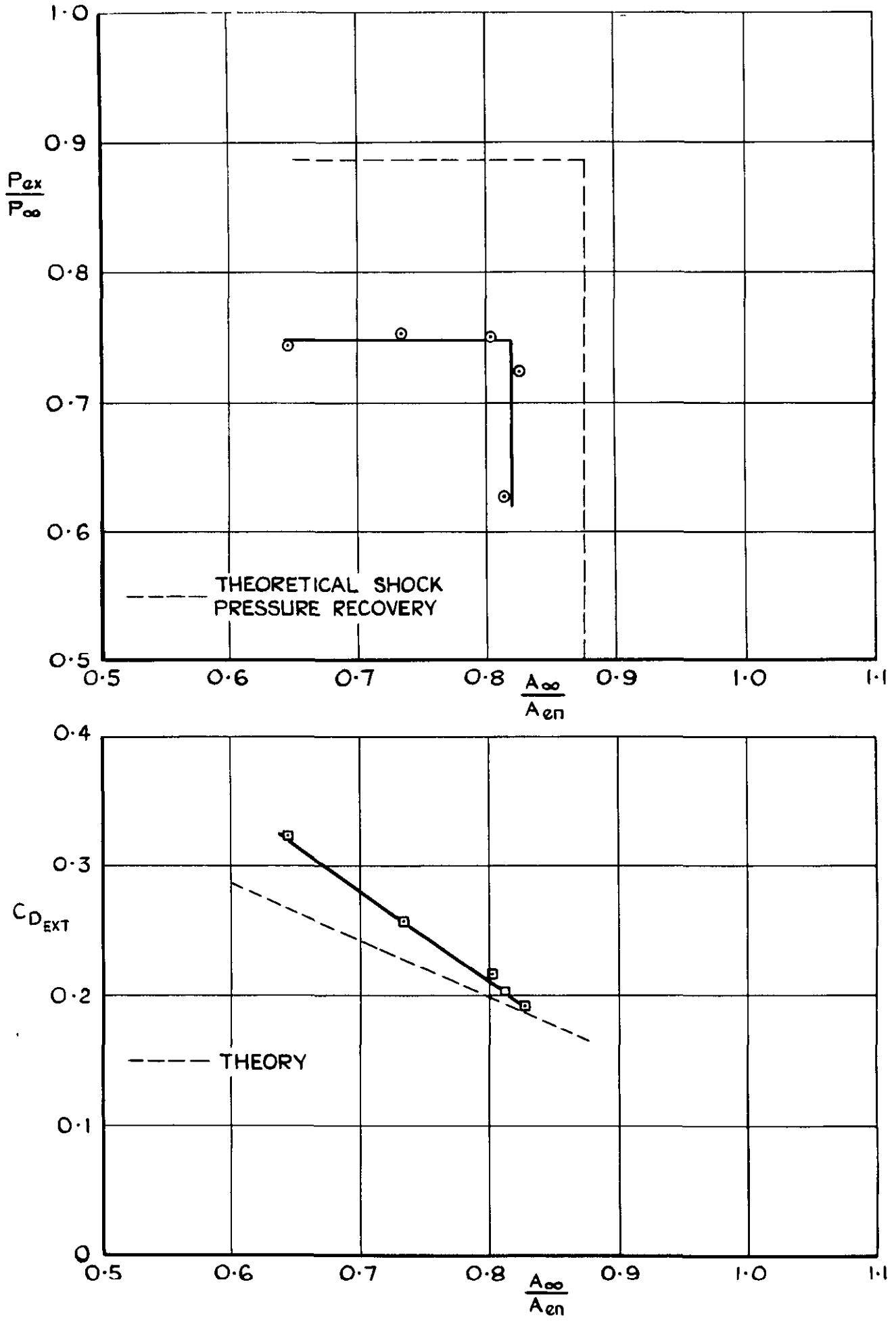

FIG. 20(b) VARIATION OF DRAG AND PRESSURE RECOVERY WITH MASS FLOW THROUGH A 20° WEDGE CENTRE BODY INTAKE AT $M_\infty = 1.86$

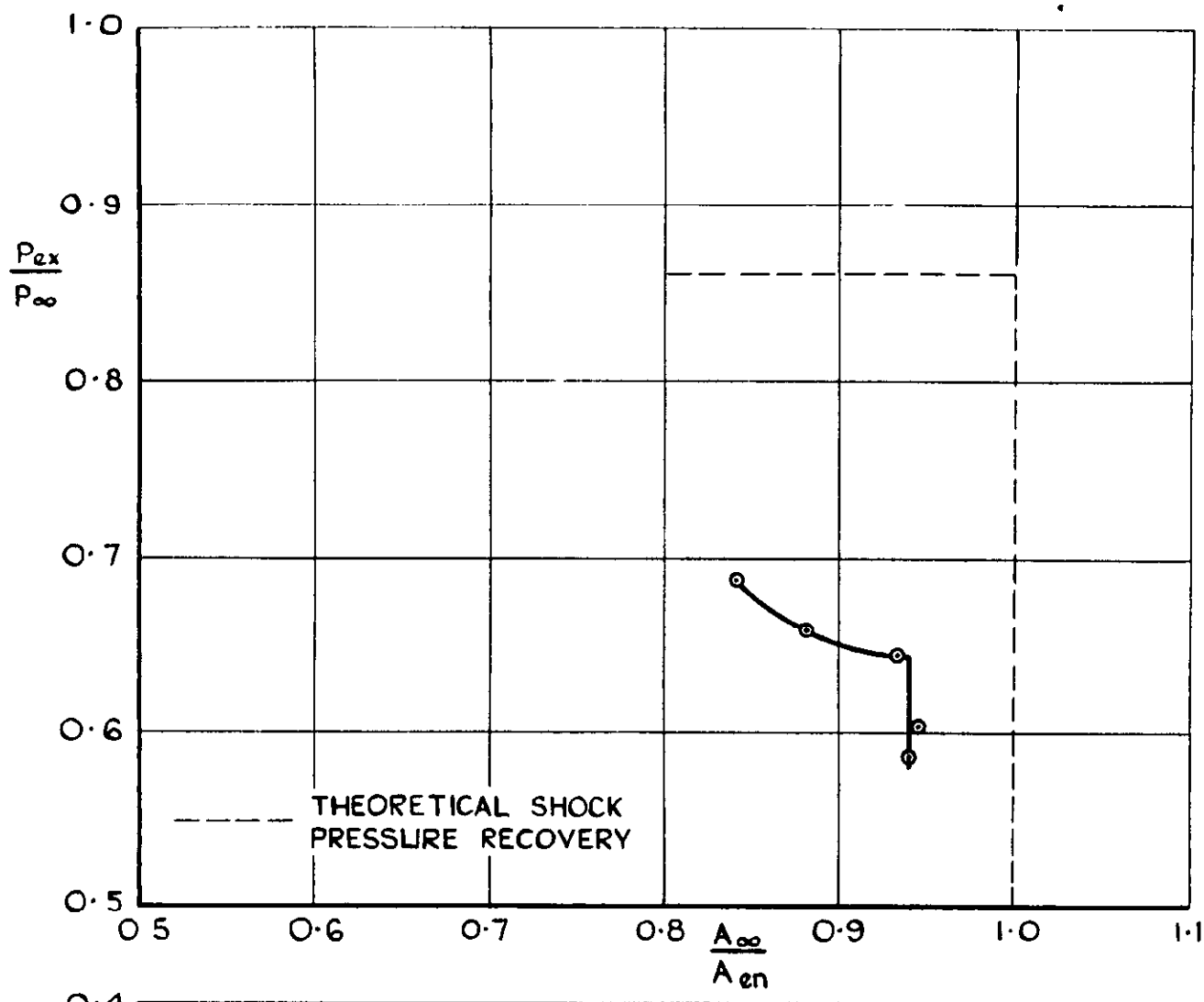

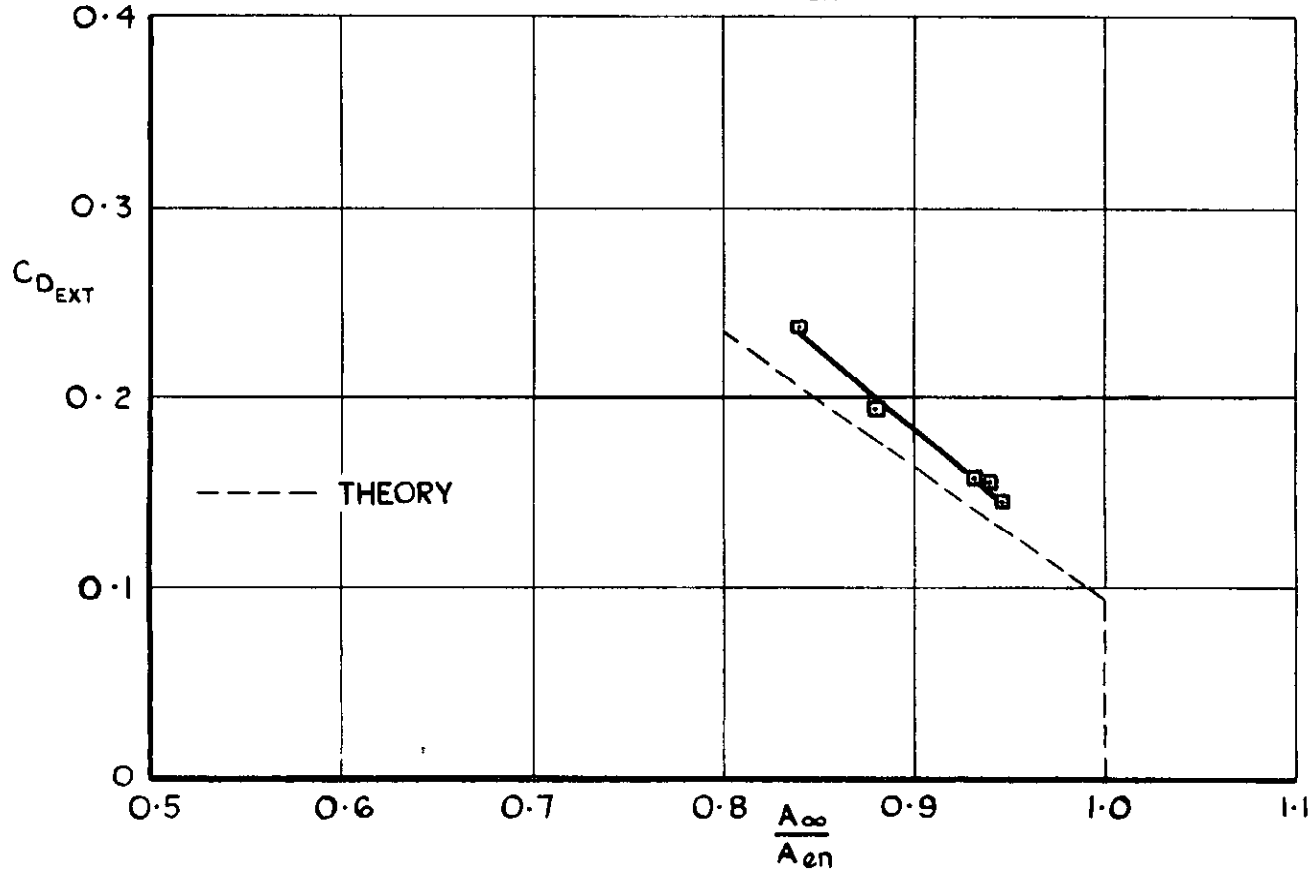

FIG 20(c) VARIATION OF DRAG AND PRESSURE RECOVERY WITH MASS FLOW THROUGH A 20° WEDGE CENTRE BODY INTAKE AT $M_\infty = 2{\cdot}14$

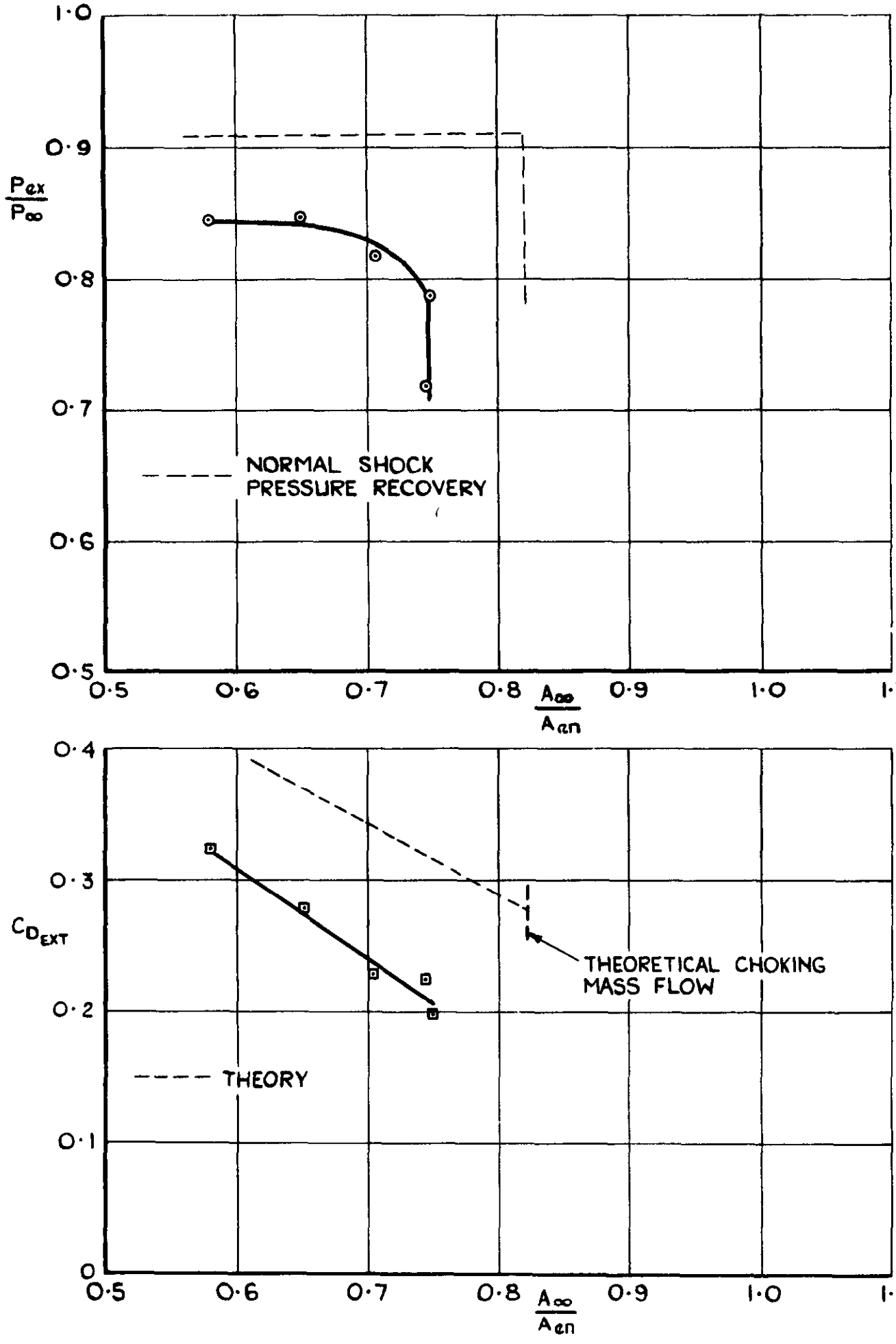

FIG. 21(a) VARIATION OF DRAG AND PRESSURE RECOVERY WITH MASS FLOW THROUGH A 24° WEDGE CENTRE BODY INTAKE AT $M_\infty = 1{\cdot}56$

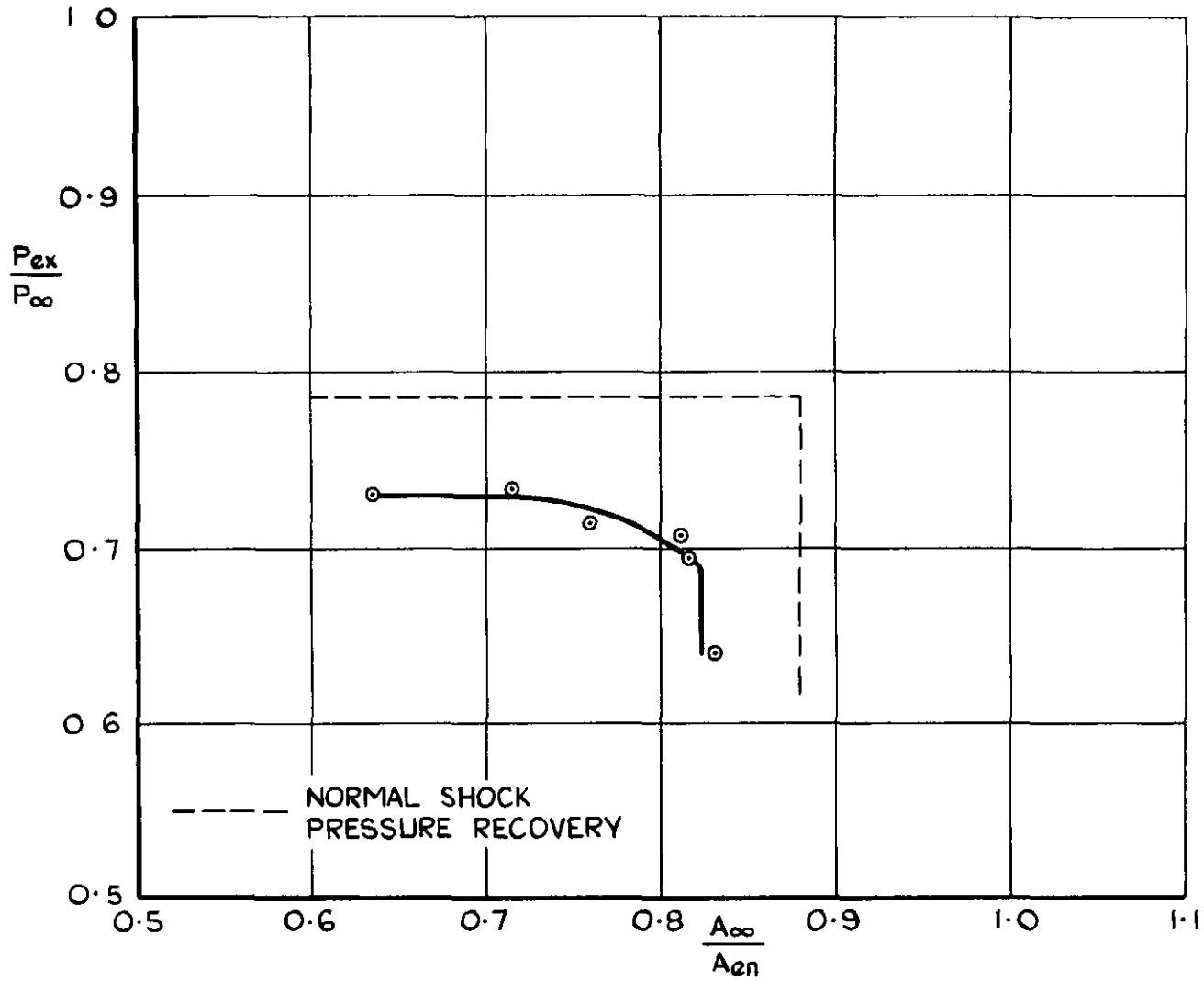

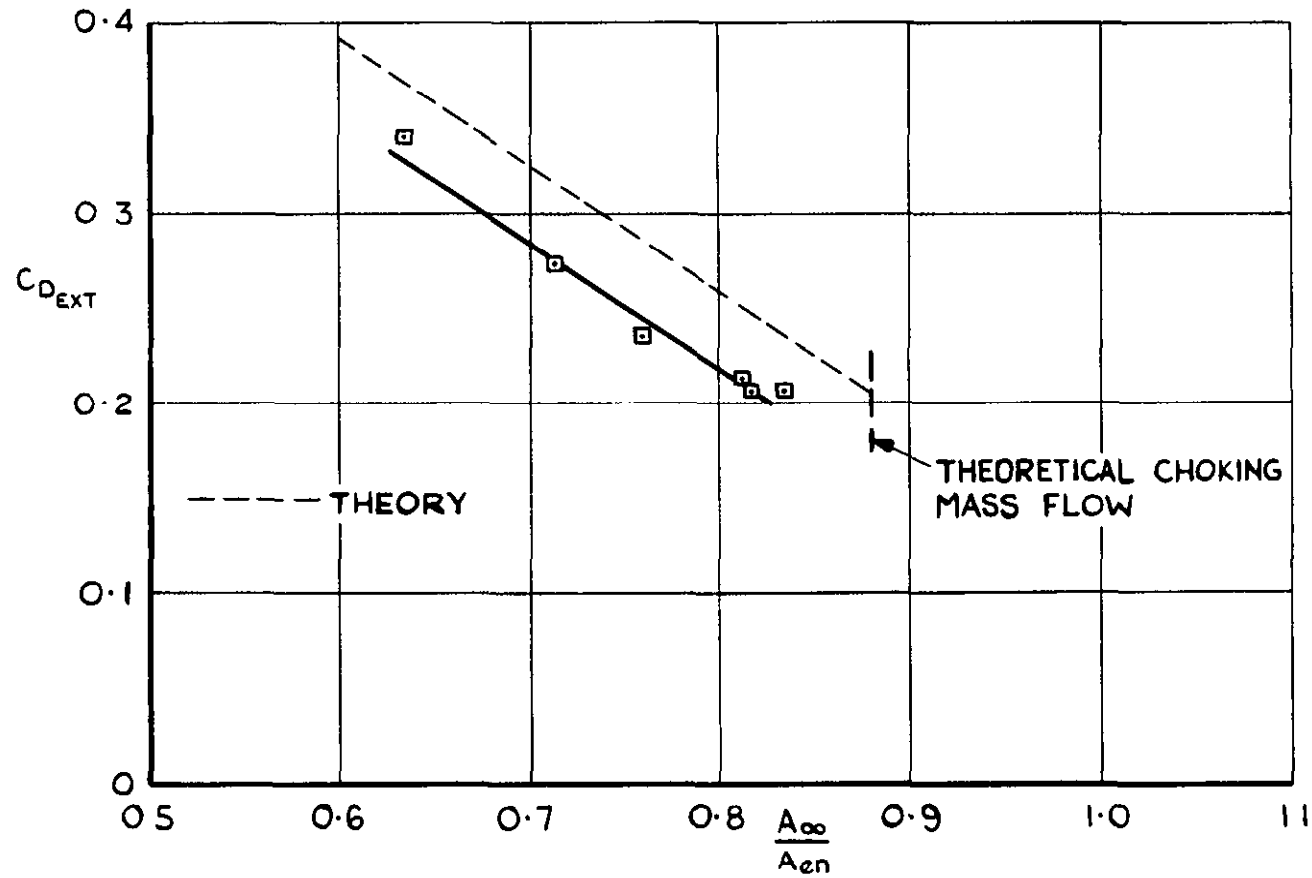

FIG. 21(b) VARIATION OF DRAG AND PRESSURE RECOVERY WITH MASS FLOW THROUGH A 24° WEDGE CENTRE BODY INTAKE AT $M_\infty = 1.86$

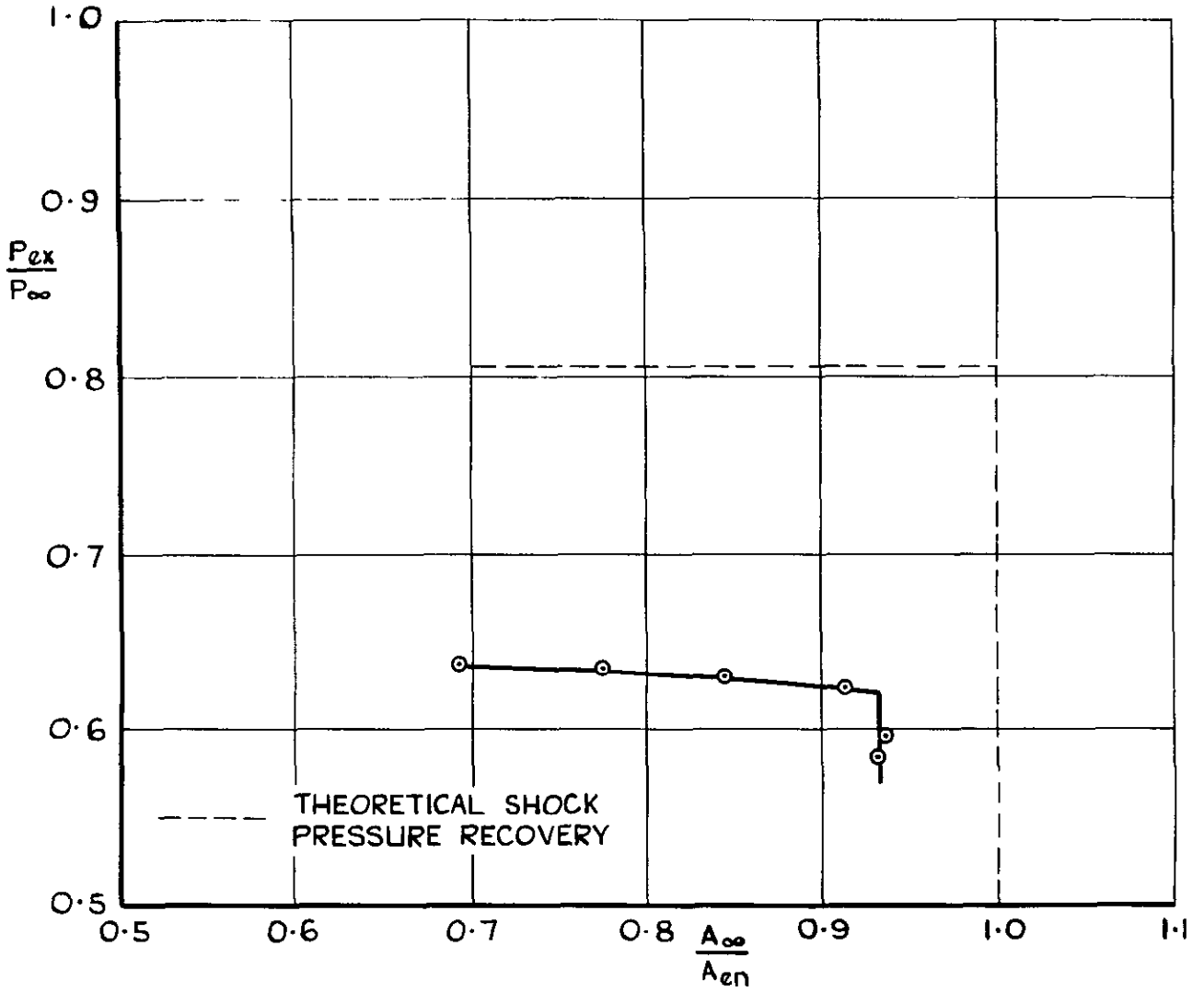

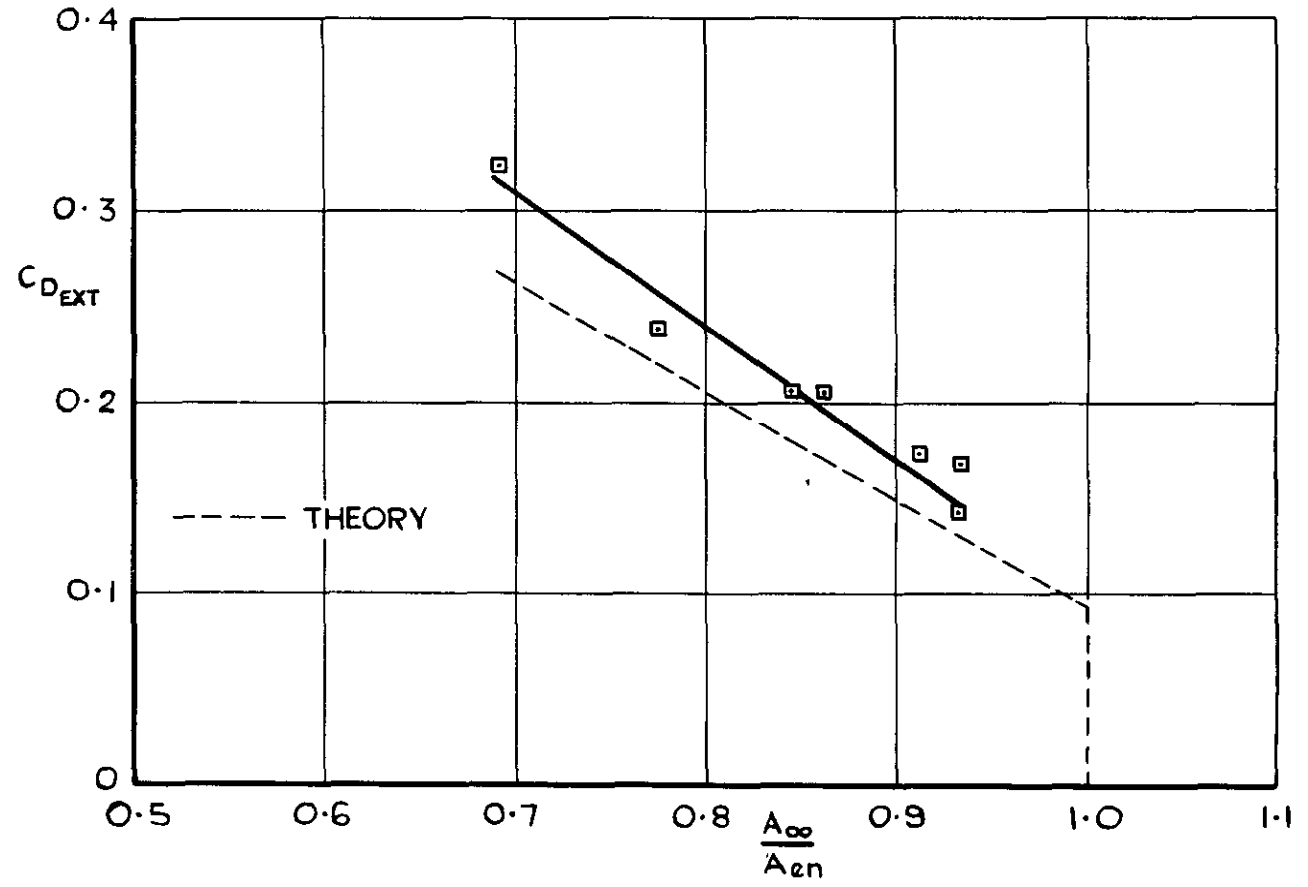

FIG. 21(c) VARIATION OF DRAG AND PRESSURE RECOVERY WITH MASS FLOW THROUGH A 24° WEDGE CENTRE BODY INTAKE AT $M_\infty = 2{\cdot}14$

Printed in England for Her Majesty's Stationery Office by the Royal Aircraft Establishment, Farnborough. Dd.129528. K.4.

A.R.C. C.P. No. 968
July 1966

Dutton, R.A.
Goldsmith, E.L.

533.697.25 :
533.6.013.12 :
531.652 :
533.6.011.72 :
533.6.011.5

THE DRAG OF SOME WEDGE CENTRE-BODY INTAKES AT MACH NUMBERS OF 1.56, 1.86 AND 2.14

Experiments are described in which measurements have been made of the drag and pressure recovery of a wedge centre-body intake of rectangular cross-section. Intakes with four different wedges (12°, 16°, 20° and 24° semi apex angle) were tested at Mach numbers of 1.56, 1.86 and 2.14. The measurements were obtained for the following three different flow states; with both the wedge and cowl lip shocks attached, with only the wedge shock attached, and finally with the wedge shock detached. The results obtained from the drag measurements are compared with those from

(over)

A.R.C. C.P. No. 968
July 1966

Dutton, R.A.
Goldsmith, E.L.

533.697.25 :
533.6.013.12 :
531.652 :
533.6.011.72 :
533.6.011.5

THE DRAG OF SOME WEDGE CENTRE-BODY INTAKES AT MACH NUMBERS OF 1.56, 1.86 AND 2.14

Experiments are described in which measurements have been made of the drag and pressure recovery of a wedge centre-body intake of rectangular cross-section. Intakes with four different wedges (12°, 16°, 20° and 24° semi apex angle) were tested at Mach numbers of 1.56, 1.86 and 2.14. The measurements were obtained for the following three different flow states; with both the wedge and cowl lip shocks attached, with only the wedge shock attached, and finally with the wedge shock detached. The results obtained from the drag measurements are compared with those from

(over)

A.R.C. C.P. No. 968
July 1966

Dutton, R.A.
Goldsmith, E.L.

533.697.25 :
533.6.013.12 :
531.652 :
533.6.011.72 :
533.6.011.5

THE DRAG OF SOME WEDGE CENTRE-BODY INTAKES AT MACH NUMBERS OF 1.56, 1.86 AND 2.14

Experiments are described in which measurements have been made of the drag and pressure recovery of a wedge centre-body intake of rectangular cross-section. Intakes with four different wedges (12°, 16°, 20° and 24° semi apex angle) were tested at Mach numbers of 1.56, 1.86 and 2.14. The measurements were obtained for the following three different flow states; with both the wedge and cowl lip shocks attached, with only the wedge shock attached, and finally with the wedge shock detached. The results obtained from the drag measurements are compared with those from

(over)

an approximate method of calculation. With the wedge shock attached, the spillage drag can be estimated reasonably well but when the wedge shock is detached the measure of agreement between experimental and calculated results is poor.

Curves showing the variation of capture ratio and pre-entry drag at full mass flow with M for particular wedge angles, and curves giving the cowl drag at full mass flow for families of both straight line and elliptical cowl profiles are presented.

an approximate method of calculation. With the wedge shock attached, the spillage drag can be estimated reasonably well but when the wedge shock is detached the measure of agreement between experimental and calculated results is poor.

Curves showing the variation of capture ratio and pre-entry drag at full mass flow with M for particular wedge angles, and curves giving the cowl drag at full mass flow for families of both straight line and elliptical cowl profiles are presented.

Published by
HER MAJESTY'S STATIONERY OFFICE

To be purchased from
49 High Holborn, London W C 1
423 Oxford Street, London W 1
13A Castle Street, Edinburgh 2
109 St Mary Street, Cardiff
Brazennose Street, Manchester 2
50 Fairfax Street, Bristol 1
35 Smallbrook, Ringway, Birmingham 5
7-11 Linenhall Street, Belfast 2
or through any bookseller

C.P. No. 968

S.O. CODE No. 23-9017-68